MULTIBODY DYNAMICS USING CONSERVATION OF MOMENTUM WITH APPLICATION TO COMPLIANT OFFSHORE FLOATING WIND TURBINES

A Dissertation

by

LEI WANG

Submitted to the Office of Graduate Studies of
Texas A&M University
in partial fulfillment of the requirements for the degree of

DOCTOR OF PHILOSOPHY

August 2012

Major Subject: Ocean Engineering

MULTIBODY DYNAMICS USING CONSERVATION OF MOMENTUM WITH APPLICATION TO COMPLIANT OFFSHORE FLOATING WIND TURBINES

A Dissertation

by

LEI WANG

Submitted to the Office of Graduate Studies of
Texas A&M University
in partial fulfillment of the requirements for the degree of

DOCTOR OF PHILOSOPHY

Approved by:

Chair of Committee,	Bert Sweetman
Committee Members,	Richard Mercier
	Jeffrey Falzarano
	Ayal Anis
Head of Department,	John Niedzwecki

August 2012

Major Subject: Ocean Engineering

ABSTRACT

Multibody Dynamics Using Conservation of Momentum with Application to Compliant Offshore Floating Wind Turbines. (August 2012)

Lei Wang, B.S., Tianjin University;

M.S., Tianjin University

Chair of Advisory Committee: Dr. Bert Sweetman

Environmental, aesthetic and political pressures continue to push for siting offshore wind turbines beyond sight of land, where waters tend to be deeper, and use of floating structures is likely to be considered. Savings could potentially be realized by reducing hull size, which would allow more compliance with the wind thrust force in the pitch direction. On the other hand, these structures with large-amplitude motions will make dynamic analysis both more challenging and more critical. Prior to the present work, there were no existing dynamic simulation tools specifically intended for compliant wind turbine design.

Development and application of a new computational method underlying a new time-domain simulation tool is presented in this dissertation. The compliant floating wind turbine system is considered as a multibody system including tower, nacelle, rotor and other moving parts. Euler's equations of motion are first applied to the compliant design to investigate the large-amplitude motions. Then, a new formulation of multibody dynamics is developed through application of the conservation of both linear momentum and angular momentum to the entire system directly. A base

body is prescribed within the compliant wind turbine system, and the equations of motion (EOMs) of the system are projected into the coordinate system associated with this body. Only six basic EOMs of the system are required to capture 6 unknown degrees of freedom (DOFs) of the base body when mechanical DOFs between contiguous bodies are prescribed. The 6×6 mass matrix is actually composed of two decoupled 3×3 mass matrices for translation and rotation, respectively. Each element within the matrix includes the inertial effects of all bodies. This condensation decreases the coupling between elements in the mass matrix, and so minimizes the computational demand. The simulation results are verified by critical comparison with those of the popular wind turbine dynamics software FAST.

The new formulation is generalized to form the momentum cloud method (MCM), which is particularly well suited to the serial mechanical N-body systems connected by revolute joints with prescribed relative rotation. The MCM is then expanded to multibody systems with more complicated joints and connection types.

To my wife, Chang Liu

for her trust, support and sacrifice

ACKNOWLEDGMENTS

This dissertation is composed of the main result of my four-year research since I have been enrolled in Texas A&M University in 2008. I would like to express my sincere gratitude to my advisor, Professor Bert Sweetman, for his insightful guidance and consistent encouragement along the way. His efforts have helped transform a ship designer into a researcher. I especially appreciate his great patience and tolerance during these years because I am a stickler for technical opinions. I also wish to express my sincere thanks to Professor Richard Mercier, Professor Jeffrey Falzarano and Professor Ayal Anis, for taking time out of their busy schedules to serve as my committee members. I truly appreciate their valuable advices on my research and constructive comments on this dissertation.

TABLE OF CONTENTS

CHAPTER Page

CHAPTER Page

LIST OF TABLES

LIST OF FIGURES

FIGURE Page

FIGURE Page

FIGURE Page

CHAPTER I

INTRODUCTION

This dissertation focuses on the development of a new multibody formulation methodology underlying a time-domain dynamic simulation tool of the compliant floating wind turbine system. In Section A of this introduction chapter, the background of the problem are introduced, including the development of floating wind turbine concepts, presentation of complaint designs and motivation for research on the new formulation. In Section B, relevant historical literatures about offshore wind turbines and multibody dynamics are reviewed. Main contributions and organization of the presented work are summarized in Section C and D, respectively.

A. Background

Offshore wind energy has enormous development potential. Compared to the onshore counterparts, the offshore wind turbines have many advantages [1]: a higher velocity, steadier wind field in the offshore area could enable more electricity generated per square meter of swept rotor area; transportation and installation capacities of marine shipping and handling equipment exceed the installation requirements for multi-megawatt wind turbines; wind turbines can be larger because visual intrusion is minimized and noise emissions can be ignored offshore; offshore turbines can be located close to high-value urban load centers, simplifying transmission of power and

---

The journal model is *IEEE Transactions on Automatic Control.*

increasing efficiency. Potential development of floating wind turbine systems has become an area of intensive research field recent years.

Although various types of floaters have been presented to support wind turbine payloads, the overall cost of the entire system is still a significant concern for the utilization of floating wind turbine concepts. A cost analysis [1] shows that the economics of deep-water wind turbines will be determined primarily by the additional costs of the floating structure and power distribution system, because the costs of topside facilities are similar to that of bottom-fixed turbine systems. Musial [2] indicates that the wind turbine platform and mooring system should provide the most potential for system cost reduction because the application is new and the most significant cost saving design tradeoffs have not yet been explored.

The compliant floating wind turbine design presented in this dissertation applies a truncated spar cylinder as the floater. Although technical challenges posed by this compliant structural design are significant, meaningful weight savings could be realized, which can be demonstrated using simple dimensional analysis. Fig. 1 shows the predominant loads on a spar-type floating wind turbine. Considering the static equilibrium of a tower subject to four constant forces representing each of these loads combined with the use of simple dimensional analysis yields considerable insight into the potential for weight savings. Other important forces such as waves and the water-plane stiffness are neglected from this very basic thought experiment. Considering just the four forces and arbitrarily defining pitch as the direction of the rotational motion caused by wind forces, pitch motion will be in static equilibrium if the couple created by the wind and mooring forces is equal to that of the buoyancy

and gravity forces. The wind force and tower height are assumed to be approximately constant, which implies some constant wind moment must be reacted by buoyancy and gravity. A small increase in the design static pitch angle would allow either: 1) a decrease in the required buoyancy and ballast weight, or 2) a decrease in the required restoring moment arm, which implies a decrease in the structural distance between the center of gravity and center of buoyancy, or some combination of the two. Either option 1) or 2) implies a lighter structure. Simple dimensional analysis can also be used to investigate cost implications, if costs of installation, operation and maintenance are not considered. Sclavounos [3] estimates that the cost of the floater, ballast and mooring system increase linearly with the size of wind turbine.

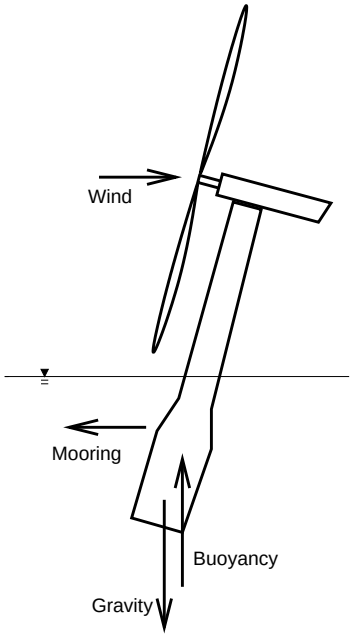

Fig. 1. Predominant forces on a floating wind turbine with the spar floater

The compliant design allows large-amplitude rotation of the floater, which can be described by Euler angles to accurately obtain the instantaneous position of the floating system. Accurate calculation of the instantaneous position is necessary for load estimation and design optimization. The external loads on the compliant floating wind turbine caused by wind, waves and mooring lines all depend on the motion of the floater and topside facilities. Accurate structural motions are also needed for accurate calculation of internal loads, such as gyroscopic effects of the topside facilities on the tower and blades bending moment on the hub, which are critical design criteria for the wind turbine system. Additionally, precise prediction of the instantaneous position is important to the design optimization of the compliant floating wind turbine: both the estimation of power output and the optimization of control algorithms are very sensitive to large-amplitude motion of the structure.

Compliant floating wind turbines offer unique technical challenges especially when subject to large-amplitude rotation. A new computational methodology has been developed and implemented into a time-domain simulation tool that retains the full nonlinearity of the equations of motion (EOMs). External loads from wind, wave and mooring lines are all nonlinear and there is coupling between the structural motion and external loads. Further, large-amplitude rotation described by Euler angles introduces nonlinear inertial loads, which cannot be adequately addressed using linear EOMs. Finally, the real-time control mechanisms used on floating wind turbines, such as nacelle yaw control and blade pitch control, significantly influence the structural dynamics of the entire system. Not all of these effects can be captured using only frequency-domain simulation. Time-domain simulation results are

also necessary for statistical analysis, such as extreme environmental loads, extreme internal loads and fatigue analysis. Although dynamic simulation of floating wind turbines has been investigated by others using fully coupled time-domain simulators, the EOMs associated with Euler angles have not been applied in previous studies.

The main development underlying the new time-domain simulation method is the establishment of the EOMs of the compliant system. Formulation of these EOMs generally falls within the broad field of multibody dynamics. Multibody system analysis is commonly used to simulate complex systems as a system of rigid bodies connected by mechanical joints. Here, the compliant floating wind turbine system is considered as a multibody system including several rigid components, such as tower, nacelle and rotor, which are mechanically connected by the yaw bearing, hub, etc. There are various classical analytical methods for the establishment of the EOMs of multibody system: Newton-Euler (NE, 1750) method is based on the conservation of momentum for each body, while Euler-Lagrange (EL, 1788) and Kane's methods (1985) formulate the EOMs from the perspective of energy of the system. These methods are then combined with various numerical implementations to achieve time-domain simulations of multibody systems. From the perspective of numerical efficiency, the optimum formulation of multibody dynamics varies depending on the specifics of the mechanical system and simulation objectives.

In this dissertation, the theorem of conservation of momentum is applied to establish the EOMs of the compliant floating wind turbine with large-amplitude motion. Initially, Euler's equations of motion resulting from the conservation of angular momentum are applied to each body of a 2-body wind turbine model respectively

to investigate large-amplitude motion of compliant design and its influence on gyroscopic moments. As the work progresses, new EOMs are established and gradually refined to enable an increased number of bodies. These improvements result from direct application of the conservation of both linear and angular moments to the entire multibody system.

The new formulation is primarily motivated by the opportunity to develop a more efficient time-domain simulation tool specially applicable to the floating wind turbines with prescribed DOFs of relative motion between contiguous bodies. In the new method, a base body is prescribed within the multibody system, and the EOMs of the entire system are projected into the coordinate system relevant to this body. Only six basic EOMs of the system are required to capture 6 unknown DOFs of the base body when mechanical DOFs between contiguous bodies are prescribed. The 6×6 mass matrix is actually composed of two decoupled 3×3 mass matrices for translation and rotation, respectively. Each element within the matrix includes the inertial effects of all bodies. This condensation decreases the coupling between elements in the mass matrix, and so minimizes the computational demand. This new formulation method is later expanded to multibody systems with more complicated joints and connection types. More complicated joints require coupled solution of six basic EOMs as well as control and constraint EOMs.

The method presented here is an effective alternative to the existing classical methods in multibody dynamics. Any one of these methods may be optional for a specific application, depending on analysis needs and body configuration. The new formulation is particularly well-suited for cases in which the computational de-

mands required to solve the basic EOMs are much larger than those of the control and constraint EOMs. Cases for which the control EOMs represent pure mechanical control and relative motions between contiguous bodies are known or easy to obtain, such as that in robotics, are optional candidates for application of the new method. Cases for which the control EOMs are complicated by introducing springs and dampers, the new method may be less optional. Similarly, cases for which the constraint EOMs would require solution of a large number of simultaneous equations also may not be optional candidates. For example, representing a mooring line as a series of rigid elements along the the line may require more computation efforts than solution of the basic EOMs. An additional strength of the new method is its direct applicability to large-amplitude rotation. However, the method is equally applicable to small-amplitude rotation of the base body; the angular velocities of conventional roll, pitch and yaw motions can be used in the calculation of the angular momentum, instead of Euler angular velocities. Finally, the new method derives much of its efficiency by avoiding the need to calculate internal loads. Much of that efficiency is lost in cases for which internal loads are needed at many joints. Cases including complicated connection types or highly interconnected topology, such as tree-type systems combined with loops, may also not be ideal candidates for the new method if internal loads is needed. Calculation of internal loads within any overdetermined system cannot be accomplished using presented inverse dynamics, which preclude application of the new formulation to these cases.

B. Literature Review

1. Offshore Wind Turbines

The research and utilization of offshore wind power for generation of electricity has seen a rapid growth worldwide in the past two decades. In 2003, Henderson [4] reviewed the development of offshore wind energy in Europe, where many offshore wind farms composed of bottom-fixed wind turbines in shallow water have been established. Especially, a project called "Concerted Action on Offshore Wind Energy in Europe" (CAOWEE) was presented to gather, evaluate, synthesize and distribute knowledge on all aspects of offshore wind energy, including offshore technology, electrical integration, economics, environmental impacts and political aspects. Meanwhile, European success has made offshore wind energy more attractive for the United States. In 2006, Musial [2] indicated that offshore wind generated electricity in the United States has the potential to become a major contributor to the domestic energy supply. Preliminary studies performed by the National Renewable Energy Laboratory (NREL) estimate the offshore resource to be greater than 1000 GW for the United States. Future projections show this potential could result in over 100 billion of revenue to the offshore industry over the next 30 years in the construction and operation of offshore wind turbines and the infrastructure needed to support them. In 2007, Manwell [5] reviewed the external design conditions applicable to offshore wind energy systems in the United States from the perspective of statistics, including wind and wave loads as well as extreme events, such as hurricane. Quite recently, Brenton [6] investigated the potential for offshore wind energy in Europe

and North America, including existing plans for the development of offshore wind farms, current technical developments and promising new solutions offered by this technology.

The application of floating wind turbines is an attractive concept in the nascent offshore wind energy field. The deep-water wind resource worldwide has been shown to be extremely abundant, with the U.S. potential ranked second only to China [7]. Compared to current wind farms composed mainly of bottom-fixed turbines, many potential benefits motivate research on the technology of floating wind turbines, such as steadier and stronger wind fields, flexibility in site location, less visual and noise pollution, etc. Musial [7] indicated that the application of floating wind turbines should be based on the combination of current experience in offshore oil and gas industries and the expertise of shallow-water wind turbines. Although the technology of oil and gas platforms are relatively mature, new technology is still needed to make wind energy economically competitive over a broad range of deep water sites. Preliminary investigation [1] in 2004 shows that the costs for deployment of deep-water wind turbines could reach down to 0.051 $/kWh in the near future, pending sufficient research and development into technology improvements, and volume production. Floating wind turbine platforms may be the most economical means for deploying wind turbines in the coastal waters beyond view from densely populated urban load centers [7].

The balance between feasibility and cost has been investigated by many researchers, covering various floater types. Butterfield [8] divided the physical elements used to achieve first-order static stability of floating platforms into three general cat-

egories: ballast, mooring lines and buoyancy. In practice, all floating concepts are actually hybrid designs that gain static stability from all three aspects, although relying on one primary source of stability. In general, spar type platforms have better heave performance than semisubmersibles due to their deep draft reducing vertical wave-exciting forces, but they have increased pitch and roll motions because the water plane area contribution to stability is reduced. Tension-leg platforms (TLPs) have very good heave and angular characteristics, but the complexity and cost of the mooring and installation cannot be ignored. Sclavounos [3] reviewed research efforts for floating wind turbines at MIT in recent years and highlighted two families of floater concepts: TLP and spar buoy. Henderson [9] also investigated various typical platform options (the TLP, spar and semisubmersible) as well as the feasibility of multiple-turbine floaters, such as a space-frame vessel. Roddier [10] reviewed several recent floating wind turbine projects, including the Statoil Hywind spar,the Blue H semi/TLP hybrid prototype, the SWAY spar/TLP hybrid, and the Force Technology WindSea semisubmersible. He also proposed a semisubmersible type design, WindFloat, which uses three columns to provide stability to support the turbine.

Hywind project [11] is of special note because it is the first floating wind turbine worldwide. It has 2.3 MW wind turbine, and is located in 200 m water depth off the south-west coast of Norway. One design goal in this first floating structure was to minimize tower motion, which makes the technological leap from bottom-founded towers to floating structures relatively smaller.

Two extremely significant aspects of the structural design of wind turbine systems are the calculation and combination of external loads, and the estimation of

internal load effects. API [12] presented the rules and regulations for fixed offshore platforms design. IEC [13, 14] released relevant standards for the design of offshore wind turbines based on the estimation of load effects under various load cases, but indicated that the design requirements specified in these standards are not necessarily sufficient to ensure the engineering integrity of floating offshore wind turbines. DNV regulations [15] apply partial safety factor method based on direct simulation of combined load effects of simultaneous load processes for design of support structures and foundations for offshore wind turbines. Obviously, internal and external loads are critical for these designs. Krogh [16] applied the simulation of wind turbine loads for the purpose of comparing different design codes. Freudenreich [17] used the previous IEC standard [13] to determine the extreme blade bending moments by applying stochastic and statistical analysis. Henderson [18] calculated external loads of floating wind turbines in the time domain and then transferred the results into the frequency domain for use in fatigue analysis based on internal loads.

Accurate calculations of internal and external loads require a coupled dynamic analysis model of the offshore wind turbine system. The study of Bush [19] shows that accurate structural dynamics is required to produce accurate long-term tower loads by comparing various foundation models. Henderson [20] indicates that the determination of the design wave loads will involve selection of appropriate structural dynamics models. Camp [21] also concludes that the integrated modelling of wind and wave action is essential for accurate design load calculations as well as fatigue and extreme loading analysis. Additionally, coupled dynamic analysis is required for optimum design of offshore wind turbines: the Markovian power curves of wind tur-

bines including consideration of relative wind speed was investigated by Anahua [22]; the effect of control mechanisms on mitigating tower dynamic loads was discussed by Write [23].

Simulations in either the frequency or time domain are used to analyze the coupled dynamic models of floating wind turbines. Frequency-domain simulation is chosen by some researchers due to its simplicity and its consistency with conventional dynamic analysis of oil and gas offshore platforms. Lee [24] analyzes the RAOs of the responses of a spar buoy floater with tension legs and with taut mooring lines, respectively. Wayman [25] evaluates dynamic performance of several floaters using coupled structural, hydrodynamic and aerodynamic analysis models in the frequency domain. Sclavounos [3] presented a fully coupled linear dynamic analysis of floating wind turbines in the frequency domain that integrated the linear external loads and structural EOMs. However, as Henderson [18] indicates, frequency domain models could be used only for concept exploration of floating wind turbines, and not for design and optimization, because they usually exclude many nonlinear effects. Thus, many time-domain simulators have been developed for the design of floating wind turbines. To mention a few examples, Withee [26] integrates commercially structural dynamic software ADAMS with various external loads calculation subroutines to establish a fully coupled dynamic simulator and applies it to estimate the feasibility of a tension leg spar buoy floater. Skaare [27] et al. develop a simulation tool for dynamic response of conceptual designs of Hywind by integrating existing computer programs, HAWC2 from Riso National Laboratory and SIMO/RIFLEX from MARINTEK. Jonkman [28, 29] from NREL combines FAST, AeroDyn [30] and

WAMIT [31] to generate a coupled structural-aero-hydro dynamic simulator. Matha [32] applies the FAST simulator to evaluate the modeling, loads and dynamics of the TLP concept.

2. Multibody Dynamics and Application

A multibody system is defined as an assembly of two or more rigid bodies imperfectly joined together, and having the possibility of relative movement between them [33]. Dynamic simulation of multibody systems has broad applicability in engineering, including application in robotics, industrial machinery, aerospace, and automobile systems. Prior works have been done to simulate dynamic systems subject to large-amplitude displacements. For example, Stoneking [34] presents the derivation of the exact nonlinear dynamic EOMs for a multibody spacecraft connected by spherical gimbal joints. Kurfess [35] systematically models the dynamics of robots using conventional methods of formulation of equations of motion. Featherstone [36] investigates the dynamics formulation of a floating-base rigid-body system, in which the base body is free to move in the space.

Generally, multibody systems can be classified into open-chain or closed-chain systems [33]. Open-chain systems are made up of bodies without closed branches, while closed-chain systems include loops of rigid bodies. The simplest open-chain system is a series of rigid bodies connected by joints and does not include any branch, such as serial manipulator in robotics. The key components in multibody system are the joints, which permit certain DOFs of relative motion between contiguous bodies and constrain others. For example, a revolute joint only allows one relative rotation

between bodies, while a prismatic joint only allows one relative translation.

Kinematics and dynamics are two main aspects in multibody system analysis [33]. Kinematics problems investigate the position or motion of the multibody system without need to consider dynamic factors, such as the mass matrix, inertial tensor etc., while dynamics problems require the solution to the EOMs governed by the balance of external and inertial loads. Dynamic analysis may further include forward and inverse dynamic problems. The forward dynamic problem (dynamic simulation) focuses on the resultant motion of the system subject to the applied loads and given initial conditions, and implies the solution of a system of differential EOMs, which are repeatedly numerically integrated at sequential time steps starting from the initial conditions. Efficient methods to formulate the EOMs of the system are needed to decrease the burden of these numerical calculations. The inverse dynamic problem calculates the internal loads applied at the joints between rigid bodies, given the velocities and accelerations, as well as known external loads resulting from the forward dynamics solution.

Many books summarize conventional analytical techniques for multibody dynamics and the generalized formulations of EOMs (e.g. [35, 37, 38]). The NE equations are usually established by separating the free-body diagrams of each rigid body in the system. A key advantage of the NE method is that the effect of a newly added body on the EOMs can be conveniently represented by a recursive formulation procedure. A key disadvantage is that the internal forcing at each joint must be considered to solve the EOMs of the system at every time step, which may not be efficient if only a few internal forces are needed. The EL method avoids the calculation

of any internal forcing that does not perform work. However, the method requires derivation of partial derivatives of energy function with respect to generalized DOFs, which can be laborious. Kane's method combines the advantages of previous two methods and enables the user to formulate the EOMs through application of virtual power theory, which avoids the calculation of internal forcing and the differentiation of energy function, but still requires laborious rederivation of the EOMs when a new body with additional DOFs is added to the system.

Essentially all methods for obtaining the EOMs are equivalent, but the application scope may differ, depending on specific applications [39]. Mason [40] applies various NE algorithms to systematically solve dynamics of robots. Garrad [41–44] uses EL method to investigate the dynamics of bottom-fixed wind turbine models with different DOFs. Kane's method is employed in the well-recognized wind turbine dynamics aero-elastic simulator, the NREL FAST [45, 46]. Hansena [47] combines the Kane's method with modal shape function to reduce the DOFs of the EOMs.

C. Main Contributions

A new rigid-body dynamic methodology is developed to complement various classical analytical methods for the establishment of the EOMs and is applied to compliant floating wind turbine designs with truncated spar floaters, which are presented to reduce the cost of the entire system. Euler angles are introduced to describe the large-amplitude rotation of this compliant design. A time-domain simulation tool is developed based on the new method to investigate the dynamics of such multibody wind turbine system. As shown in Fig. 2, the new dynamic simulator is formed by

interfacing the structural dynamics method with the calculation of various nonlinear external loads, including aerodynamics, hydrodynamics and mooring dynamics. The new method for derivation of the EOMs of the multibody system forms the computational core of the simulation tool.

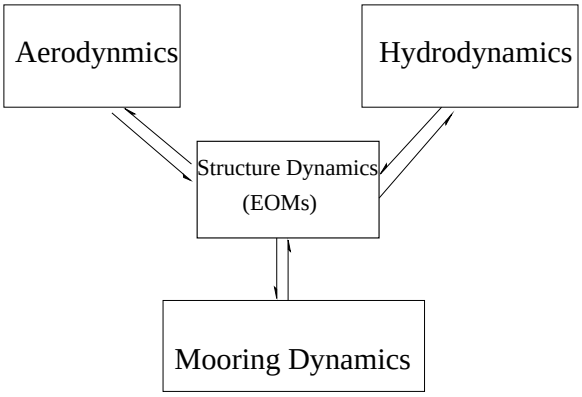

Fig. 2. Fully coupled simulation of compliant floating wind turbines

The multibody dynamics problem is solved by applying the conservation of momentum to the compliant floating wind turbine system. The first development and application is for a 2-body wind turbine model. Two sets of Euler's equations of motion resulting from the conservation of angular momentum are applied to each body of the 2-body model composed of the tower and topside facilities. Two sets of 3-1-3 sequenced Euler angles are chosen to dramatically simplify the equations. Further, the two sets of equations are mathematically connected and solved using constraint relations between two sets of Euler angles. These relations result from

the connections between bodies, which decrease the DOFs of the system and enable simulation of the 2-body wind turbine model using only one set of dynamic equations in Euler space.

The conservation of both linear and angular momentum is then applied to the entire multibody system to directly formulate the EOMs of the compliant floating wind turbine. The rotation of the tower is described by 1-2-3 sequenced Euler angles, which is consistent with conventional pitch-roll-yaw of floating structures in the case of small-amplitude motion. Only six equations are needed to describe the global motion of the floating wind turbine system, because the system is made of known relative mechanical motions among contiguous bodies. The six equations consist of three translational equations for the position of the center of mass (CM) of the system and another three rotational equations for the large-amplitude rotation of the tower. Arbitrary locations of the CM of each body, combined with relative motion among bodies generally change the CM of a multibody system. Modern turbines are generally configured with the CM of the nacelle downwind of the centerline of the tower. Subsequently, the CM of the floating wind turbine is not constrained to any-body within the system as the nacelle yaws relative to the tower, but depends on the varying position of the CM of each body within the system. The theoretical developments presented here enable application of the method including this realistic aspect of the configuration. A key point of the formulation of the rotational equations is to calculate the angular momentum of each rigid body and sum them in a unified translating-rotating coordinate system to obtain the total angular momentum of the entire system, the derivative of which is equal to the sum of externally applied mo-

ments. Meanwhile, formulating the EOMs about the CM of the system decouples the inertial loads in the translational and rotational equations, which facilitates efficient numerical integration of the EOMs.

A floating wind turbine system is typically subject to wind forcing, wave forcing and mooring forcing, each of which is coupled with the dynamic response of the structure. In the case of large-amplitude motion, this coupling is highly nonlinear and should not be ignored. The introduction of Euler angles enables more accurate calculation of the position of the floater. This position is combined with the relative motions among bodies to obtain the accurate position of each body at each time step. A system of transformation matrices that cascade between the various coordinate systems are applied to compute this motion, which enables preservation of the full nonlinear coupling between external excitation and large-amplitude motion of the wind turbine system.

The new multibody dynamic formulation methodology has application beyond derivation of the EOMs of floating wind turbines. The method is generalized for application to any N-body system. The theoretical derivations for both forward and inverse dynamics are systematized using standardized notations. The generalized formulation procedure is named the momentum cloud method (MCM) and it can be applied to establish the EOMs using standard vector and matrix calculations. The resulting EOMs are not coupled between translation and rotation beyond the first-order and so facilitate numerical integration. A key advantage over conventional energy methods is that the MCM avoids tedious rederivation of the EOMs if new rigid bodies are added to the system. In the MCM, the momentum associated with any

newly added body is already included in the derivation and can be added directly to the existing expressions of momentum for the overall system. The systematic formulation of the MCM is based on a serial mechanical N-body system connected by revolute joints with prescribed relative rotation, and is then expanded for application to multibody systems with more complicated forms and more complicated joints, such as open-chain systems with branches, closed-chain systems and cylindrical joints with both unknown translation and rotation between contiguous bodies.

D. Organization of Dissertation

The organization of this dissertation is based on continuous improvement and refinement of conservation of momentum with application to compliant floating wind turbine models.

In Chapter 2, a 2-body model composed of the tower and topsides consisting of the nacelle and rotor is applied for the dynamics investigation of the compliant floating wind turbine. Only rotational motion is to be investigated, so the CM of the system can be prescribed to be fixed in the space. The conservation of angular momentum is applied to two bodies respectively to establish the EOMs. The global motions of the tower and topsides described by Euler angles are shown. The effects of the gyroscopic moments are quantified in this work and found to introduce significant internal loads.

In Chapter 3, both the translation and rotation of a 2-body model are considered. The CM of the system is moving in the space but constrained to the tower axis. The conservation of both linear and angular momentum is applied to the system directly

to establish six translational and rotational EOMs. The resulting simulation tool is then applied to a family of compliant floating wind turbines with different truncated spar lengths to investigate the feasibility of compliant designs through statistical analysis of the simulation results.

In Chapter 4, the method is extended to develop the EOMs of a 3-body model composed of the tower, nacelle and rotor. Unlike Chapter 3, the CM of the system is no longer constrained to the tower axis, but moves with any nacelle yaw. The improvement to the formulation enables consideration of the effect of the unconstrained CM of the system in the derivation of both translational and rotational EOMs. Simulation results are compared to that from Chapter 3 to quantify this effect.

In Chapter 5, the conservation of momentum is applied to a serial N-body system to generalize the derivation of the EOMs and form the momentum cloud method (MCM). The expansion of the MCM for general N-body systems with more complicated forms and connection joints is also investigated. An open-chain system with branches is presented as a 6-body wind turbine model composed of tower, nacelle, hub and three blades. This 6-body model is used to demonstrate the simulation of global motion and computation of internal loads.

Finally, conclusions and recommendations for future work are presented in Chapter 6.

CHAPTER II

EULER DYNAMIC EQUATIONS FOR 2-BODY MODEL

A. Overview

The compliant design with truncated spar cylinder is proposed to support the floating offshore wind turbine in deep water, where environmental forcing could subject the rotor to meaningful angular displacements in both precession and nutation, offering design challenges beyond conventional bottom-founded structures. The tower and rotor-nacelle-assembly (RNA) are considered as two rotational bodies in the space, for which two sets of 3-1-3 sequenced Euler angles are defined to describe the large-amplitude rotations and investigate the gyroscopic moments generated by the RNA on the tower. Two systems of Euler dynamic equations of motion are established and solved through the relation of two sets of Euler angles. Transformations between the various coordinate systems are derived to enable solution for motion of the tower with gyroscopic, environmental and restoring effects applied as external moments. An example is presented to simulate time-histories of a floating tower with RNA. The results are also verified by FAST, the well-recognized dynamic simulation software of wind turbines.

B. Introduction and Background

Environmental, aesthetic and political pressures continue to push for siting offshore wind turbines beyond sight of land, where waters tend to be deeper, and use of floating structures is likely to be considered. Design of a floating wind turbine

support structure capable of maintaining a near-vertical tower requires buoyancy far exceeding the weight of the equipment being supported. Savings could potentially be realized by reducing hull size, which would allow more compliance with the wind thrust force in the pitch direction.

Design of these increasingly compliant floating towers will make computation of structural dynamics both more challenging and more important. A specific design challenge associated with large-amplitude rotation is gyroscopic moments relevant to inertial loading of topside facilities. Gyroscopic moments for conventional, stiff, bottom-founded structures are primarily generated by mechanical precession of the spin axis into the shifting winds, and so are limited by the maximum nacelle yaw rate [9]. However, no such limit exists for gyroscopic moments of floating structures because they result from both shifting winds and irregular motions of the tower. H. Matsukuma et al. [48] analyzed the dynamic response of a 2 MW downwind turbine mounted on a spar-type floating platform for pitch amplitudes up to around 10 degrees and concluded that the platform motions are considerably influenced by gyro moments associated with rotor spin. Shim and Kim [49] also investigated rotor-floater-tether coupled dynamic analysis of offshore floating wind turbines using an integrated time-domain simulator and indicated that the dynamic coupling between the rotating blades and the floater is significant and should be considered in the design.

Reasonable quantification of gyroscopic effects of the compliant floating wind turbine requires the establishment of the EOMs applicable to the large-amplitude rotation. Conventional methods applicable to small-amplitude motion have been

widely applied to dynamic analysis of offshore structures [50], including offshore wind turbines [19]. A fully coupled version of the NREL FAST aero-elastic simulator [45] is available to compute the dynamics of floating wind turbines. FAST is highly developed and well recognized, and includes the option of computing hydrodynamic radiation-diffraction analysis package WAMIT [31]. Unfortunately, large-amplitude motions exceed present capabilities of FAST: WAMIT relies on small-amplitude assumptions. FAST solves the equations of motion using transformation matrices made orthogonal by the Frobenius norm, which limits its applicability to platform rotation of less than 20 deg [46]. Prior to this work, no purpose-specific time-domain simulation tool existed for investigating the dynamics of compliant design.

Euler's equations of motion, which are associated with Euler angles, are commonly used to analyze the large-amplitude rotation of rigid bodies. The EOMs are actually derived from the conservation of angular momentum of one rigid body. Euler stated that "any two independent orthonormal coordinate frames can be related by a sequence of rotations (not more than three) about coordinate axes, where no two successive rotations may be about the same axis" [51]. The angles of these three rotations are commonly defined as Euler angles, and the axes of rotation are designated as axes 1, 2, and 3 or x, y, and z. The order in which the axes of rotation are taken is referred to as the Euler rotation sequence. There are a total of twelve of these sequences [52]: 3-1-3 (z, x, z), 1-2-3 (x, y, z) and so on including all combinations with no two succeeding rotations about the same axis. Euler's equations of motion using various sequenced Euler angles have been applied by researchers to investigate large-angle rotations. To mention a few, Guran [53] and Amer [54] used

the 3-1-3 sequenced Euler angles to analyze the rotational motion of a gyrostat about a fixed point. The 3-1-2 sequenced Euler angles are applied by Longuski [55] to investigate the attitude motion of a self-excited rigid body. The application of Euler angles is usually limited by singularity, or "gimbal lock". Any set of Euler angles where the second rotation makes the first and third rotational axes align causes a singularity [56]. In this case, the first and third rotations degenerate into a single rotation and the angular derivatives, and the EOMs become infinite. This singularity is commonly avoided by transferring the Euler angles to quaternion [57].

In this Chapter, Euler's equations of motion are applied to investigate rotational dynamics of compliant floating wind turbines because the gyroscopic effects highly depend on the rotational inertia of the RNA. A 2-body wind turbine model including the tower and RNA is used, each of which is considered as a rotational body in space and described by a set of Euler's equations of motion. The RNA represents the combination of spinning and non-spinning parts within the topside facilities, in which the latter is treated as a point-mass on the spin axis. The 3-1-3 sequenced Euler angles are applied to describe the rotations of the tower and RNA, respectively. This sequence is chosen because it enables separation of rotation of the rigid body from rotation of the body-fixed coordinate system, which simplifies derivations of the EOMs dramatically. A vertical tower position may introduce the singularity of the 3-1-3 sequenced Euler angles, but the zero pitch angle of the compliant wind turbine appears in a ratio between very small numbers in the procedure of numerical integration such that the singularity problems are avoided [53]. The number of degrees of freedom is further reduced by using the geometry of the physical connection

between two bodies. The new development enables simulation of the 2-body tower-RNA system using only one set of dynamic equations in Euler space, which enhances numerical efficiency. The effectiveness of the new theory is shown in an example by solving the EOMs of the compliant floating wind turbine subject to both irregular environmental forcing and gyro moments.

C. Theory

The 3-1-3 sequenced Euler angles are introduced in Section 1. In Section 2, the constraint equations, i.e. the relation between two sets of Euler angles of the tower and RNA, are derived to decrease the number of unknown rotational degrees of freedom. The Euler dynamic equations of the tower are established in Section 3. The external moments applied on the tower are calculated in the following sections: the external moments generated by the rotation of RNA are derived using the Euler dynamic equations of the RNA in Section 4; the effects of wind and wave forcing on the tower rotation are investigated in Sections 5 and 6.

1. Coordinate Systems and Euler Angles

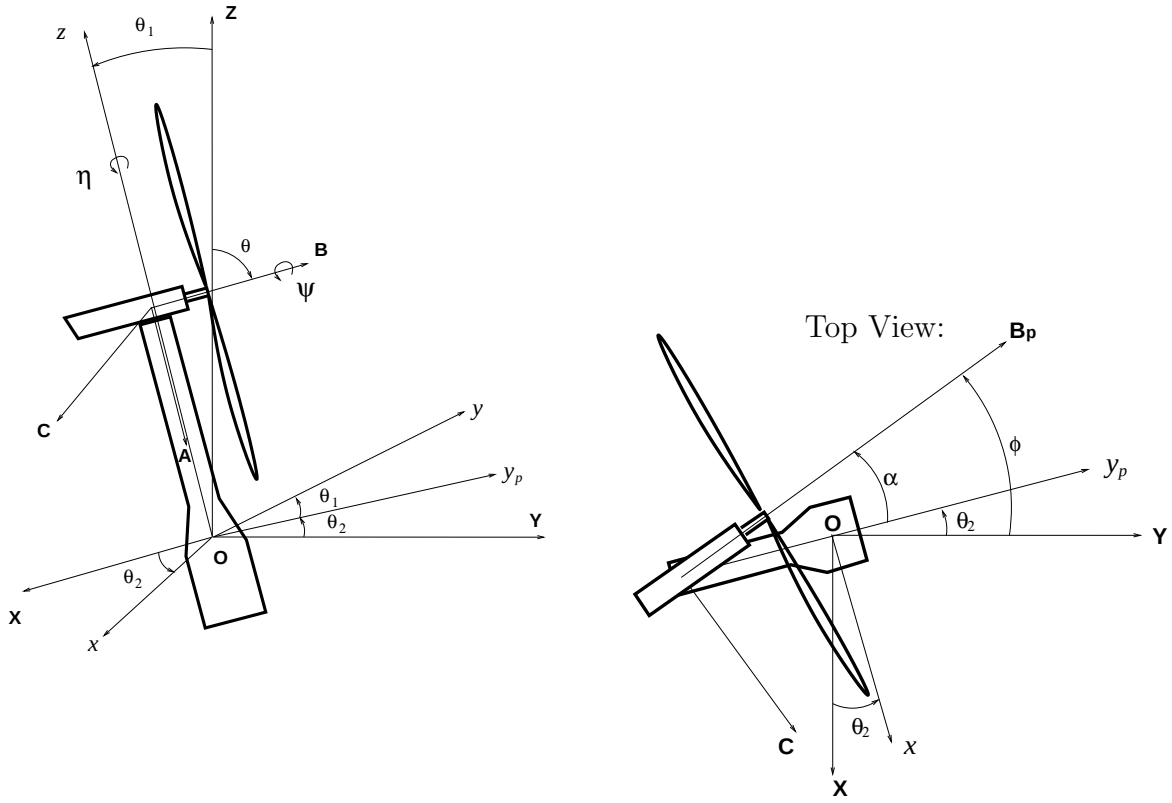

Fig. 3. Coordinate systems and two sets of Euler angles

In this methodology, the system is considered as two rigid bodies: the tower is the complete structural assembly, including the buoyant hull, that supports the RNA; the RNA is the complete assembly that can mechanically yaw relative to the tower. Coordinate systems (X, Y, Z) and (x, y, z) both originate at the center of mass of the moving tower (Fig. 3). The (X, Y, Z) system is non-rotating, while (x, y, z) is a rotating coordinate system. The z-axis defines the center of the moving tower; the

directions of x and y are not fixed to the tower. Angular differences between these coordinate systems define a set of independent Euler angles, $(\theta_1, \theta_2, \eta)$. The angle θ_1 lies between the vertical Z, and the tower centerline, z, with positive rotations right-handed about the positive x-axis. Angle θ_2 lies between Y and y_p with positive right-handed along positive Z-axis, and corresponds to the tower revolving around Z; y_p is the projection of y on the horizontal X-Y plane, and opposite to the projection of z onto X-Y. The first two Euler angles, θ_1 and θ_2, fully define the location of the (x, y, z) coordinate system. A third Euler angle, η, describes rotation about the moving z-axis, with positive rotations being right-handed about positive z.

For large angular displacements in space, the order in which the angles of rotation are applied is important; there are twelve possible Euler angles sequences. Here, 3-1-3 sequenced angles are used to describe the position of the rotating tower and of the spinning RNA (e.g., [58]). For the tower, a 3-1-3 sequence indicates the Euler sequence is z-x-z, or in detail: 1) first, rotate the upright tower about the z-axis (then coincident with Z) through an angle θ_2 measured in the horizontal plane XOY; 2) next, rotate the resultant tower about the resulting x-axis through an angle θ_1 measured in the vertical plane ZOy_p, and 3) finally, rotate the tower about the new z-axis (not coincident with Z for non-zero θ_1) through the third Euler angle, η. The Euler equations of motion of the tower and RNA are established, respectively, and solved in terms of θ_2, θ_1, and η. This sequence enables considerable simplification in the derivation of Euler's kinematic equations, which in turn results in dramatically simpler equations of motion, and improved numerical efficiency.

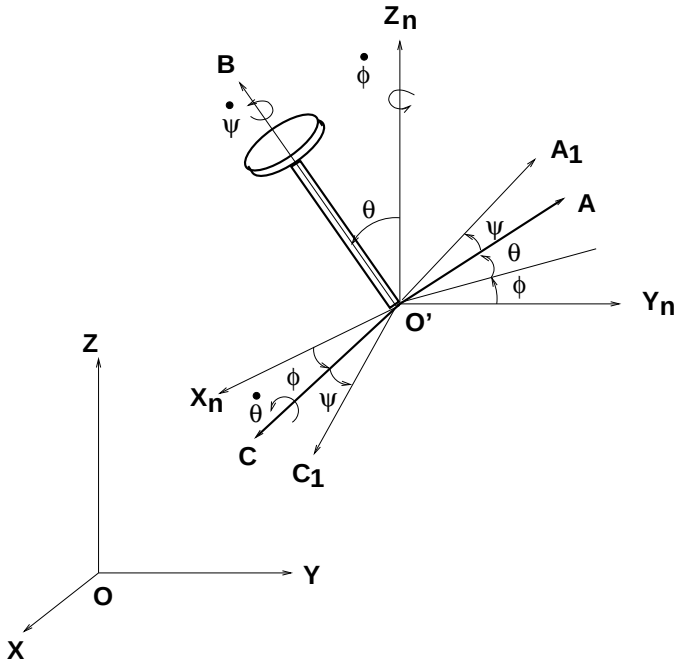

Fig. 4. Rotation of (A, B, C) in terms of ϕ, θ and ψ

Additional axes and angles are necessary to describe the position of the RNA. The translating coordinate system (X_n, Y_n, Z_n) and the rotating system (A, B, C) are used to form a second set of Euler angles, which is associated with the rotating machinery at the top of the tower. The origin of the disk-based (A, B, C) coordinate system is fixed at the center of mass of the RNA, here assumed to be at the intersection of the spin axis (B) and the yaw axis (z). The A-axis is generally not exactly parallel to z (Eqn. (2.5)). The angle α is the difference between the y_p-axis and B_p, the projection of the spin axis onto the horizontal: $\alpha = \phi - \theta_2$, with positive in the same direction as ϕ. A nutation angle of $\theta = -\pi/2$ indicates a horizontal B-axis.

The (A, B, C) coordinate system of the RNA is also positioned using the 3-1-3 sequence Euler angles ϕ-θ-ψ, as shown in Fig. 4. The (X_n, Y_n, Z_n) coordinate system has translation relative to the earth and shares the same origin with (A, B, C). The angular transformation from (X_n, Y_n, Z_n) to (A, B, C) is the order of: 1) rotate the disk coordinate system (A, B, C) about the z_n-axis by an angle ϕ in the X_n-Y_n plane; 2) next rotate about the resulting C-axis by an angle θ, and then finally 3) rotate about the resulting B-axis by an angle ψ. In this 3-1-3 sequence, precession and spin are applied along the same moving axis, since the initial B-axis coincides with the z_n-axis. The angular velocity components of precession, nutation and spin are Euler angular velocities $\dot{\phi}$, $\dot{\theta}$ and $\dot{\psi}$, each with positive as a right-hand rotation about its rotation axis. Similar to the (x, y, z) system, the (A, B, C) system is not body-fixed. (A_1, B, C_1) is an exact body-fixed coordinate system on the RNA and has spinning motion relative to (A, B, C). This definition of the (A, B, C) coordinate system greatly simplifies derivation of Euler kinematics equations of the RNA and computation of gyroscopic moments.

2. Connecting the Two Sets of Euler Angles

Motion of the tower is described by Euler rotations θ_2, θ_1, and η, while RNA rotations are described by ϕ, θ, and ψ. These two sets of angles describe bodies that are physically connected in space, so the number of degrees of freedom can be reduced by expressing the motion of the RNA in terms of θ_1, θ_2, and η using vector projection. Fig. 5 shows both (A, B, C) and (x, y, z) coordinate systems, which are relocated to the origin, O, for convenience.

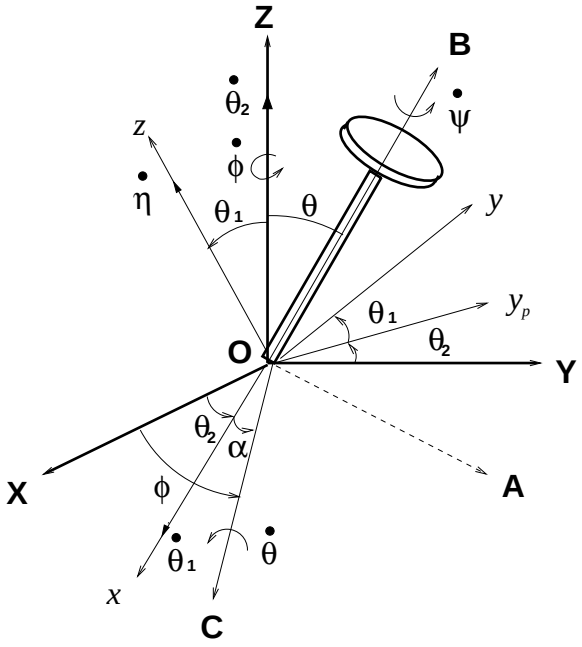

Fig. 5. Projection of Euler angular velocities

The nutation angular velocity and acceleration are obtained by projecting $\dot{\theta}_1$, $\dot{\theta}_2$ and $\dot{\eta}$ onto the C-axis and differentiating:

$$\begin{aligned}
\dot{\theta} &= \dot{\theta}_1 \cos\angle COx + \dot{\theta}_2 \cos\angle COZ + (\dot{\eta} + \omega_{yaw}) \cos\angle COz && (2.1)\\
&= \dot{\theta}_1 \cos\alpha - (\dot{\eta} + \omega_{yaw}) \sin\theta_1 \sin\alpha && (2.2)\\
\ddot{\theta} &= \ddot{\theta}_1 \cos\alpha - \dot{\theta}_1 \dot{\alpha} \sin\alpha - (\ddot{\eta} + \dot{\omega}_{yaw}) \sin\theta_1 \sin\alpha \\
&\quad -(\dot{\eta} + \omega_{yaw})(\dot{\theta}_1 \cos\theta_1 \sin\alpha + \dot{\alpha} \sin\theta_1 \cos\alpha) && (2.3)
\end{aligned}$$

where ω_{yaw} is yaw rate, angular motion of the RNA relative to the tower along z-axis, and $\dot{\omega}_{yaw}$ is its time derivative. The nutation angle, θ, has been obtained

geometrically in separate work by the authors [59], which is more accurate than numerical integration of $\dot{\theta}$ in Eqn. (2.2), and decreases the required number of degrees of freedom:

$$\theta = -\frac{\pi}{2} + \lambda \tag{2.4}$$

$$= -\frac{\pi}{2} + \arctan(\tan\theta_1 \cos(\phi - \theta_2)) \tag{2.5}$$

where λ is the angle between the B- and B_p-axes.

The derivation of the precession angular velocity, $\dot{\phi}$, is based on the definition of yaw rate:

$$\omega_{yaw} = \omega_{z,RNA} - \omega_{z,tower} \tag{2.6}$$

where $\omega_{z,RNA}$ is the absolute angular velocity of the RNA about the z-axis and can be obtained by projection of Euler angular velocities $\dot{\phi}$, $\dot{\theta}$ and $\dot{\psi}$ onto the z-axis; $\omega_{z,tower}$ is the absolute angular velocity of the tower about the z-axis and can be obtained by the projection of Euler angular velocities $\dot{\theta}_1$, $\dot{\theta}_2$ and $\dot{\eta}$ onto the z-axis:

$$\omega_{z,tower} = \dot{\theta}_1 \cos\angle xOz + \dot{\theta}_2 \cos\angle ZOz + \dot{\eta} \tag{2.7}$$

$$\omega_{z,RNA} = \dot{\phi} \cos\angle ZOz + \dot{\theta} \cos\angle COz + \dot{\psi} \cos\angle BOz \tag{2.8}$$

Considering Fig. 5, $\cos\angle ZOz = \cos\theta_1$ and $\cos\angle xOz = \cos\angle BOz = \cos(\pi/2)$. The vertical plane zOy_p is perpendicular to the horizontal plane COy_p, so $\cos\angle COz$ can be shown to be:

$$\cos\angle COz = \cos\angle zOy_p \cos\angle COy_p$$

$$= \cos(\frac{\pi}{2} + \theta_1) \cos(\frac{\pi}{2} - \alpha)$$

$$= \quad -\sin\theta_1 \sin\alpha \tag{2.9}$$

Substituting Eqns. (2.7) and (2.8) into Eqn. (2.6) yields the precession velocity:

$$\dot{\phi} \quad = \quad (\cos^2\theta_1 + \sin^2\theta_1 \cos^2\alpha)\sec\theta_1(\omega_{yaw} + \dot{\eta}) + \tag{2.10}$$

$$\dot{\theta}_2 + \dot{\theta}_1 \tan\theta_1 \sin\alpha\cos\alpha \tag{2.11}$$

Eqn. (2.11) can alternatively be derived by differentiating Eqn. (2.5) and equating the resulting $\dot{\theta}$ with Eqn. (2.2). Setting $\omega_{yaw} = 0$ in Eqn. (2.11) shows that precession velocity, $\dot{\phi}$, is a function of overall tower motions; further assuming relatively small θ_1, Eqn. (2.11) can be reduced to $\dot{\phi} \approx \dot{\theta}_2 + \dot{\eta}\cos\theta_1$, which helps to clarify the relationship between θ_2 and η. Differentiating Eqn. (2.11) yields the precession acceleration:

$$\begin{aligned} \ddot{\phi} \quad = \quad & (\omega_{yaw} + \dot{\eta})(\dot{D}\sec\theta_1 + D\sec\theta_1\tan\theta_1\dot{\theta}_1) + \\ & (\dot{\omega}_{yaw} + \ddot{\eta})D\sec\theta_1 + \ddot{\theta}_2 + \dot{\theta}_1\dot{\alpha}\cos 2\alpha\tan\theta_1 + \\ & \frac{1}{2}(\ddot{\theta}_1\tan\theta_1\sin 2\alpha + \dot{\theta}_1^2\sec^2\theta_1\sin 2\alpha) \end{aligned} \tag{2.12}$$

in which $D = \cos^2\theta_1 + \sin^2\theta_1\cos^2\alpha$ and $\dot{D} = -\dot{\theta}_1\sin^2\alpha\sin 2\theta_1 - \dot{\alpha}\sin^2\theta_1\sin 2\alpha$

3. Equations of Motion of the Tower

Beginning at first principles, the sum of the moments resulting from externally applied forces about the center of mass of a body in a translating-rotating system, (x, y, z), equals the change of the momentum within the coordinate system plus that

associated with the movement of the coordinate system (e.g. [58]):

$$\sum \vec{M} = \dot{\vec{H}}_O = (\dot{\vec{H}}_O)_{xyz} + \vec{\Omega} \times \vec{H}_O \tag{2.13}$$

Vector $\vec{\Omega}$ describes the angular velocity of (x, y, z) with respect to (X, Y, Z). The x-, y- and z-axes are chosen as the principal axes of the body, so the products of inertia in $\vec{H_O}$ disappear, and locating the coordinate system at the center of mass decouples the rotational and translational degrees of freedom. Following e.g. Hibbeler [58], Eqn. (2.13) expands to three scalar equations:

$$\sum M_x = I_x\dot{\omega}_x - I_y\omega_y\Omega_z + I_z\omega_z\Omega_y \tag{2.14}$$

$$\sum M_y = I_y\dot{\omega}_y - I_z\omega_z\Omega_x + I_x\omega_x\Omega_z \tag{2.15}$$

$$\sum M_z = I_z\dot{\omega}_z - I_x\omega_x\Omega_y + I_y\omega_y\Omega_x \tag{2.16}$$

where $\vec{\omega}$ describes the rotation of the tower in space. The more conventional form of Eqns (2.14)–(2.16) has $\vec{\omega} = \vec{\Omega}$, such that the coordinate system is fixed to the body. The difference between motion of the (x, y, z) coordinate system, $\vec{\Omega}$, and that of the body, $\vec{\omega}$, is the Euler angle η: $\vec{\omega} = \vec{\Omega} + \dot{\eta}\vec{k}$. The associated Euler kinematic equations are:

$$\vec{\omega} = \omega_x\vec{i} + \omega_y\vec{j} + \omega_z\vec{k} \tag{2.17}$$

$$= \dot{\theta}_1\vec{i} + (\dot{\theta}_2 \sin\theta_1)\vec{j} + (\dot{\theta}_2 \cos\theta_1 + \dot{\eta})\vec{k} \tag{2.18}$$

Continuing to follow e.g. [58], component-wise expressions for $\vec{\omega}$, $\dot{\vec{\omega}}$ and $\vec{\Omega}$ are substituted into a component-wise expansion of Eqn. (2.13). Principal moments of inertia of the tower, I_x, I_y and I_z, are taken about the x-, y- and z-axes. The tower is

symmetrical such that $I_x = I_y = I$. The resulting Euler dynamic equations are:

$$\sum M_x = I(\ddot{\theta}_1 - \dot{\theta}_2^2 \sin\theta_1 \cos\theta_1) + I_z \dot{\theta}_2 \sin\theta_1 (\dot{\theta}_2 \cos\theta_1 + \dot{\eta}) \quad (2.19)$$

$$\sum M_y = I(\ddot{\theta}_2 \sin\theta_1 + 2\dot{\theta}_1 \dot{\theta}_2 \cos\theta_1) - I_z \dot{\theta}_1 (\dot{\theta}_2 \cos\theta_1 + \dot{\eta}) \quad (2.20)$$

$$\sum M_z = I_z(\ddot{\eta} + \ddot{\theta}_2 \cos\theta_1 - \dot{\theta}_1 \dot{\theta}_2 \sin\theta_1) \quad (2.21)$$

The moments on the left hand side of Eqns. (2.19)–(2.21) are externally applied about the center of mass of the tower.

$$\sum M_x = M_{RNAx} + M_{FTx} + M_{wavex} - M_{mooringx} - M_{hydrostatic} \quad (2.22)$$

$$\sum M_y = M_{RNAy} + M_{FTy} + M_{wavey} - M_{mooringy} \quad (2.23)$$

$$\sum M_z = M_{RNAz} + M_{FTz} + M_{wavez} - M_{mooringz} \quad (2.24)$$

where $\vec{M}_{RNA}$ represents the total moment applied by the RNA on the top of the tower; $\vec{M}_{FT}$ is the total moment resulting from the RNA forces, those forces applied to the top of the tower by the RNA: $\vec{M}_{FT} = \vec{r} \times \vec{F}_T$. Vector $\vec{r}$ is from the mass center of the tower to the RNA; the RNA forces, $\vec{F}_T = \vec{F}_b - m_R \vec{a}_R$, where m_R is the mass of the RNA, and $\vec{a}_R$ is the linear acceleration of the RNA caused by rotation of the tower. This acceleration, $\vec{a}_R$, is the derivative of the velocity at the top of the tower; $\vec{F}_b$ is the thrust force on the blade area. $\vec{M}_{wave}$ is the hydrodynamic forcing. The mooring restoring moment, $\vec{M}_{mooring}$, can be calculated as a sum of cross-products, with each mooring line represented by a cross-product between the radius vector from the center of mass of the tower to the fairlead and the force vector. Hydrostatic restoring moment, $\vec{M}_{hydrostatic}$, is generally zero in the y- and z-directions.

4. Moments Caused by Rotational Motion of the RNA

Rotational motions of the RNA are treated the same way as the rotational equations of motion of the tower in Section 3: as a single rigid body using the 3-1-3 Euler sequence, with the body rotating separately from the rotating coordinate system. The rotational motion of the RNA differs from that of the coordinate system (A, B, C) only by the spinning rate along the B-axis:

$$\vec{\omega} = \omega_A \vec{i}_{ABC} + \omega_B \vec{j}_{ABC} + \omega_C \vec{k}_{ABC} \tag{2.25}$$

$$= (\dot{\phi}\sin\theta)\vec{i}_{ABC} + (\dot{\phi}\cos\theta + \dot{\psi})\vec{j}_{ABC} + \dot{\theta}\vec{k}_{ABC} \tag{2.26}$$

where $\vec{i}_{ABC}$, $\vec{j}_{ABC}$ and $\vec{k}_{ABC}$ are unit vectors along the A-, B- and C-axes.

Following a derivation similar to Section 3, the resulting Euler dynamic equations can be applied to compute the RNA moments applied by the tower on the RNA:

$$M_A = I_A(\ddot{\phi}\sin\theta + 2\dot{\theta}\dot{\phi}\cos\theta) - I_B\dot{\theta}(\dot{\psi} + \dot{\phi}\cos\theta) \tag{2.27}$$

$$M_B = I_B(\ddot{\phi}\cos\theta - \dot{\theta}\dot{\phi}\sin\theta) - M_{windB} \tag{2.28}$$

$$M_C = I_C(\ddot{\theta} - \dot{\phi}^2\sin\theta\cos\theta) + I_B\dot{\phi}\sin\theta(\dot{\psi} + \dot{\phi}\cos\theta) \tag{2.29}$$

The moments of inertia are those of a rigid body representing the RNA; the parts of the RNA not rotating at $\dot{\psi}$ are assumed to be a point-mass on the B-axis. Moments I_A and I_C are about the A- and C-axes, and I_B can realistically be taken as the moment of inertia of the blades about B. Contributions to M_A and M_C due to

asymmetrical external forcing are neglected, such as asymmetric wind loading. The non-zero M_{windB} is the rotor torque used to generate electricity. The spin velocity is assumed constant, $\ddot{\psi} = 0$, in accordance with typical wind turbine operations.

Any terms in Eqns. (2.27)-(2.29) including spin, $\dot{\psi}$, which disappear when the rotor is parked, are the gyroscopic moments:

$$M_{gyroA} = -I_B \dot{\theta} \dot{\psi} \tag{2.30}$$

$$M_{gyroB} = 0 \tag{2.31}$$

$$M_{gyroC} = I_B \dot{\phi} \sin\theta \dot{\psi} \tag{2.32}$$

The gyro moments of bottom-fixed wind turbine can be estimated as those corresponding to a static, upright tower. Considering only the gyroscopic moments and substituting $\theta = -\frac{\pi}{2}$ and $\dot{\theta} = 0$ into Eqns. (2.27)-(2.29) yields precisely the results given by e.g. Henderson [9] when θ_1 motion is neglected. On large bottom-founded turbines, gyroscopic moments are limited by active yaw control such that the precession angular velocity remains small. On compliant floating turbines, however, significant gyroscopic moments can be developed about the A- and C-axes. The A-axis lies nearly along the axis of the tower, with M_{gyroA} moments resulting from nutation of the RNA, as noted by Jonkman [46].

The RNA moments must be transformed from the (A, B, C) coordinate system into the (x, y, z) system for application in the equations of motion of the tower:

$$\begin{bmatrix} M_{RNAx} \\ M_{RNAy} \\ M_{RNAz} \end{bmatrix} = T \begin{bmatrix} -M_C \\ -M_A \\ -M_B \end{bmatrix} \tag{2.33}$$

The transformation matrix T is obtained by first rotating (x, y, z) back to the (X, Y, Z) system and then rotating from (X, Y, Z) to the final (C, A, B) rotational system (Fig. 5). The (X, Y, Z) and (x, y, z) systems translate together with the tower, so translation does not influence the transformation matrix. The transformation matrix from the (C, A, B) to (x, y, z) results from the product of a sequence of element rotation matrixes:

$$T = T_{x_1}(-\theta_1)T_{x_3}(-\theta_2)T_{x_3}(\phi)T_{x_1}(\theta) \tag{2.34}$$

where $T_{x_1}(-\theta_1)T_{x_3}(-\theta_2)$ indicates rotation from (x, y, z) back to initial (X, Y, Z), in which both the ordering of rotation and the directions of the rotational angles must be reversed. Element rotation matrices T_{x_1} and T_{x_3} are defined in Section 6.

5. Transformation of Moments Resulting from RNA Forces

The environmental and inertial forcing in Eqns. (2.22)-(2.24) can be computed considering both the wind and waves acting on the structure, and the relative motion of the tower through the air and water. The linear velocity of the RNA through the air is computed from the angular velocities:

$$\vec{v}_{\theta_1} = \dot{\vec{\theta}}_1 \times \vec{r}_s = \dot{\theta}_1 l \tag{2.35}$$

$$\vec{v}_{\theta_2} = \dot{\vec{\theta}}_2 \times \vec{r}_s = \dot{\theta}_2 l \sin\theta_1 \tag{2.36}$$

where $\vec{v}_{\theta_1}$ and $\vec{v}_{\theta_2}$ are linear-velocity components at a location along the z-axis (here, the RNA); angular velocity $\vec{v}_{\theta_1}$ is along the negative direction of the y-axis and $\vec{v}_{\theta_2}$ is along the positive direction of the x-axis. In Fig. 6, vector $\vec{r}_s$ is the radius from

the center of mass of the system, O_s, to that location, and l is the magnitude of $\vec{r}_s$. Direction vectors (i_I, j_I, k_I) and (i, j, k) are along (X, Y, Z) and (x, y, z) respectively. Linear acceleration of the RNA is needed to calculate the RNA forces, F_T. This acceleration, $\vec{a}_R$, is computed by taking the derivative of the vector sum of $\vec{v}_{\theta_1}$ and $\vec{v}_{\theta_2}$ and then transforming into the (x, y, z) coordinate system.

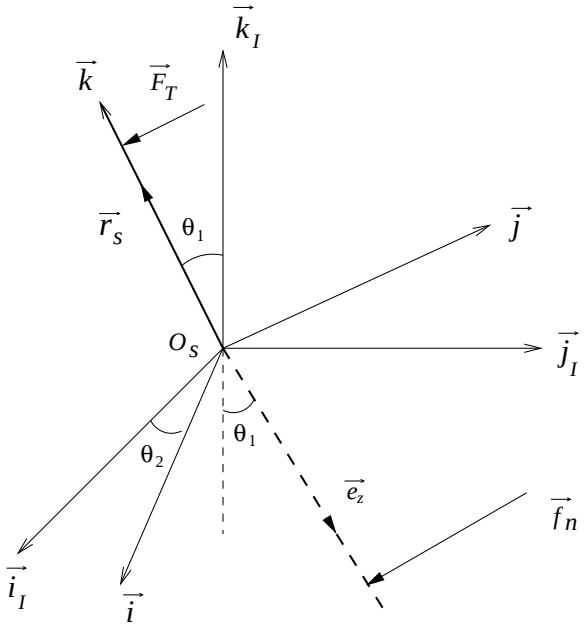

Fig. 6. Coordinate system for derivation of inertial and environmental forcing

An expression for the velocity of the wind relative to the RNA, V_{rb}, along the negative B-axis, can be developed from Eqns. (2.35) and (2.36) and direction cosines, which

can be derived geometrically or through use of transformation matrices:

$$\vec{V_{rb}} = \vec{v}_w + \vec{v}_{\theta_1}(-\cos\angle BOy) + \vec{v}_{\theta_2}\cos\angle BOx \tag{2.37}$$

$$V_{rb} = -v_w + \dot{\theta}_1 l(\cos\theta_1 \sin\theta\cos\alpha - \cos\theta\sin\theta_1) + \dot{\theta}_2 l\sin\theta_1\sin\theta\sin\alpha \tag{2.38}$$

where $v_w = |\vec{v}_w|$ and is along the negative B-axis. The resulting relative velocity can be used to compute the wind forces acting on the RNA in the (X, Y, Z) coordinate system, after which they must be transformed into the (x, y, z) system for application in the equations of motion. Moments resulting from RNA forces include both wind and inertial loads.

$$\vec{M}_{FT} = \vec{r} \times \vec{F}_T = \vec{r} \times (\vec{F}_b - m_R\vec{a}_R) = \vec{M}_{wind} - \vec{r} \times m_R\vec{a}_R \tag{2.39}$$

where $\vec{r}$ originates at the center of mass of the tower. The wind moments result from decomposing the thrust force, $\vec{F}_b$, onto the (x, y, z) system, and calculating moments as a cross product expressed as a cofactor expansion:

$$\vec{M}_{wind} = \vec{r} \times \vec{F}_b = \begin{bmatrix} \vec{i} & \vec{j} & \vec{k} \\ 0 & 0 & l \\ -F_b\cos\angle BOx & -F_b\cos\angle BOy & -F_b\cos\angle BOz \end{bmatrix} \tag{2.40}$$

6. Transformations for Wave Forcing

Similar to the calculation of wind forcing, wave forces are computed in the (X, Y, Z) coordinate system, decomposed into the (x, y, z) system, and used to compute the moments. Waves are assumed to progress down the negative Y-axis. The wave kinematic velocity relative to the moving tower is $\vec{V_{rt}}$. Determination of $\vec{V_{rt}}$ requires

expression of velocity vectors for both the tower and the wave kinematics normal to the axis of the tower in the (X, Y, Z) coordinate system. In general, 3-D rotation matrices of a regular right-handed (x_1, x_2, x_3) coordinate system can be expressed in a general form e.g. [52]. Here, the location of the centerline of the tower is fully defined by (θ_1, θ_2), with the final rotation about the z-axis being irrelevant, so the transformation matrix from (x, y, z) to (X, Y, Z) can be computed from the general form as in [59].

$$\begin{aligned} T_{x_3}(\theta_2)T_{x_1}(\theta_1) &= \begin{bmatrix} \cos\angle XOx & \cos\angle XOy & \cos\angle XOz \\ \cos\angle YOx & \cos\angle YOy & \cos\angle YOz \\ \cos\angle ZOx & \cos\angle ZOy & \cos\angle ZOz \end{bmatrix} \\ T_Z(\theta_2)T_x(\theta_1) &= \begin{bmatrix} \cos\theta_2 & -\cos\theta_1\sin\theta_2 & \sin\theta_1\sin\theta_2 \\ \sin\theta_2 & \cos\theta_1\cos\theta_2 & -\cos\theta_2\sin\theta_1 \\ 0 & \sin\theta_1 & \cos\theta_1 \end{bmatrix} \end{aligned} \tag{2.41}$$

The instantaneous unit vector along the negative z-axis can be deduced directly from Fig. 6:

$$\vec{e_z} = -\cos\angle XOz\vec{i_I} - \cos\angle YOz\vec{j_I} - \cos\angle ZOz\vec{k_I} \tag{2.42}$$

The direction cosines appear as matrix elements in Equation 2.41. The unit vector $\vec{e_z}$ can then be used to find the relative normal velocity:

$$\vec{V_{rt}} = \vec{e_z} \times (\vec{V_r} \times \vec{e_z}) \tag{2.43}$$

where $\vec{V_r}$ is the relative velocity of the wave to the submerged tower: $\vec{V_r} = \vec{V} - \vec{V_t}$, in which $\vec{V} = (0, u_Y, u_Z)$ is the wave kinematic velocity in the YOZ plane.

The transformation matrix, Eqn. (2.41), is again used to compute the structural velocity, $\vec{V_t}$. Linear velocities $\vec{v}_{\theta_1}$ and $\vec{v}_{\theta_2}$, are found as in Eqns. (2.35) and (2.36), with $\vec{r}_s$ originating at the center of mass of the system and now along the negative direction of the z-axis of the submerged tower, such that linear velocity $\vec{v}_{\theta_1}$ is along the positive direction of the y-axis and $\vec{v}_{\theta_2}$ is along the negative direction of the x-axis. Decomposing into the (X, Y, Z) system:

$$\begin{aligned} \vec{V_t} &= \vec{v}_{\theta_1,XYZ} + \vec{v}_{\theta_2,XYZ} \qquad (2.44) \\ &= (\vec{v}_{\theta_1} \cos\angle XOy - \vec{v}_{\theta_2} \cos\angle XOx)\vec{i_I} \\ &\quad +(\vec{v}_{\theta_1} \cos\angle YOy - \vec{v}_{\theta_2} \cos\angle YOx)\vec{j_I} \\ &\quad +(\vec{v}_{\theta_1} \cos\angle ZOy - \vec{v}_{\theta_2} \cos\angle ZOx)\vec{k_I} \qquad (2.45) \end{aligned}$$

It may also be useful to know the absolute kinematic wave-particle acceleration in absence of tower motion, $\dot{\vec{V}}_n$. Similar to Eqn. (2.43), the normal component of wave acceleration, $\dot{\vec{V}}_n$, can be expressed as:

$$\dot{\vec{V}}_n = \vec{e}_z \times (\dot{\vec{V}} \times \vec{e}_z) \qquad (2.46)$$

where $\dot{\vec{V}} = (0, \dot{u_Y}, \dot{u_Z})$ is the wave acceleration vector in the YOZ plane.

Wave moments in the (x, y, z) coordinate system necessary for application in the Euler equations of motion can be computed using the relative velocities and accelerations resulting from Eqns. (2.43) and (2.46) at finite slices of the cylinder, then transforming the resulting forces into the (x, y, z) system (Eqn. (2.41)) and

numerically integrating over the submerged length of the tower:

$$\vec{f}_{n,xyz} = [T_Z(\theta_2)T_x(\theta_1)]^{-1}\,\vec{f}_n \tag{2.47}$$

$$\vec{M}_{wave} = \int_r (\vec{r} \times \vec{f}_{n,xyz})dr \tag{2.48}$$

$$\vec{M}_{wave} = M_{wavex}\vec{i} + M_{wavey}\vec{j} + M_{wavez}\vec{k} \tag{2.49}$$

where M_{wavex}, M_{wavey} and M_{wavez} are three components of the moments of wave forces in the (x, y, z) coordinate system. In practice, the integral in Eqn. (2.48) is computed as a finite sum. Use of relative velocities in computation of wave forcing introduces damping in the θ_1- and θ_2-directions.

D. Example

The motions and RNA loads of a floating wind turbine are simulated using this implementation which applies the existing ODE45 solver in MATLAB. The example is based on the OC3-Hywind model [60], with the hull modified to allow large-amplitude motion. The RNA is the same as that of OC3 Hywind: the moments of inertia of the RNA about the (A, B, C) coordinate system are $I_A = 2.35\times10^7$ kg·m^2, $I_B = 4.37\times10^7$ kg·m^2, $I_C = 2.54\times10^7$ kg·m^2; the rotor speed is 12.1 rpm.

Modifications to the standard Hywind model were made to enable large amplitude motion and to simplify the simulation. To increase rotational motions, the submerged length of the spar hull is reduced from 120 m to 84.4 m. The tower between the hull and RNA is treated as a rigid body and its moments of inertia are combined with those of the hull: 3.57×10^9 kg·m^2 and 9.28×10^7kg·m^2 in the tilt (roll or pitch) and yaw, respectively. The four taught-leg mooring lines are each assumed

to be a straight axial spring with stiffness $EA = 3.84 \times 10^8$ N and length 409 m in a 320 m water depth location.

The first example case presented is free-vibration in absence of environmental loading; the second is forced-vibration with environmental loading computed using irregular winds and waves. Irregular wind velocities are simulated by IECwind [61] and Turbsim [62]. The mean wind velocity at hub height is 18.2 m/s. The thrust force due to wind on the blade area is computed as a function of thrust coefficient, C_T, times relative velocity squared. Here, the value of C_T depends solely on relative wind velocity and is taken directly from Nielsen [63]. The thrust coefficient generally decreases with increasing relative wind speed and is assumed to change instantaneously. The steady moment along the B-axis that generates electricity, M_{windB}, is estimated by dividing the rated efficiency of turbine by $\dot{\psi}$ (Eqn. (2.28)). Wave forces are computed using the Morison equation and a first-order time-domain representation of irregular waves is simulated directly from a JONSWAP spectrum with a significant wave height of 5.0 m and peak period of 11.2 s using a uniform phase distribution.

The thrust force for wind perpendicular to the swept area of the blades is approximately (e.g., [63]):

$$F_b = \frac{1}{2} C_T \rho_a A_b V_{rb}^2 \tag{2.50}$$

where ρ_a is the density of air; A_b is the swept area of the blades; C_T is the thrust coefficient. The force is in the direction of V_{rb}, the velocity of the wind relative to the RNA along the negative B-axis.

Wave loads are estimated using the well-known Morison equation in the (X, Y, Z)

system (e.g., [64]):

$$\vec{f_n} = C_m \rho \frac{\pi}{4} D^2 \dot{\vec{V}}_n - C_a \rho \frac{\pi}{4} D^2 \dot{\vec{V}}_t + \frac{1}{2} \rho C_d D \vec{V}_{rt} |\vec{V}_{rt}| \tag{2.51}$$

where ρ is the density of sea water; D is the diameter of the tower; $C_m = 2.0$ is the inertia coefficient; $C_a = 1.0$ is the added mass coefficient, and $C_d = 0.6$ is the drag coefficient. All velocities, accelerations and forces are normal to the central axis of the tower: $\vec{f_n}$ is the wave force per unit length of the tower (Fig. 6). The kinematic acceleration normal to the axis of the tower is $\dot{\vec{V}}_n$. The second acceleration term, which includes the tower acceleration $\dot{\vec{V}}_t$, is technically a force resulting from a hydrodynamic pressure, but this term effectively has been moved to the inertial side of the equation as the basis for calculation of added mass. Added mass is included in the calculation of the center of mass and moment of inertia of the body, and so should not be included here. The result is that the relative velocity, $\vec{V_{rt}}$, is applied in the Morison drag term, but the absolute acceleration, $\vec{V_n}$, is applied in the acceleration term. Damping in the z-direction can be added directly to the R.H.S. of Eqn. (2.24).

1. Verification for Small Angles

This case directly compares results from the large-angle theory presented here with the small-angle theory applied in FAST. The observed undamped free-vibration results from initial conditions of a θ_1 offset of 0.1 rad and zero θ_2. The resulting motion corresponds to an inverted pendulum moving in a single nearly-vertical plane; the plane is not exactly vertical because Hywind has the center of mass of the RNA slightly offset from the tower centerline. Representation of precisely the same physical

system in both models is enabled by replacing the default restoring moment calculations in FAST with a user subroutine that was custom-developed to yield identical hydrostatic and mooring stiffness, and by turning off the translational motion calculations in FAST. Fig. 7 shows resulting time-histories for θ_1, θ_2 and η. The 3-1-3 Euler sequence does not admit negative values of θ_1, so the tower passing through vertical is consistent with π rad jumps in θ_2; similar results are found by e.g. [53]. Direct comparison of Euler-angle results is impossible because FAST computes roll, pitch and yaw about an earth fixed coordinate system. Simulation results can be directly compared by projecting angular velocities onto the earth-fixed coordinate system, as shown in Fig. 8 and Fig. 9. Results show excellent agreement for this small-angle case.

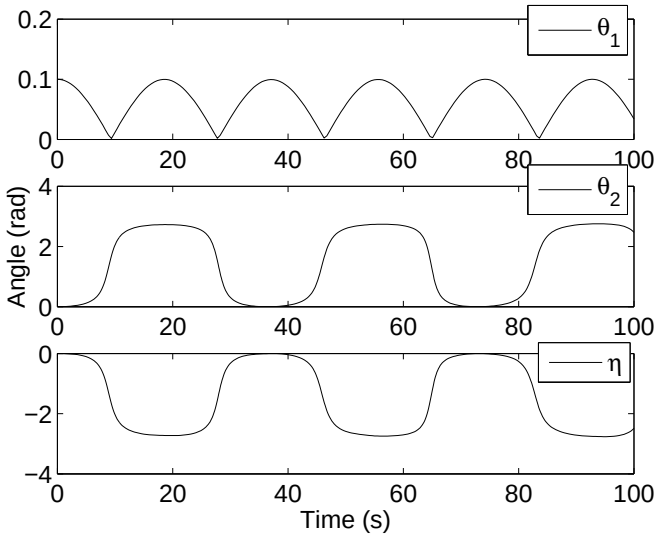

Fig. 7. Free vibration described by three Euler angles

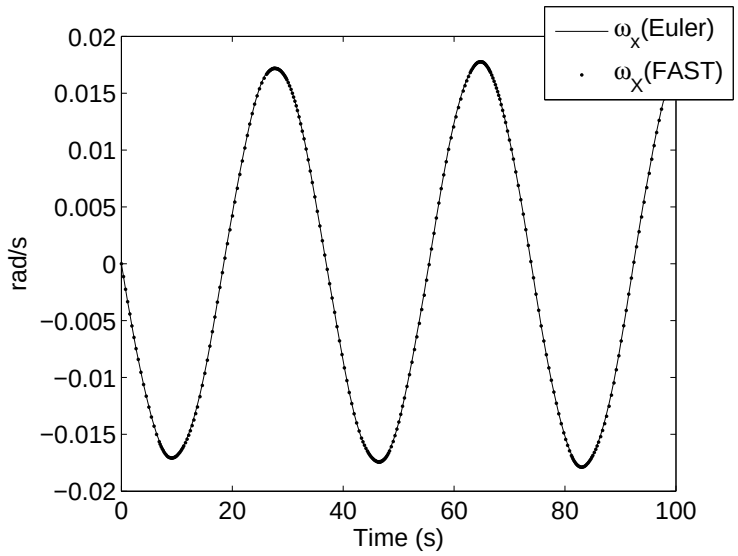

Fig. 8. Comparison of ω_X

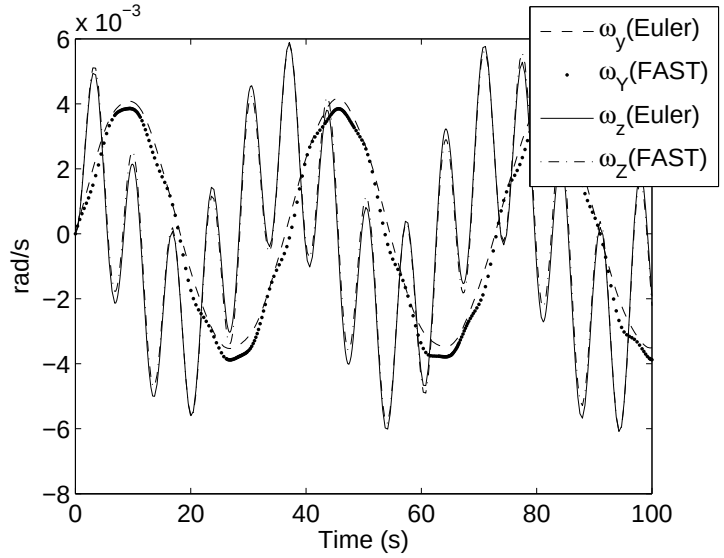

Fig. 9. Comparisons of ω_Y and ω_Z

2. Yaw of the RNA

This case is used to investigate the behavior of the dynamic system subject to irregular winds, waves and a large wind shift. The wind time-history is generated by superimposing a time-history of a sudden 45 degree shift from IECwind [61] at a time 100 seconds into an irregular operating condition from Turbsim [62]. A typical yaw control algorithm is assumed, which includes a 10-second lag before yaw activation and a 10-second acceleration or deceleration period. Fig. 10 shows precession of the RNA. In case of gust, precession angle is dominated by yaw of the RNA, which is active from 110 seconds to about 260 seconds, when the precession angle of the RNA changes from 0 rad to about 0.8 rad. Fig. 11 shows the gyro moments in the A- and C-directions. For a conventional bottom-fixed turbine, $M_{gyroA} = 0$ because the spin axis remains horizontal and M_{gyroC} is dominated by the mechanical precession velocity (Eqns. 2.27–2.29 with $\theta = \text{-}\pi/2$). For this compliant floating structure, however, the precession velocity is dominated by tower motions rather than yaw of the RNA relative to the tower. Tower-motion induced gyro moments can be substantial. Continuous operation of the yaw control mechanism to offset tower motions could minimize these moments, but such control would require a wholly new yaw control strategy.

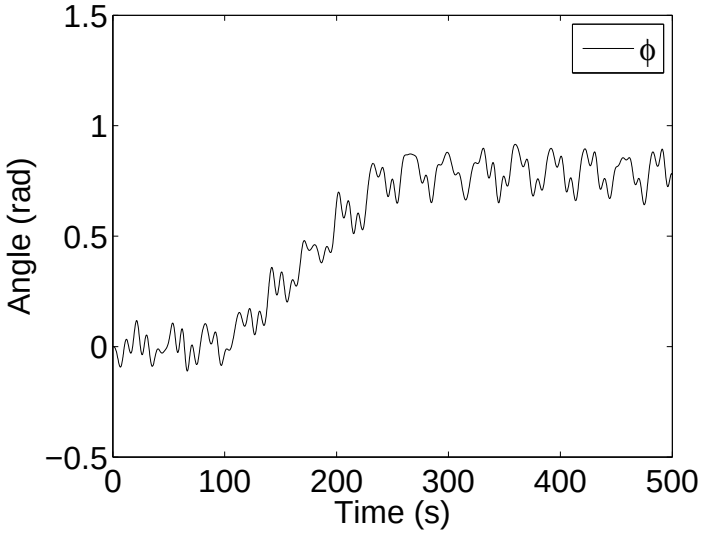

Fig. 10. Precession angle of the RNA

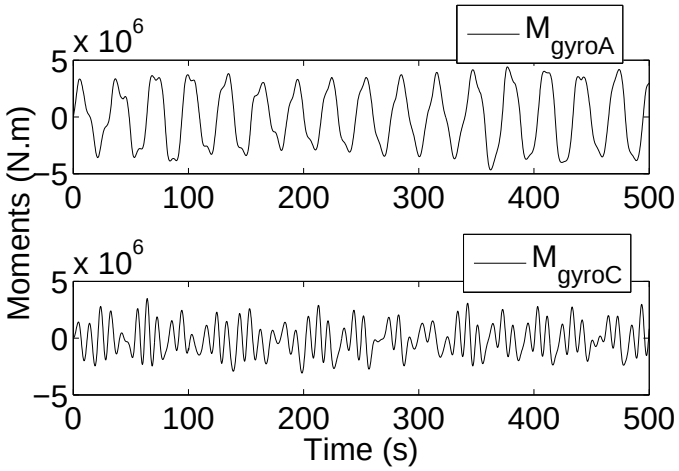

Fig. 11. Gyro moments acting on the RNA

E. Conclusions

In this Chapter, a new method has been developed to apply Euler dynamic equations in a 3-1-3 sequence to the motion of a simple 2-body compliant floating wind turbine. The tower and RNA are considered as two rotational bodies in the space, for which two sets of Euler angles are defined and used to develop two systems of Euler dynamic equations of motion. The number of degrees of freedom is reduced by using the geometric constraints of the physical joint between the tower and RNA to express one set of Euler angles as a function of the other. Full dynamic coupling is preserved through the loads on the interface between the two bodies (the RNA loads), which include gyroscopic moments. The new theory is implemented as part of a time-domain numerical simulation methodology, which retains the full nonlinear coupling between external forcing and large-angle rotations of the tower. Motions and external forcing are transformed at each time step between the non-rotating (X, Y, Z) and rotating (x, y, z) using matrices developed in terms of Euler angles for the rigid body. One example demonstrates that the new methodology yields substantially identical results to the well-known FAST software for a small-angle free-vibration case. Another example shows that there are two major components of gyroscopic loading on a compliant floating structure: one due to precession velocity of the spin axis and another due to nutation velocity, both of which can be substantial. Overall, the new theory is found to be effective for computation of the very complex dynamic behavior of these structures.

CHAPTER III

CONSERVATION OF MOMENTUM FOR 2-BODY MODEL

A. Overview

In this Chapter, a new formulation of the nonlinear equations of motion (EOMs) is derived by directly applying the theorem of conservation of angular momentum and linear momentum (Newton's second law) to the entire compliant floating wind turbine system. In the 2-body model composed of the tower and RNA, the large-amplitude rotation of the tower is described by the 1-2-3 sequence Euler angles, which are consistent with conventional pitch-roll-yaw motions of offshore structures. Other than six degrees of freedom (DOFs) of the tower, two additional DOFs of the RNA relative to the tower, nacelle yaw and rotor spin, are prescribed by mechanical control and are also included in the EOMs of the entire system. Results from the EOMs are transformed among different coordinate systems for use in the computation of hydrodynamics, aerodynamics and restoring forces, which preserves the nonlinearity between external excitation and structural dynamics. The new method is verified by critical comparison of simulation results with those of the popular wind turbine dynamics software FAST. A new time-domain simulator based on this new formulation is then applied to a family of compliant designs with different lengths of truncated spar cylinders to investigate dynamic performance and power efficiency.

B. Introduction and Background

Chapter 2 offers a simple and convenient simulation tool to investigate the dynamics of a compliant floating wind turbine rotating about a fixed point. The conservation of angular momentum (Euler dynamics equations) are applied to the tower and RNA, respectively. The model is useful to quantify a phenomena specific to wind turbines: internal loads due to gyroscopic moments. However, the 3-1-3 sequenced Euler angles may not be an intuitive measure of global motion. Instead, the 1-2-3 sequenced Euler angles are introduced in this Chapter to describe the large-angle rotations of the compliant design. Non-repeated axis sequences are more consistent with the conventional pitch, roll and yaw motions of offshore structures. For example, Mulk and Falzarano [65] introduced 3-2-1 sequenced Euler angles to analyze the nonlinear ship rolling motion. In addition to the sequence change, the work presented in this Chapter improves the formulation of the EOMs in Chapter 2 by adding the translation of the tower. The conservation of both linear and angular momentum are applied to the floating wind turbine system directly, which combines the advantages of conventional momentum and energy methods for multibody formulations.

As mentioned in Chapter 1, multibody system analysis can be used to simulate a complex system made up of rigid bodies connected by mechanical joints. The compliant floating wind turbine system is considered as a multibody system including tower, rotor, nacelle and other moving parts, which are mechanically connected by the yaw bearing, hub, etc. Thus, formulation of the EOMs of the floating wind turbine system falls within the field of multibody dynamics. Several conventional analytical methods exist. Both motions and internal loads are obtained simultane-

ously in NE method, which include global motion and all internal loads at joints (active forces from mechanical control and constraint forces). Thus, the NE method is a comprehensive way to solve multibody dynamics, but may be inefficient in the case that only global motion is concerned. EL method solves the multibody dynamics from the perspective of energy and precludes internal loads in the derivation. However, the differentiation of scalar energy functions (the Lagrangian) is laborious, especially for a large multibody system. Kane's method [66] combines the advantages of both the NE and EL methods. Internal loads are eliminated through the application of the virtual power theory to the entire system in that the work done by all these loads is offset. The differentiation required to compute velocities and accelerations can be obtained through the use of algorithms based on vector products. Unfortunately, rederivation is needed for any body newly added to the system. Additionally, each equation includes the coupling of all DOFs due to the calculation of virtual power.

The method presented in this Chapter combines the advantages of energy methods (EL, Kane) and momentum methods (NE) by applying the conservation of momentum to the floating wind turbine system directly. The calculation of unknown internal loads can be avoided in the solution for global motion. Translational and rotational EOMs are decoupled in terms of inertial forcing, which increases the efficiency of numerical integration and simplifies the rederivation for newly added bodies. The new method makes direct use of the known interactions between mechanical components in the wind turbine, which are directly controlled or explicitly defined, to derive the rotational equations of motion of the entire wind turbine system. The

conventional Euler dynamic equations are normally applied to only one rigid body; here, the known relationships between the rigid body components enable the application of the theorem of conservation of angular momentum to the entire system. Transformation matrixes are used to transfer the angular momentum of each rigid body to a unified coordinate system to obtain the total angular momentum of the entire system, the derivative of which is equal to the sum of external moments applied to the system. The resulting rotational EOMs are combined with translational equations governed by conservation of linear momentum (Newton's second law) of the entire multi-body system to develop a system of six equations. A key advantage of the new methodology is that the EOMs use fewer equations than previous conventional methods because only three rotational DOFs of the base body (tower) described by Euler angles and three translational DOFs need to be solved. Known relative DOFs along the rigid-body chain (nacelle yaw and blade spin) do not require additional EOMs. Mechanical systems with known geometric relationships between components are common, especially in rotating machinery. Thus, the methodology here is developed for floating wind turbines, but is broadly applicable to other types of interconnected dynamic mechanical systems.

The nonlinearities of various external forces and moments due to their coupling with structural motions are included in this work. Aerodynamics and hydrodynamics are calculated including the motion of body through the fluid, and the instantaneous position of the structure is accurately computed to incorporate nonlinearities of both the mooring and hydrostatics. In the numerical simulation, the motions and external excitation (including both external forces and moments) are transformed between

various coordinate systems at each time step using matrices developed in terms of Euler angles for the rigid body. Thus, the full nonlinear coupling between external excitation and large-amplitude motion of the tower is preserved.

C. Theory

The 1-2-3 sequenced Euler angles and relevant coordinate systems are introduced in Section 1. Then, the translational and rotational EOMs of the entire floating wind turbine system are derived in Section 2. The external loads on the system, i.e. the restoring and environmental forcing, are calculated in Sections 3 and 4. Section 5 investigates the internal moments between the tower and RNA within the 2-body model.

1. Coordinate Systems and Euler Angles

The methodology considers the system as two rigid bodies: the tower is the complete structural assembly that supports the rotor-nacelle assembly (RNA), including the buoyant hull; the RNA is the complete assembly that can mechanically yaw relative to the tower. The implementation of the new method requires use of several coordinate systems to derive the EOMs for the complete system. The external excitation applied in the dynamic equations is computed consecutively and projected into the corresponding coordinate systems. Fig. 12 shows both the (X, Y, Z) and the (X_M, Y_M, Z_M) systems, which are earth-fixed global coordinate systems with the origins located at the center of mass (CM) of the entire system and at the still water level, respectively, when the system is in equilibrium status with zero displacements.

The (x_t, y_t, z_t) and the (A, B, C) systems are body fixed and originate at the CM of the tower and RNA, respectively. The CM of the RNA, G_R, is assumed to be on the centerline of the tower to guarantee that the CM of the system, G_s, is fixed on the tower. The (x_s, y_s, z_s) system is parallel to (x_t, y_t, z_t) and originates at the instantaneous CM of the entire system, which is also assumed to be on the centerline of the tower. Thus (x_s, y_s, z_s) coincides with the (X, Y, Z) system for zero displacement.

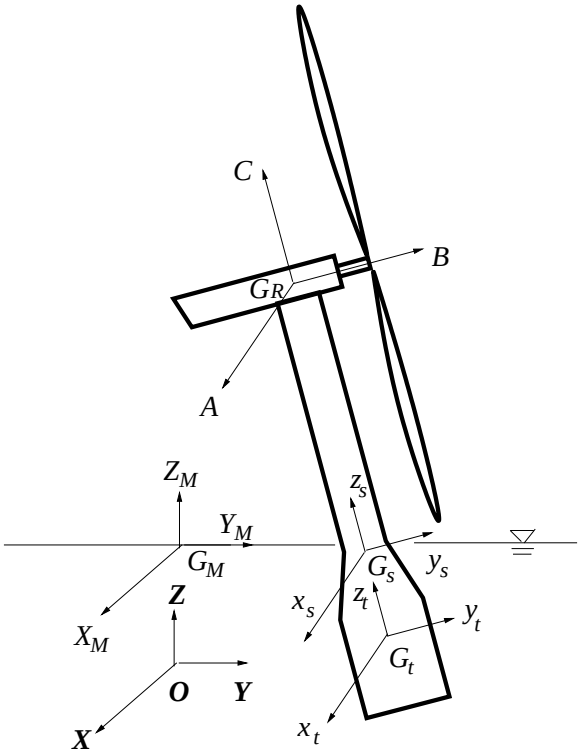

Fig. 12. Coordinate systems used in the 2-body model

The (X, Y, Z) and (x_s, y_s, z_s) coordinate systems are used for application of both the Newton's second Law and the theorem of moment of momentum on the entire system. Two body-fixed Cartesian frames, (A, B, C) and (x_t, y_t, z_t), are assumed to be on the principal axes of inertia in order to simplify the calculation of angular momentum of the two rigid bodies. The (A, B, C) system is assumed to be on the principal axes of both the rotor and the nacelle. The (X_M, Y_M, Z_M) system is defined to enable comparison of simulation results with those of FAST, in which the reference point is usually prescribed to be on the still water level.

Fig. 13 shows the Euler angles used to describe large-amplitude rotational motion. For large angular displacements in space, the order in which the angles of rotation are applied is important; there are 12 possible Euler angles sequences. Here, 1-2-3 sequenced Euler angles X_4-X_5-X_6 are used to describe the position of the rotating tower. The (x', y', z') is a translating coordinate system with respect to the (X, Y, Z) system, with the origin located at the CM of the tower. The (x_t, y_t, z_t) system can be transformed from the (x', y', z') by: first rotating the upright tower about the x'-axis by angle X_4, and then rotating about the resulting second coordinate axis through an angle X_5, and finally, rotating the tower about the z_t-axis through the third Euler angle, X_6.

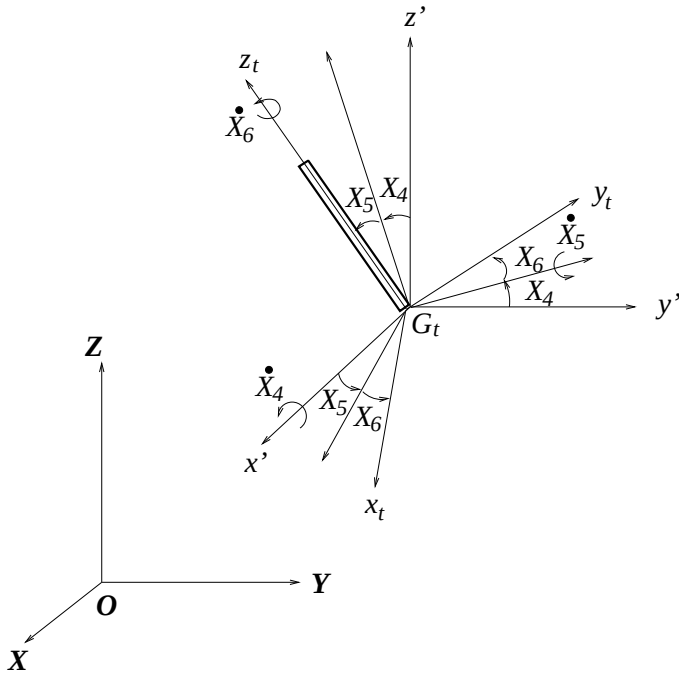

Fig. 13. 1-2-3 sequenced Euler angles in terms of X_4, X_5 and X_6

2. Equations of Motion of the System

The well-known Euler equations of motion are conventionally derived using conservation of angular momentum applied to a single rigid body. Here, the theorem of moment of momentum is directly applied to the complete wind turbine system, which consists of two rigid bodies: the tower and the RNA. Six unknown DOFs of tower (translation and rotation) and two known DOFs of RNA (nacelle yaw and rotor spinning) are considered in the model. Using the presented method, only one set of equations of motion are needed to compute the rotational dynamics of the

integrated multi-body system. The angular momentum of the entire system results from the sum of angular momentum of each rigid body, which is computed within the respective local coordinate system and then transformed into a unified system with the origin located on the CM of the wind turbine system. Similar to the application of Newton-Euler dynamics equations to one rigid body, the coupled motions are computed using rotational EOMs combined with translational equations governed by Newton's Second Law of multi-body systems.

Beginning with conservation of angular momentum, the sum of the moments resulting from externally applied forces about the CM of a system of particles in the translating-rotating system, (x_s, y_s, z_s), equals the change of amplitude of the momentum within the coordinate system plus the change of direction of the momentum with respect to global coordinate system [58]:

$$\sum \vec{M} \quad = \quad \dot{\vec{H}}^s_{G_s} = (\dot{\vec{H}}^s_{G_s})_{x_s y_s z_s} + \vec{\omega}_t \times \vec{H}^s_{G_s} \tag{3.1}$$

The LHS, $\sum \vec{M}$, represents the moments from all of external forces: $\sum \vec{M} = \vec{M}_{wind} + \vec{M}_{wave} + \vec{M}_{restoring}$, where the restoring moment $\vec{M}_{restoring}$ includes the effect of both hydrostatics and mooring lines; the environmental moments $\vec{M}_{wind}$ and $\vec{M}_{wave}$ result from wind and wave forces. In the RHS, $\vec{H}^s_{G_s}$ is the angular momentum of entire system calculated about that CM of the multi-body system and decomposed into the (x_s, y_s, z_s) system. The vector $\vec{\omega}_t$ describes the angular velocity of (x_s, y_s, z_s) with respect to the global coordinate system (X, Y, Z), which is the absolute angular velocity of the tower because the (x_s, y_s, z_s) system is parallel to the body-fixed coordinate system (x_t, y_t, z_t). In general, angular momentum of a system, $\vec{H}^s_{G_s}$, can

be decomposed into any coordinate system with the origin located at the CM of the entire multi-body system. Here, choosing the orientation of (x_s, y_s, z_s) parallel to (x_t, y_t, z_t) simplifies the calculation of angular momentum and its derivative. The angular momentum of the system, $\vec{H}^s_{G_s}$, is obtained by superimposing the momenta of the RNA and the tower and then decomposing the sum onto the (x_s, y_s, z_s) system: $\vec{H}^s_{G_s} = \vec{H}^R_{G_s} + \vec{H}^t_{G_s}$, in which the angular momenta of two rigid bodies, $\vec{H}^R_{G_s}$ and $\vec{H}^t_{G_s}$, are calculated about the CM of the system, G_s. These momenta can be further related to the angular momenta about the respective CM of these two rigid bodies by [58]:

$$\vec{H}^t_{G_s} = \vec{\rho}_{G_t/G_s} \times m_t \vec{v}_{G_t} + \vec{H}^t_{G_t} \tag{3.2}$$

$$\vec{H}^R_{G_s} = \vec{\rho}_{G_R/G_s} \times m_R \vec{v}_{G_R} + \vec{H}^R_{G_R} \tag{3.3}$$

where radius vectors, $\vec{\rho}_{G_R/G_s}$ and $\vec{\rho}_{G_t/G_s}$, are from G_s to the CM of RNA and tower, respectively, and projected onto the (x_s, y_s, z_s) system; $\vec{v}_{G_R}$ and $\vec{v}_{G_t}$ represent the corresponding linear velocities of the CM; m_R and m_t are the masses of these two rigid bodies. Those terms including radius vectors correspond to the effect of distance in the parallel axis theorem, and can be further represented by expanding $\vec{v}_{G_R}$ and $\vec{v}_{G_t}$ in terms of the linear velocity of G_s, $\vec{v}_{G_s}$:

$$\vec{\rho}_{G_t/G_s} \times m_t \vec{v}_{G_t} = \vec{\rho}_{G_t/G_s} \times m_t(\vec{v}_{G_s} + \vec{\omega}_t \times \vec{\rho}_{G_t/G_s}) \tag{3.4}$$

$$\vec{\rho}_{G_R/G_s} \times m_R \vec{v}_{G_R} = \vec{\rho}_{G_R/G_s} \times m_R(\vec{v}_{G_s} + \vec{\omega}_t \times \vec{\rho}_{G_R/G_s}) \tag{3.5}$$

Combining Eqns. (3.4) and (3.5):

$$\begin{aligned}\vec{\rho}_{G_t/G_s} \times m_t\vec{v}_{G_t} + \vec{\rho}_{G_R/G_s} \times m_R\vec{v}_{G_R} &= \vec{\rho}_{G_t/G_s} \times (m_t\vec{\omega}_t \times \vec{\rho}_{G_t/G_s}) \\ &\quad +\vec{\rho}_{G_R/G_s} \times (m_R\vec{\omega}_t \times \vec{\rho}_{G_R/G_s}) \qquad (3.6)\end{aligned}$$

Those terms including the linear velocity of the CM of the system disappear because $m_R\vec{\rho}_{G_R/G_s} + m_t\vec{\rho}_{G_t/G_s} = 0$, which decouples the angular momentum of the system and its derivative from the translational DOFs. This decoupling significantly simplifies solution of Eqn. (3.1), which increases the efficiency of numerical solution to the final coupled 6-DOFs equations of motion.

The angular momentum of the tower, $\vec{H}^t_{G_t}$ in Eqn. (3.2), is calculated in the (x_t, y_t, z_t) coordinate system, parallel to the (x_s, y_s, z_s) system, and originated from the CM of the tower. If the body-fixed coordinate system (x_t, y_t, z_t) are composed of principal axes of inertia, the angular momentum of the tower can be obtained by first calculating the product of the inertia tensors and the angular velocities, and then transforming into the (x_s, y_s, z_s) system: $\vec{H}^t_{G_t} = T_{t\to s}(I_t\vec{\omega}_t)$, where $T_{t\to s}$ is the transformation matrix from (x_t, y_t, z_t) to (x_s, y_s, z_s) and equal to the elementary matrix because these two coordinate systems are parallel; the inertia tensor of the tower, I_t, is a diagonal matrix with diagonal elements equal to I_{x_t}, I_{y_t} and I_{z_t}, i.e. the moments of inertia of the tower about its principal axes. The absolute angular velocity of the tower, $\vec{\omega}_t$, is decomposed into the body-fixed coordinate system (x_t, y_t, z_t) and can

be represented in terms of 1-2-3 sequenced Euler angles by (e.g. [67]):

$$\vec{\omega}_t = \begin{bmatrix} \dot{X}_4 cos X_5 cos X_6 + \dot{X}_5 sin X_6 \\ -\dot{X}_4 cos X_5 sin X_6 + \dot{X}_5 cos X_6 \\ \dot{X}_4 sin X_5 + \dot{X}_6 \end{bmatrix} \tag{3.7}$$

The angular momentum of the RNA in Eqn. (3.3), $\vec{H}^R_{G_R}$, is calculated by further separating the RNA into the nacelle and the rotor (including all spinning parts within the RNA). The (A, B, C) system is assumed to be the principal coordinate system of inertia of the nacelle. The angular momentum of the nacelle is transformed from its principal axes to the (x_s, y_s, z_s) by: $\vec{H}^n_{G_R} = T_{n\to s}(I_n \vec{\omega}_n)$, in which $T_{n\to s}$ is the transformation matrix from (A, B, C) to (x_s, y_s, z_s); I_n is the inertia tensor of the nacelle calculated about the (A, B, C) system. The angular velocity of the nacelle within the (A, B, C) system, $\vec{\omega}_n$, is obtained by first calculating it in the (x_t, y_t, z_t) system in terms of nacelle yaw rate and then transforming into the (A, B, C) system: $\vec{\omega}_n = T_{t\to n}\vec{\omega}_{n,t} = T_{t\to n}(\vec{\omega}_t + \vec{\omega}_{yaw})$, where the transformation matrix from (x_t, y_t, z_t) to (A, B, C), $T_{t\to n}$, can be calculated by the inverse of $T_{n\to s}$, which is just the transpose since the transformation matrix is orthogonal; $\vec{\omega}_{n,t}$ represents the absolute angular velocity of the nacelle with respect to the (x_t, y_t, z_t) system; the vector $\vec{\omega}_{yaw}$ has positive nacelle yaw rate component along z_t-direction, i.e. $\vec{\omega}_{yaw}=(0, 0, \omega_{yaw})$.

Here, the (A, B, C) axes are assumed to be on the principal axes of the rotor to simplify the calculation of angular momentum. This angular momentum depends on both the moments of inertia and the angular velocities of the rotor in the (A, B, C) system. The exact moments of inertia of the rotor are preserved in the (A, B, C) system and are not the function of time. Similar to the calculation of $\vec{\omega}_n$, the angular

momentum of the rotor can be calculated by: $\vec{H}^r_{G_R} = T_{n\to s} I_r \vec{\omega}_{r,n} = T_{n\to s} I_r (\vec{\omega}_n + \dot{\vec{\psi}})$, in which $\vec{\omega}_{r,n}$ represents the absolute angular velocity of the rotor with respect to the (A, B, C) system; I_r is the inertia tensor of the rotor calculated about the (A, B, C) system; the spinning vector $\dot{\vec{\psi}}$ has a positive component about B-direction, i.e. $\dot{\vec{\psi}}=(0, \dot{\psi}, 0)$. Combining the angular momentums of nacelle and rotor, the angular momentum of RNA is $\vec{H}^n_{G_R}+\vec{H}^r_{G_R} = T_{n\to s}(I_n+I_r)\vec{\omega}_n+T_{n\to s} I_r \dot{\vec{\psi}}$, in which the moments of inertia of the nacelle and rotor can be combined into that of RNA within the (A, B, C) system:

$$\vec{H}^R_{G_R} = T_{R\to s}(I_R \vec{\omega}_n) + T_{R\to s} I_R \dot{\vec{\psi}} \tag{3.8}$$

In Eqn. (3.8), the nacelle and the rotor are treated as a single unit, with yaw motion along the C-axis and spinning motion along the B-axis. The change of I_r to I_R directly has no influence on the calculation because in the inertia tensor, only that element associated with spinning matters in this term. Considering the (A, B, C) system as the principal coordinate system of inertia of the RNA, the transformation matrix from (A, B, C) to (x_s, y_s, z_s), $T_{R\to s}$, is equal to $T_{n\to s}$ and can be represented as [52]:

$$T_{R\to s}(\beta) = \begin{bmatrix} \cos\beta & -\sin\beta & 0 \\ \sin\beta & \cos\beta & 0 \\ 0 & 0 & 1 \end{bmatrix} \tag{3.9}$$

where the relative degree of freedom, β, describes the rotation of (A, B, C) to (x_s, y_s, z_s) and depends on the yaw angle of the nacelle, which is continually adjusted by the yaw control mechanism; I_R is the inertia tensor of the RNA in the form of diagonal

matrix with diagonal elements equal to I_A, I_B and I_C. Combining Eqns. (3.2) and (3.3), the angular momentum of the system in the (x_s, y_s, z_s) system, $\vec{H}^s_{G_s}$, can be arranged as: $\vec{H}^s_{G_s} = I_s\vec{\omega}_t + \vec{H}'$, which is a generalized validation of Leimanis's conclusion [68]: the angular momentum of a two-rigid-body system can be separated into one part due to transport of the whole system considered as a rigid body and another part due to the relative motion between the bodies. The inertia tensor associated with the transport of the system, I_s, can be expressed as:

$$I_s = \begin{bmatrix} I_{11} & I_{12} & I_{13} \\ I_{21} & I_{22} & I_{23} \\ I_{31} & I_{32} & I_{33} \end{bmatrix} \tag{3.10}$$

in which

$$\begin{aligned}
I_{11} &= (I_A cos^2\beta + I_B sin^2\beta + m_R\rho^2_{G_R/G_s}) + (I_{x_t} + m_t\rho^2_{G_t/G_s}) \\
I_{12} &= (I_A - I_B)cos\beta sin\beta \\
I_{21} &= (I_A - I_B)cos\beta sin\beta \\
I_{22} &= (I_A sin^2\beta + I_B cos^2\beta + m_R\rho^2_{G_R/G_s}) + (I_{y_t} + m_t\rho^2_{G_t/G_s}) \\
I_{33} &= I_C + I_{z_t} \\
I_{13} &= I_{23} = I_{31} = I_{32} = 0
\end{aligned}$$

where ρ_{G_t/G_s} and ρ_{G_R/G_s} are the moduli of corresponding vectors in Eqns. (3.2) and (3.3). The off-diagonal terms in the inertia tensor result from the included angle between the B and y_s-axes. The effect of the parallel axis theorem is obvious

in the diagonal terms. The angular momentum of the RNA relative to the tower can be expressed by collecting terms independent of the rotation of the tower, $\vec{\omega}_t$: $\vec{H}' = (-I_B\dot{\psi}sin\beta, I_B\dot{\psi}cos\beta, I_C\omega_{yaw})$. The angular momentum associated with the spinning blades corresponds to projections onto both x_s- and y_s-directions, while the angular momentum associated with the nacelle yaw is only along the z_s-axis.

The absolute time derivative in Eqn. (3.1) includes changes in both the direction and amplitude of the angular momentum vector. The latter can be expressed as:

$$(\dot{\vec{H}}^s_{G_s})_{x_s y_s z_s} = \dot{I}_s\vec{\omega}_t + I_s\dot{\vec{\omega}}_t + \dot{\vec{H}}' \tag{3.11}$$

where the derivative of inertia tensor, $\dot{I}_s$, is computed by taking time derivative element by element in the matrix according to the definition of matrix derivative. Thus, only the time-dependent terms in the inertia tensor are considered, which include the angle β since $\dot{\beta} = \omega_{yaw}$. This derivative of angular momentum is simplified considerably by the selection of the (x_s, y_s, z_s) system parallel to the body-fixed (x_t, y_t, z_t), because all the time-dependent terms are explicitly defined by the yaw control mechanism and the geometrical configuration.

Computation of transitional motions is relatively straightforward. The theorem of the motion of the center of mass is applied to the entire wind turbine system to solve the translational DOFs:

$$\sum \vec{F} = m_s\vec{a}_{G_s} \tag{3.12}$$

where $\vec{a}_{G_s}$ is the linear acceleration of the CM of the system, $\vec{a}_{G_s} = (\ddot{X}_1, \ddot{X}_2, \ddot{X}_3)$; m_s is the mass of the whole system; the force vector $\sum \vec{F}$ represents the external forces of

the entire system in the inertia coordinate system (X, Y, Z), including environmental forces, restoring forces and gravity: $\sum \vec{F} = \vec{F}_{wind} + \vec{F}_{wave} + \vec{F}_{restoring} + \vec{G}$. Each of these components must be decomposed to the inertia coordinate system (X, Y, Z) for application of Newton's second Law. Restoring forces, $\vec{F}_{restoring}$, include contributions from buoyancy of the hull and tension of the mooring lines.

3. Restoring Forces

The restoring forces (including both the external forces and moments) resulting from the contribution of hydrostatics and mooring lines are also computed for large-amplitude motions. Restoring forces are calculated about the CM of the system, G_s, which may experience large excursions from the original equilibrium position. The large-amplitude motions preclude use of the conventional stiffness matrix method in which restoring forces can be computed as a stiffness matrix times a displacement vector with each column of the matrix corresponding to unit motion in one DOF and zero displacements in other DOFs. This section addresses the nonlinear hydrostatic and mooring forcing due to coupled large-amplitude translational and rotational motions.

The LHS of the rotational equations of motion (Eqn. (3.1)) is the sum of the external moments in the translating-rotating system (x_s, y_s, z_s); the LHS of the translational equations (Eqn. (3.12)) is the external forces in the inertial system (X, Y, Z). The transformation matrix between these two coordinate systems is a function of 1-2-3 sequenced Euler angles X_4-X_5-X_6 since the (x_s, y_s, z_s) system is defined parallel to the body-fixed coordinate system of the tower, (x_t, y_t, z_t). The transformation

matrix from (x_s, y_s, z_s) to (X, Y, Z) can be expressed as:

$$T_{s\to I} = T_x(X_4)T_y(X_5)T_z(X_6) = \begin{bmatrix} t_{11} & t_{12} & t_{13} \\ t_{21} & t_{22} & t_{23} \\ t_{31} & t_{32} & t_{33} \end{bmatrix} \tag{3.13}$$

in which

$$\begin{aligned} t_{11} &= cosX_5cosX_6 \\ t_{12} &= -cosX_5sinX_6 \\ t_{13} &= sinX_5 \\ t_{21} &= cosX_4sinX_6 + cosX_6sinX_4sinX_5 \\ t_{22} &= cosX_4cosX_6 - sinX_4sinX_5sinX_6 \\ t_{23} &= -cosX_5sinX_4 \\ t_{31} &= sinX_4sinX_6 - cosX_4cosX_6sinX_5 \\ t_{32} &= cosX_6sinX_4 + cosX_4sinX_5sinX_6 \\ t_{33} &= cosX_4cosX_5 \end{aligned}$$

where $T_x(X_4)$, $T_y(X_5)$ and $T_z(X_6)$ are element transformation matrices [59]. The complexity of Eqn. (3.13) results from prescribing the (x_s, y_s, z_s) system parallel to the (x_t, y_t, z_t) system instead of the (X, Y, Z) system. This resulting complexity is more than offset by avoiding the tedious calculation of the time derivative of this transformation matrix.

The hydrostatic restoring forces are calculated directly from the buoyancy of the cylindrical floater. The instantaneous buoyancy of a floating cylinder in the inertial

coordinate system (X, Y, Z) is $\vec{F}_B^I = (0, 0, \rho g \pi r^2 h_1)$ [67], where ρ is the density of sea water; g is the gravitational acceleration; r is the radius of the cylinder; h_1 is instantaneous submerged length of the cylinder along the centerline. This variable length is a function of heave motion and leaning angle of the cylinder:

$$h_1 = \frac{\rho_{G_M/O} - X_3}{cos\theta_1} - \rho_{G_M/O} + h_0 \tag{3.14}$$

where $\rho_{G_M/O}$ is the distance measured from still water level to the CM of the system in its equilibrium position, i.e. the length from G_M to O in Fig. 12; θ_1 is the leaning angle of the cylinder with respect to vertical, $cos\theta_1 = cosX_4 cosX_5$; h_0 is the initial length of h_1, i.e. the draft of cylinder in equilibrium position. For small rotations, the restoring force in heave reduces to the conventional $F_B = \rho g \pi r^2 (h_0 - X_3)$.

The center of buoyancy of a partially submerged cylinder piercing the water surface at an angle is described by the radius vector in the (x_s, y_s, z_s) system, i.e. $\vec{\rho}_{B/G_s} = (x_s^B, y_s^B, z_s^B)$, in which [67]:

$$\begin{aligned} x_s^B &= -\frac{t_{31} r^2}{4 t_{33} h_1} \\ y_s^B &= -\frac{t_{32} r^2}{4 t_{33} h_1} \\ z_s^B &= \vec{h}_G + \frac{h_1}{2} + \frac{r^2 (t_{31}^2 + t_{32}^2)}{8 t_{33}^2 h_1} \end{aligned} \tag{3.15}$$

where vector $\vec{h}_G$ indicates the position of the bottom of the cylinder measured from the (x_s, y_s, z_s) system along the centerline. To obtain the hydrostatic restoring moment in the (x_s, y_s, z_s) system, the buoyancy in the inertia coordinate system is decomposed into the (x_s, y_s, z_s) system and then combined with the vector radius $\vec{\rho}_{B/G_s}$, i.e. $\vec{F}_B^s = T_{I \to s} \vec{F}_B^I$ and $\vec{M}_B^s = \vec{\rho}_{B/G_s} \times \vec{F}_B^s$, in which the transformation matrix

from (X, Y, Z) to (x_s, y_s, z_s), $T_{I\to s}$, is the inverse of Eqn. (3.13), which is just the transpose since the transformation matrix is orthonormal. This hydrostatic calculation method is applicable to any composite body having a cylinder piercing the water-plane. The center of buoyancy of fully submerged parts of a composite body are not affected by pitch angle, and can be geometrically combined with a surface-piercing cylinder.

A simplified mooring system is assumed to consist of four radial taut lines for convenience. The change in tension in each line can easily be expressed as a function or cable stretch. Each fairlead position is calculated by summing translations and Euler angle rotations. The contribution of each mooring line is calculated consecutively and then summed. The combined restoring force in the (X, Y, Z) system and the combined restoring moment calculated about G_s in the (x_s, y_s, z_s) system are needed in the application of equations of motion of the system.

Compliance along each straight line is due to elasticity of the materials only. The radius position of any one fairlead (point A) in the inertia coordinate system (X, Y, Z) is $\vec{\rho}_{A/O} = \vec{\rho}_{G_s/O} + T_{s\to I}\vec{\rho}_{A/G_s}$, where the radius vector $\vec{\rho}_{G_s/O}$ is the position of G_s measured from the (X, Y, Z) system, $\vec{\rho}_{G_s/O} = (X_1, X_2, X_3)$ and $\vec{\rho}_{A/G_s}$ is the radius position of point A in the (x_s, y_s, z_s) system. The position of the fixed end (point E) of this mooring line on the sea bottom, $\vec{\rho}_{E/O}$, is constant in the (X, Y, Z) system. Combining the radius position from point A to point E in the (X, Y, Z) system is $\vec{\rho}_{E/A} = \vec{\rho}_{E/O} - \vec{\rho}_{A/O}$. The tension along a neutrally buoyant taut line in

the (X, Y, Z) system can be obtained by the nature of elasticity material [67]:

$$\vec{F}^I_{line} = [T_0 + \frac{ES}{L}(\rho_{E/A} - L)]\frac{\vec{\rho}_{E/A}}{\rho_{E/A}} \tag{3.16}$$

where T_0 is the pretension of one mooring line; E is Young's Modulus; S is the cross sectional area of the line; L is the initial length of the line; $\rho_{E/A}$ is the norm of the vector $\vec{\rho}_{E/A}$, i.e. the instantaneous length of the line. The restoring force of the mooring system, $\vec{F}^I_{mooring}$, is obtained by summing the force from each line.

The restoring moment from each line in the (x_s, y_s, z_s) system is obtained by decomposing the restoring force into the (x_s, y_s, z_s) system first and then multiplied by the radius vector of the fairlead, i.e. $\vec{F}^s_{line} = T_{I\to s}\vec{F}^I_{line}$ and $\vec{M}^s_{line} = \vec{\rho}_{A/G_s} \times \vec{F}^s_{line}$. The result from each line can be further summed to obtain the restoring moment from mooring system, $\vec{M}^s_{mooring}$. Finally, the restoring forces can be expressed as:

$$\vec{F}_{restoring} = \vec{F}^I_B + \vec{F}^I_{mooring} \tag{3.17}$$

$$\vec{M}_{restoring} = \vec{M}^s_B + \vec{M}^s_{mooring} \tag{3.18}$$

4. Environmental Forcing

The wind force in the (X, Y, Z) system and wind moment calculated about G_s in the (x_s, y_s, z_s) system are needed in the application of equations of motion of the system. For simplicity, an approximate wind thrust force is computed for the complete swept area of the blades following the method of Nielsen [63]:

$$F_b = \frac{1}{2}C_T\rho_a A_b V^2_{rb} \tag{3.19}$$

where ρ_a is the density of air; A_b is the swept area of the blades; C_T is the thrust

coefficient; V_{rb} is the amplitude of the velocity of the wind relative to the RNA along the B-axis. The wind force is assumed to be applied on the center of the blade area and along the B-axis, i.e., perpendicular to the blade area. The thrust coefficient, C_T, is assumed to depend solely on relative wind velocity and is taken directly from Nielsen [63] and repeated in Fig. 14. This curve is a proxy for the influence of conventional blade-pitch control on thrust. The curve was developed by assuming that the control mechanism maximizes the power output for wind speeds below the rated speed (17 m/s here) and retains constant power output after the rated speed. More accurate wind forces could be computed by linking the codes of this method with an existing rotor-aerodynamics module, e.g. AeroDyn [30].

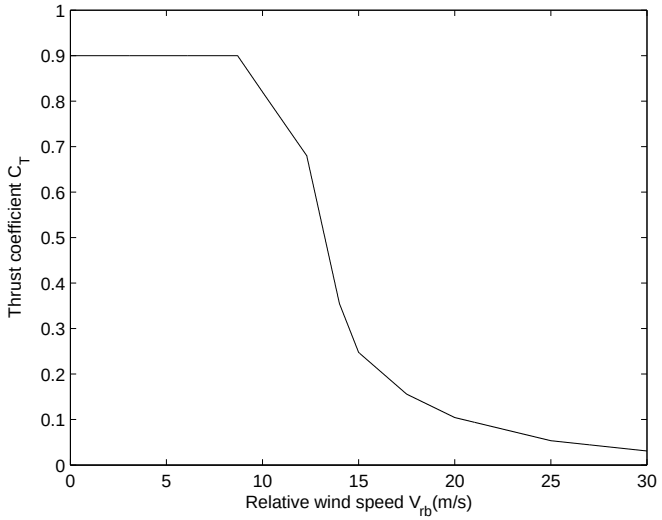

Fig. 14. Thrust force coefficient as function of relative wind velocity

The amplitude of relative velocity, V_{rb}, is computed by projecting both the wind velocity and structural velocity onto the B-axis. A unit vector $\vec{u}_B^I$ indicates the direction of the B-axis in the (X, Y, Z) system by $\vec{u}_B^I = T_{R\to I}\vec{u}_B^R$, where $\vec{u}_B^R$ is the unit vector along B-axis in the (A, B, C) system, i.e. $\vec{u}_B^R = (0, 1, 0)$. The transformation matrix from (A, B, C) to (X, Y, Z), $T_{R\to I}$, is obtained by multiplication of the transformation matrix in Eqns. (3.9) and (3.13): $T_{R\to I} = T_{s\to I}T_{R\to s}$.

The structural velocity of the center of the blade area can be expressed as: $\vec{V}_{G_R}^I = \vec{V}_{G_s} + T_{s\to I}(\vec{\omega}_t \times \vec{\rho}_{G_R/G_s})$, where $\vec{V}_{G_s}$ is the linear velocity of G_s in the inertial coordinate system (X, Y, Z): $\vec{V}_{G_s} = (\dot{X}_1, \dot{X}_2, \dot{X}_3)$ and the distance between G_R and the center of the hub is neglected. Projections of the wind velocity and structural velocity along the B-axis are obtained by dot product: $V_w = \vec{V}_{wind}^I \cdot \vec{u}_B^I$ and $V_b = \vec{V}_{G_R}^I \cdot \vec{u}_B^I$, in which $\vec{V}_{wind}^I$ is the wind velocity in the (X, Y, Z) system. The amplitude of relative velocity in Eqn. (3.19) is obtained by $V_{rb} = V_w - V_b$. Finally the wind force in the (X, Y, Z) system and the wind moment in the (x_s, y_s, z_s) system are expressed as:

$$\vec{F}_{wind} = T_{R\to I}\vec{F}_{wind}^R \tag{3.20}$$

$$\vec{M}_{wind} = \vec{\rho}_{G_R/G_s} \times \vec{F}_{wind}^R \tag{3.21}$$

where $\vec{F}_{wind}^R$ is the wind force in the (A, B, C) system: $\vec{F}_{wind}^R = (0, -F_b, 0)$. The aerodynamic torque is modeled as a constant using rated power divided by rotor speed, which is added to the wind moment.

Similar to the calculation of restoring forces, wave forces are computed in the (X, Y, Z) coordinate system and then decomposed into the (x_s, y_s, z_s) system to com-

pute the moments. The generalized Morison equation is used to calculate the wave forces per unit length normal to the axis of the leaning cylinder (e.g., [64]):

$$\vec{f}_n^I = C_m\rho\frac{\pi}{4}D^2\dot{\vec{V}}_n - C_a\rho\frac{\pi}{4}D^2\dot{\vec{V}}_t + \frac{1}{2}\rho C_d D\vec{V}_{rt}|\vec{V}_{rt}| \tag{3.22}$$

where ρ is the density of sea water; D is the local diameter of the hull; C_m is the inertia coefficient; C_a is the added mass coefficient, and C_d is the drag coefficient. All velocities and accelerations are normal to the central axis of the tower: $\dot{\vec{V}}_n$ is the normal component of wave acceleration; $\dot{\vec{V}}_t$ is the normal component of structural acceleration; $\vec{V}_{rt}$ is the normal velocity of the water particle relative to the cylinder. The term associated with C_a in Eqn. (3.22) is usually considered as the added mass. Hydrodynamic damping is included considering the relative velocity in the drag force calculation. Use of the Morison equation implicitly assumes the body has a negligible effect on the incident waves, which is reasonable here because the hull structure is relatively slender. Also, as is conventional for use of the Morison equations, dynamic pressures along the axis of the cylinder are neglected.

A unit vector along the central axis of the tower is needed to define the normal direction of kinematic vectors, i.e. $\vec{e}_3^I = T_{s\to I}\vec{e}_3^t$, where $\vec{e}_3^t$ is a unit vector along centerline of the tower in the (x_t, y_t, z_t) system, i.e. $\vec{e}_3^t = (0, 0, 1)$, and is transformed to the (X, Y, Z) system. Thus, the normal component of water particle acceleration can be expressed as: $\dot{\vec{V}}_n = \vec{e}_3^I \times (\dot{\vec{V}} \times \vec{e}_3^I)$, where $\dot{\vec{V}}$ is the wave acceleration vector in the (X, Y, Z) system. The structural velocity and acceleration of the segment along the tower can be obtained by the kinematics of rigid body:

$$\vec{V}_t = \vec{V}_{G_s} + T_{s\to I}(\vec{\omega}_t \times \vec{\rho}_{i/G_s}) \tag{3.23}$$

$$\dot{\vec{V}}_t = \vec{a}_{G_s} + T_{s\to I}[\dot{\vec{\omega}}_t \times \vec{\rho}_{i/G_s} + \vec{\omega}_t \times (\vec{\omega}_t \times \vec{\rho}_{i/G_s})] \tag{3.24}$$

where $\vec{V}_{G_s}$ and $\vec{a}_{G_s}$ are the linear velocity and acceleration of the CM of the system, G_s, in the inertial coordinate system (X, Y, Z); $\vec{\rho}_{i/G_s}$ is the vector radius from G_s to the segment with unit length. The wave kinematic velocity relative to the moving tower, $\vec{V}_{rt}$, is expressed as: $\vec{V}_{rt} = \vec{e}_3^I \times (\vec{V}_r \times \vec{e}_3^I)$, where $\vec{V}_r$ is the relative velocity of the wave to the segment of the submerged tower: $\vec{V}_r = \vec{V} - \vec{V}_t$, in which $\vec{V}$ is the wave kinematic velocity in the (X, Y, Z) system. The wave force on the cylinder, $\vec{F}_{wave}$, is obtained by summing the force on each segment from Eqn. (3.22). The wave moment in the (x_s, y_s, z_s) coordinate system can be computed by transforming the resulting forces from Eqn. (3.22) into the (x_s, y_s, z_s) system and then numerically integrating over the submerged length of the tower.

$$\vec{F}_{wave} = \int_r \vec{f}_n^I dr \tag{3.25}$$

$$\vec{M}_{wave} = \int_r (\vec{\rho}_{i/G_s} \times \vec{f}_n^s) dr \tag{3.26}$$

where $\vec{f}_n^s = T_{I\to s}\vec{f}_n^I$.

5. RNA Moments and Gyroscopic Moments

Computation of the RNA moments and gyroscopic moments is not necessary to simulate the global motions of the tower. However, these internal moments between RNA and tower, especially gyro moments, are a significant concern in design, and can be calculated by application of the Euler dynamic equations about the rigid body

RNA:

$$\sum \vec{M}_R \;=\; \dot{\vec{H}}^R_{G_R} = (\dot{\vec{H}}^R_{G_R})_{ABC} + \vec{\omega}_n \times \vec{H}^R_{G_R} \tag{3.27}$$

where the angular momentum of the RNA is decomposed to the (A, B, C) system with angular velocity $\vec{\omega}_n = (\omega_{n,A}, \omega_{n,B}, \omega_{n,C})$ and can be represented as $\vec{H}^R_{G_R} = [I_A\omega_{n,A}, I_B(\omega_{n,B} + \dot{\psi}), I_C\omega_{n,C}]$. The reaction moments of $\sum \vec{M}_R$ are defined as RNA moments applied by RNA on the top of tower $(MRNA_A, MRNA_B, MRNA_C)$. The gyro moments are that part of the RNA moments resulting from the time derivative of angular momentum associated with the spinning rate in Eqn. (3.27). If the (A, B, C) system is used to decompose the angular momentum of the gyro, the absolute time derivative is $\dot{\vec{H}}^{gyro}_{G_R} = (\dot{\vec{H}}^{gyro}_{G_R})_{ABC} + \vec{\omega}_n \times \vec{H}^{gyro}_{G_R}$, where the angular momentum related to spin can be expressed in the (A, B, C) system as $\vec{H}^{gyro}_{G_R} = (0, I_B\dot{\psi}, 0)$. Thus, the time change of the amplitude of this angular momentum within the (A, B, C) system, $(\dot{\vec{H}}^{gyro}_{G_R})_{ABC}$, is zero for constant spinning rate. Further, the gyro moments applied by the RNA on the top of the tower are:

$$M^{gyro}_{G_R} \;=\; -\vec{\omega}_n \times \vec{H}^{gyro}_{G_R} = \begin{bmatrix} I_B\dot{\psi}\omega_{n,C} \\ 0 \\ -I_B\dot{\psi}\omega_{n,A} \end{bmatrix} \tag{3.28}$$

The gyro moments have non-zero components in the A- and C-directions, both of which are perpendicular to the spin vector along the B-axis. The cross product in the equations of motion results in the transfer of angular momenta between the A- and C-directions. The angular velocity of the nacelle of a rigid bottom-fixed wind turbine is always along the C-axis and equal to the yaw rate, ω_{yaw}. In this

case, the gyro moments can be reduced to $(I_B\dot{\psi}\omega_{yaw}, 0, 0)$, which is the conventional expression for gyro moment in nutation [9]. The angular velocity of the nacelle for a floating wind turbine also has a non-zero component in the A-direction, which results in a component of gyro moments in the C-direction and proportional to the angular velocity of the nacelle along the A-axis (Eqn. (3.28)).

D. Example

Two different support-structure designs are used to demonstrate the new method. First, the OC3-Hywind model [60] is used to verify the new method presented here by comparison with the popular wind turbine dynamics software FAST [46] for a small-amplitude motion case. The OC3-Hywind is a conceptual design of the Hywind system developed to support the NREL 5-MW wind turbine. This design is stiff in pitch rotation and provides a realistic benchmark case against industry-standard software. The mooring system of OC3-Hywind is simplified by using two linear springs with stiffness equal to 5×10^4 N/m in the surge and sway directions such that it could be modeled in both FAST and the new method for verification. The truncated cylinder model is developed on the basis of OC3-Hywind by reducing the cylinder length from the 120 m of OC3-Hywind to 84.4 m. Physical properties of the tower and RNA are the same as those presented in example of Chapter 2.

1. Free Vibration Verified by FAST

Figs. 15–17 show the comparison of time histories from FAST and the method presented here for a small-amplitude free vibration case including blade spin but no

nacelle yaw. Here both hydrodynamics and aerodynamics have been turned off in FAST. The only external forces acting on the body are from the mooring lines and buoyancy, both of which are represented simply as a 6×6 restoring matrix in the user-defined subroutine (UserPtfmLd) in FAST. Stiffness values are linearized to be consistent with the method presented in section 3 and tuned to reproduce the correct natural frequencies. The initial conditions of FAST are prescribed as roll equal to 0.1 rad, pitch equal to 0.1 rad and sway equal to 0.5 m with respect to a reference point on still water level. The Euler rotations are roughly equivalent to roll, pitch and yaw in FAST for small-amplitude rotation [69]. Rotational results in FAST are defined about the inertial reference frame and superimposed. The small-amplitude assumption leads to a nearly orthogonal transformation matrix, which is corrected by Frobenius Norm to guarantee its orthogonality [46], while the new method does not need any correction in terms of the superposition of rotational motion. It can be seen in Figs. 15–17 that both the motions and moments from the new method match the results of FAST very well. One inconsistency between the models is that FAST considers relative motion within the RNA while the new method considers a unified RNA with a single spin rate. In Fig. 15, the yaw motion results from excitation by the gyro moments along the centerline of the tower. The translation shown in Fig. 16 is measured from the reference point on still water level, the origin of (X_M, Y_M, Z_M) system. In Fig. 17, the RNA moments are compared to the internal moments in the tower-top coordinate system located at the yaw bearing in FAST, which is similar to the (A, B, C) coordinate system in absence of nacelle yaw, located at the center of the RNA. Figs. 15–17 show good agreement for this small-amplitude case and

agreement improves for decreasing amplitudes. The next two example cases are for large-amplitude motion of the truncated spar model.

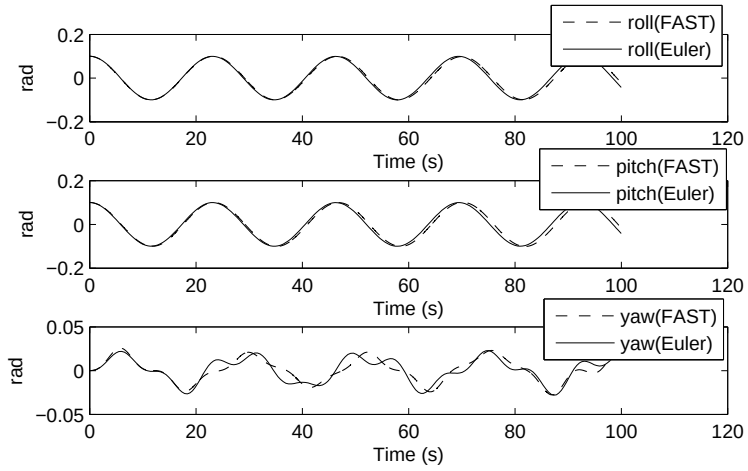

Fig. 15. Rotation compared to FAST (2-body)

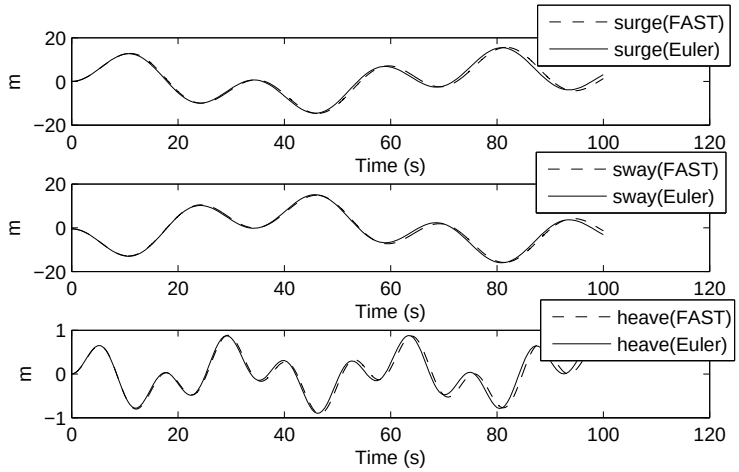

Fig. 16. Translation compared to FAST (2-body)

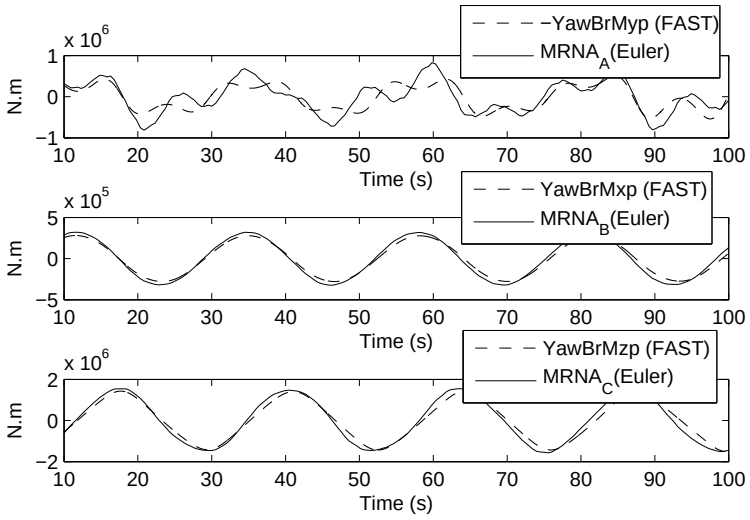

Fig. 17. RNA moments comparison

2. Forced Vibration without Nacelle Yaw

Figs. 18–20 show results for the more compliant truncated spar model in a large-amplitude forced-vibration case. Environmental loading is computed using irregular winds and waves along the negative direction of the Y-axis. The mean wind velocity at hub height is 18.2 m/s. Irregular wind velocities are simulated using TurbSim [62]. The wave environment is represented by a JONSWAP spectrum with a significant wave height of 5.0 m and peak period of 10 sec. Wave forces are computed using the Morison equation from a first-order time-domain representation of irregular waves simulated directly from the wave spectrum using a uniform phase distribution. The inertia coefficient C_m in Eqn. (3.22) is assumed to be 2.0; the added mass coefficient

C_a is assumed to be 1.0; the drag coefficient C_d is assumed to be 0.6. Figs. 18–20 show the 6-DOFs motions of the tower and gyro moments without consideration of nacelle yaw, i.e. without relative motion between the nacelle and the tower. In Fig. 18, the translation of the tower is measured from the CM of the entire wind turbine system, i.e. the origin of (X, Y, Z) system in Fig. 12. The nonzero mean of X_2 results from the surge motion in the wind direction. Fig. 19 shows 1-2-3 sequenced Euler angles X_4, X_5 and X_6, which describe the large-amplitude rotational motion of the tower. The gyro moments shown in Fig. 20 are significant and cannot be ignored in the design. Different from the bottom-fixed wind turbine, the gyro moment in the A-direction still exists due to the self-rotation of tower about its centerline even in absence of nacelle yaw. The gyro moment in the C-direction results from the angular velocity of tilt motion, and has the same frequency as X_4. Thus, the frequency of gyro moment is relevant to the frequency of motion of the tower and further depends on the frequency of environmental forcing.

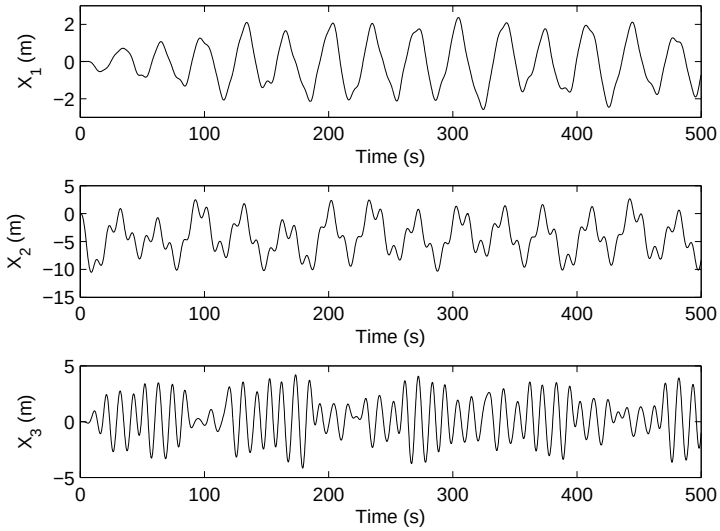

Fig. 18. Translational motion without nacelle yaw

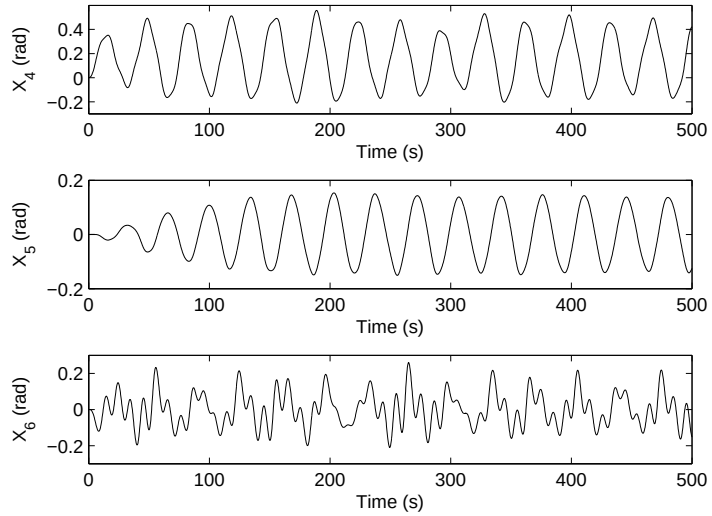

Fig. 19. Rotational motion without nacelle yaw

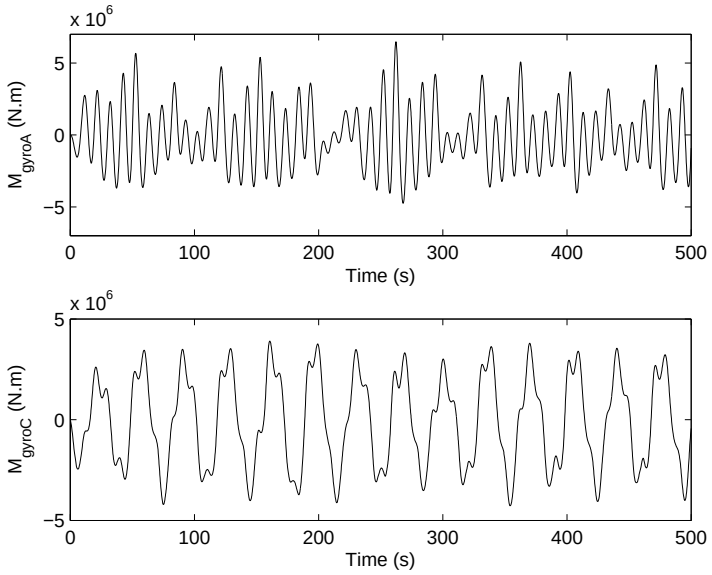

Fig. 20. Gyro moments without nacelle yaw

3. Forced Vibration with Nacelle Yaw

Figs. 21–23 show results for the same compliant spar model and the same wave conditions as the previous case, but with a sudden wind-shift imposed to show the effect of nacelle yaw. The wind direction is along the negative direction of the Y-axis during the first 100 sec and then rotates by $\pi/4$ rad toward the negative direction of the X-axis in the XOY plane to simulate the sudden shift. The yaw rate of the nacelle is 0.3 deg/sec. The wind shift causes the yaw control mechanism of the nacelle to activate at 100 sec and deactivate at around 250 sec. Fig. 21 shows the translation of the tower measured from the CM of the entire system. The amplitude

of X_1-direction motion increases because the new wind direction results in a larger wind force in the sway direction. Similarly, the Euler angle X_5 increases as shown in Fig. 22 after the wind direction changes. Comparison of Figs. 23 and 20 indicates the nacelle yaw does not significantly change the amplitudes of the gyro moments. These yaw-induced moments are relatively small because the yaw rate is much smaller than the angular velocity of self rotation of the tower about its centerline.

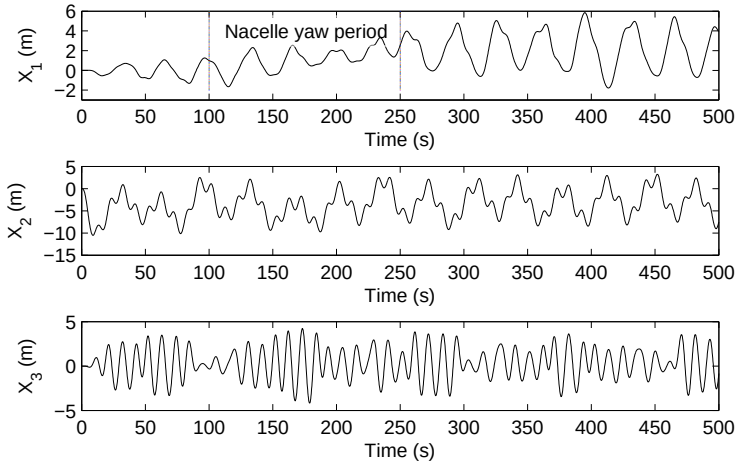

Fig. 21. Translational motion with nacelle yaw

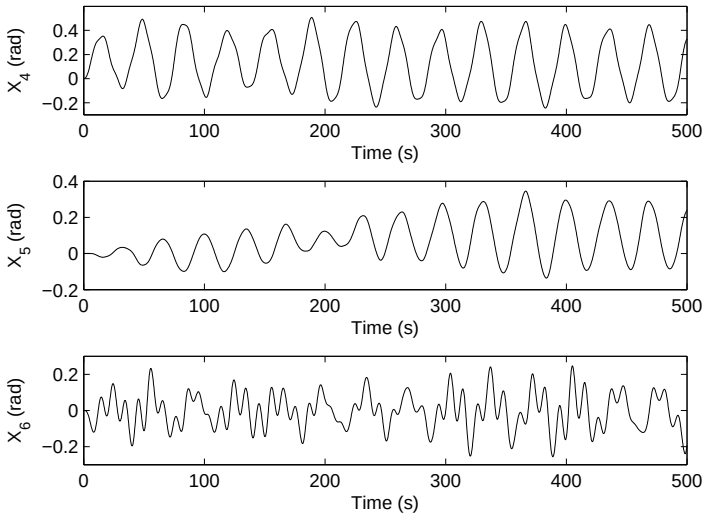

Fig. 22. Rotational motion with nacelle yaw

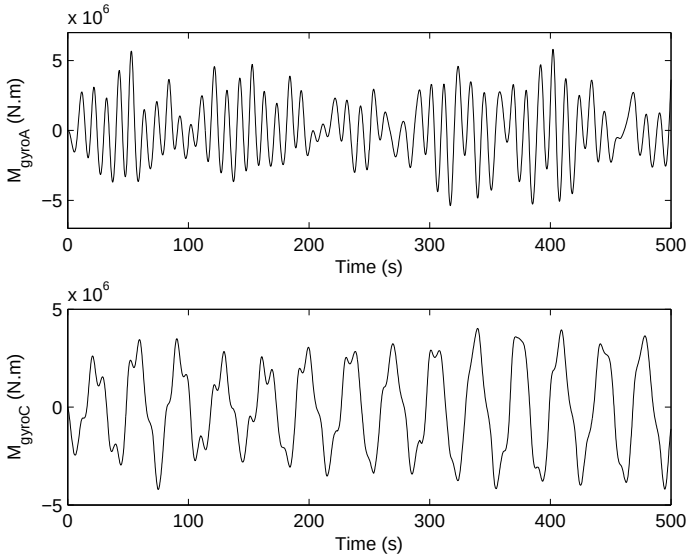

Fig. 23. Gyro moments with nacelle yaw

E. Application

In this Section, the time-domain simulation tool based on the new method is applied to roughly estimate the feasibility of compliant floating wind turbines. Three compliant designs are first developed based on the OC3-Hywind design, with drafts ranging from 84 m to the 120 m of the original OC3-Hywind. The family of floating wind turbine designs with different lengths of spar cylinders, the original OC3-Hywind plus the three new design alternates, are then analyzed through dynamic simulation to compare their dynamic performance and comparative energy harvesting efficiency.

1. A Family of Compliant Designs

As mentioned in Chapter 1, the first full-scale offshore floating wind turbine in the world, Hywind, has been installed in 2009 [11], which integrated a 2.3-MW turbine on a 65 m height tower. The base case of the investigation presented here is the OC3-Hywind, which is itself a conceptual design introduced by Jonkman [60] as an enlarged version of the installed 2.3-MW Hywind platform. The OC3-Hywind has a tower height of 87.6-m, supported by a 108-m underwater spar cylinder plus a taper and smaller cylinder for a total 120-m draft (Fig. 24). Much of the structural steel in the design is in the 108 m spar cylinder, the primary purpose of which is to maintain the tower in a near-vertical condition when subject to the very large horizontal wind force at the hub height. Additional angular stability is provided through use of barite ballast in the bottom of the 120-m deep structure.

In this Section, three smaller conceptual designs are developed from the OC3-Hywind by decreasing the ballast weight and truncating the length of the spar cylin-

der. Reducing the ballast directly reduces the amount of buoyancy required to support the structure, and reducing the cylinder length directly reduces the required structural steel. The diameter of the cylinder remains constant for all four designs. The diameter of the upper small cylinder is 6.5 m; the diameter of lower large cylinder is 9.4 m. They are connected by a tapered structural cone, the height of which is 8 m. The main criterion for design is hydrostatic equilibrium: the available buoyancy provided by the spar cylinder must equal the weight of complete structure plus the vertical component of the top tension of the mooring lines. Buoyant volume and center of buoyancy calculations included the large cylinder, small cylinder and taper. Calculation of the physical weight includes the weights of hull, ballast, tower and RNA. For all designs, the diameter and the weight per length of the spar cylinder were held constant, and were based on the original OC3-Hywind design. Various combinations of length and ballast were investigated using a trial-and-error methodology to find three design alternatives that spanned a wide range of cylinder lengths. The four conceptual designs selected for further analysis are outlined in Fig. 24 and Table I.

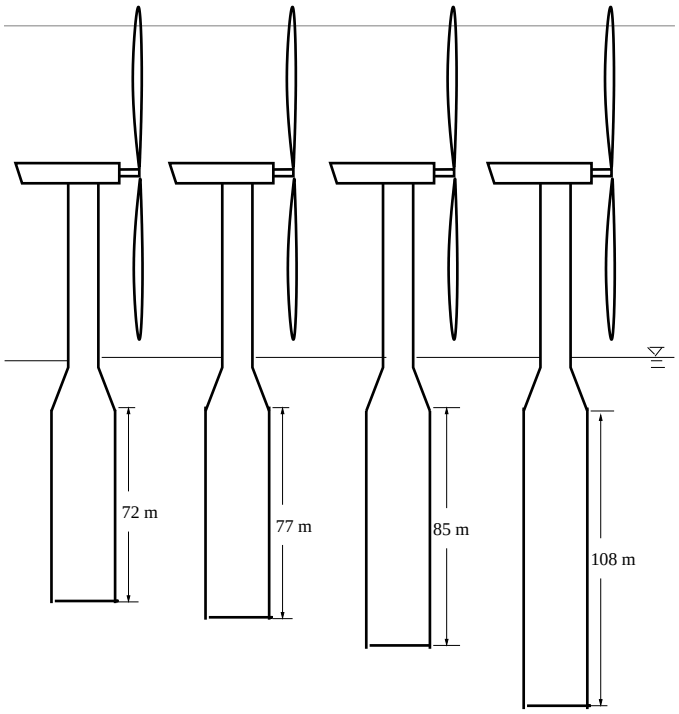

Fig. 24. Truncated cylinder designs

Table I. Properties of alternate designs and original OC3-Hywind

	Truncated			**Hywind**
Cylinder Length (m)	72	77	85	108
Platform Draft (m)	84	89	97	120
Hull Weight (tonnes)	816	860	940	unknown
Ballast (tonnes)	4,208	4,503	5,038	unknown
Platform Weight (tonnes)	5,024	5,363	5,978	7,466

2. Dynamic Behavior and Power Efficiency

The dynamic behavior of the truncated spar is analyzed and shown to be meaningfully influenced by the blade-pitch control strategy. The present time-domain simulator does not include any advanced control simulation capability. In the dynamic studies presented here, the possible control algorithms are bounded by two extremes. Optimal energy harvesting should result from ideal blade-pitch adjustments in which the blade pitch is adjusted instantaneously to the apparent wind velocity relative to the moving tower. Here, that strategy is implemented by applying Eqn. (3.19) with the thrust coefficient, C_T, updated at every time step based on the computed apparent wind and Fig. 14. These very rapid blade-pitch adjustments may not be realistically practical in the field. At the other extreme from instantaneous adjustment is to set the coefficient of thrust based on Fig. 14 using the mean wind speed and leave it at that fixed value throughout the simulation.

The four designs outlined in Table I and Fig. 24 are analyzed to assess their global behavior and relative efficiency. Fig. 25 shows both the mean and standard deviation of the platform pitch for each of the four competing designs with the standard deviation magnified by a factor of 10. The figure was generated by combining results of 10 realizations of a 180-minute irregular sea state and irregular wind time histories, using the same wind and wave time histories for each of the bounding blade-pitch control strategies: fixed vs variable C_T. The four sets of combined wind-wave conditions used here are taken directly from Nielsen [63]: mean wind velocities of 8 m/s, 17 m/s, 20 m/s, 25 m/s with corresponding wave conditions of significant wave heights 3 m, 5 m, 9 m, 14 m and peak periods 10 s, 12 s, 13 s, 15 s, respectively.

The wind and wave process are assumed to be stationary for the full 180-minutes. The reference height for the four specific wind speeds is 87.6 m (hub height).

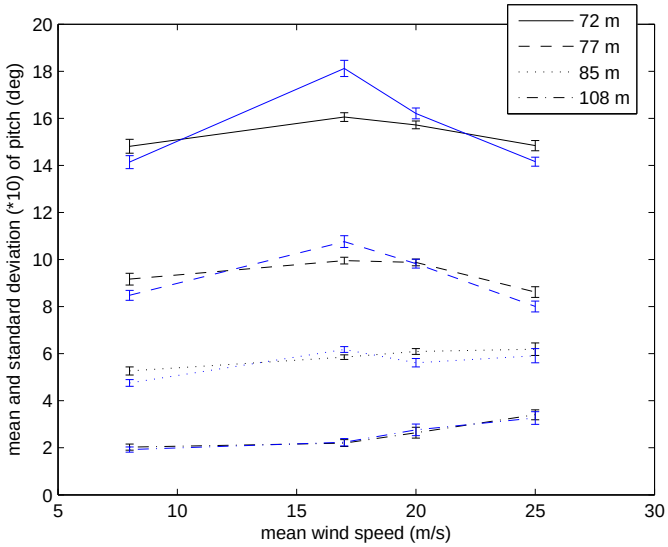

Fig. 25. Platform pitch for various cylinder lengths and blade-pitch control strategies (blue lines indicates variable C_T)

Considering the results shown on Fig. 25, mean platform pitch angle shows the expected increase with decreasing cylinder length. The general behavior of these compliant systems is to have a large, relatively steady mean offset and dynamic variation about that mean. The standard deviation shown is the square root of the variance of the process, and therefore indicates the magnitude of the dynamic motions about the mean. It also appears that increasing tower pitch corresponds to

greater difference between the fixed- and variable C_T cases. This effect probably results from computing the inflow velocity in the variable C_T cases as the component of velocity perpendicular to the blade area, so for large angles, the average C_T in the variable C_T cases corresponds to a lower average inflow velocity than that of the fixed C_T cases. Greater differences between the two control strategies can also be seen at the 17 m/sec rated wind speed than at other speeds, presumably because the slope of C_T curve in Fig. 14 is steepest near the rated wind speed. The general trend for the fixed C_T cases is to have smaller standard deviation than variable C_T cases due to the greater aerodynamic damping, as also noted in [63].

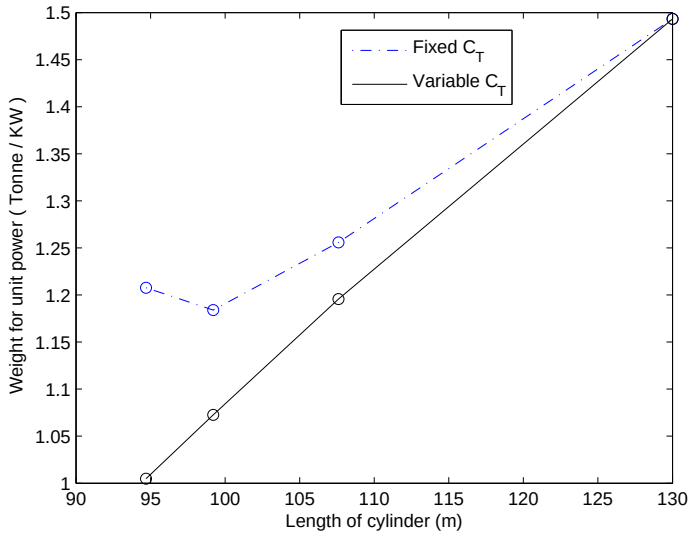

Fig. 26. Weight of supporting structure per unit power output

For each of the time-history realizations of rated wind case, the power output is calculated as $P = \frac{1}{2} C_p \rho_a A_b V_{rb}^3$, where A_b is the swept area of the blades; C_p is a power coefficient($C_p = 0.7 C_T$), which guarantees that output power of OC3-Hywind model is 5-MW. The results of the power calculation are presented as Fig. 26, which shows the ratio of the hull structural weight to the output of power. Results presented here explicitly consider platform motions in the power calculation. Designs with greater platform pitch angles generate slightly less power because the inflow velocity perpendicular to the blades is slightly reduced (or, equivalently, the projected area of the blades perpendicular to the wind is slightly reduced). Here the power is computed as 4.16 MW, 4.53 MW, 4.76 MW, 5.0 MW. The slight decrease in energy harvesting efficiency is counter-balanced by decreased structural weight. The most effective design is that with the lowest weight per kW. The figure also shows a substantial difference between the harvesting efficiency of the fixed versus variable C_T cases. This result emphasizes the importance of optimal control system design. The energy harvesting effectiveness of a wind turbine with a realistic blade-pitch control system is expected to be between these two extremes.

F. Conclusions

In this Chapter, a new method has been developed to directly apply conservation of linear momentum (Newton's second Law) and angular momentum to an entire floating wind turbine system including RNA and tower, resulting in a new formulation to simulate translation and large-amplitude rotation of the system. Motions of an 8-DOF system are represented as six EOMs of the tower. The 1-2-3 sequence Euler

angles are introduced to describe the rotation of the tower and the transformation matrixes between various coordinate systems. The restoring forcing and environmental forcing are calculated by considering nonlinear coupling among translational and rotational DOFs. Further, motions and external forcing are transformed at each time step between different coordinate systems such that the fully nonlinear coupling between external forcing and large-amplitude motion of the system is preserved. The new method is verified by comparison with the well-known software FAST for a small-amplitude case, for which the nonlinear coupling effects are small. Simulation results in terms of 6-DOFs motions of tower and gyro moments for the floating wind turbine with large-amplitude motions are also shown. A major strength of this new method is that it can be readily expanded to a large number of rigid bodies as long as the relative motion between contiguous bodies is explicitly defined. The decoupling of translational and rotational accelerations also dramatically increases the efficiency of numerical integration.

The time-domain simulator based on the new formulation is also applied to investigate the feasibility of compliant designs. Four alternate spar-based floating wind turbine designs have been analyzed and compared in terms of rigid-body dynamics and energy harvesting efficiency. The first of these designs is the OC3-Hywind, and the remaining three are developed by shortening the spar hull and reducing the ballast of the OC3-Hywind design. It is found that blade-pitch control has significant influence on the dynamic performance of compliant designs. It is also found that there is a significant opportunity for improved efficiency through active blade-pitch control using the real-time inflow velocities including tower motions, as compared

with a passive control strategy in which the blade pitch is set using only the mean wind speed.

CHAPTER IV

CONSERVATION OF MOMENTUM FOR 3-BODY MODEL

A. Overview

The methodology in this Chapter is applied to the system including three rigid bodies: the tower, the nacelle and the rotor, which is one more body than in Chapter 3. The large-amplitude rotation of the tower is described by 1-2-3 sequence Euler angles as 3 rotational degrees of freedom (DOFs); translation of the system is described by Newton's second Law and transferred to 3 translational DOFs of the tower. Additionally, two prescribed DOFs governed by mechanical control, nacelle yaw and rotor spin, are combined with the 6 DOFs of the tower to formulate the 8-DOF equations of motion (EOMs) of the system. Unlike the 2-body model in Chapter 3, the center of mass (CM) of the wind turbine system is generally time-varying and not constrained to any rigid body due to arbitrarily located CM of each body and relative mechanical motions among the bodies, i.e. the prescribed mechanical DOFs here. In this Chapter, these two effects are considered in both the solution to 3 translational DOFs and the calculation of angular momentum of each body for 3 rotational DOFs. The theorem of conservation of momentum is applied to the entire multibody system directly to solve 6 unknown DOFs. Motions computed using the six nonlinear EOMs are transformed to each body in a global coordinate system at every time-step for use in the computation of hydrodynamics, aerodynamics and restoring forcing, preserving the nonlinearity between external excitation and structural dynamics. The new method is demonstrated by simulation of the motion of highly compliant floating

wind turbine, the results of which are verified by critical comparison with those of the popular wind turbine dynamics software FAST. The effect of the unconstrained CM of the system is demonstrated by comparing to the resulting motions with those based on 2-body model in Chapter 3.

B. Introduction and Background

Chapter 3 formulates the EOMs of the compliant floating wind turbine by a 2-body model including the tower and RNA. Two relative DOFs, nacelle yaw and rotor spin, are considered in the calculation of the angular momentum of the entire system by assuming that the nacelle is a mass point attached to the spin axis of the rotor. The simple 2-body configuration is applied to conveniently demonstrate the derivation of new method. In this Chapter, a more realistic 3-body model is introduced to generalize the effect of relative motion between bodies on the total angular momentum. Three rigid bodies in the system are the tower, nacelle and rotor. The tower is the complete support structure of topsides facility, including the buoyant hull; the nacelle is the no-spinning part of the topsides; the rotor is the spinning part of the topsides, including the hub and blades. The rotor spins relative to the nacelle, and the combined nacelle and rotor mechanically yaws relative to the tower.

There is another important extension to that work: the 2-body model in Chapter 3 was configured with the CM of the nacelle centered above the axis of the tower, such that the CM of the system remained at a fixed point on the tower axis, regardless of nacelle yaw. However, having the CM of each body being arbitrarily located and

allowing relative motion among bodies generally change the CM of a multibody system. Modern turbines are generally configured with the CM of the nacelle downwind of the centerline of the tower. Subsequently, the CM of the floating wind turbine system changes as the nacelle yaws relative to the tower, and is not constrained to any body in the system. The unknown unconstrained CM must first be obtained at each time step in a numerical simulation because the conservation of both the angular and linear momentum are applied about this point. Meanwhile, the motion of each body in space is generally of interest. Here, the wind and wave forcing on the floating wind turbine are exerted on the topsides and floater, respectively. Accurate computation of these forces requires consideration of the spatial relation between the CM of each rigid body and that of the system.

The CM of the system depends on that of each body; a common coordinate system should first be chosen for measurement of the position of each CM, from which the relative position can be determined. A convenient solution is to choose the inertial coordinate system to formulate the CM of each body. The conservation of linear momentum (Newton's second Law) can be applied to the entire system in the form of $F = \Sigma m_i a_i$ based on the expression of kinematics of each body along the kinematic chain using six unknown DOFs of the tower (base body) and two known mechanical DOFs, nacelle yaw rate and rotor spin rate. However, this method introduces the combination of the translational and rotational DOFs in the formulation, which indicates the differential EOMs with complicated coupling.

The relative position between the CM of the system and that of each body is shown to be independent of the translation of the tower, and only associated

with relative rotation between bodies. Therefore, the body-fixed coordinate system attached to the base body (tower) is chosen to calculate all radius vectors at each time step. The derivatives of these radius vectors are also derived analytically. The efficient formulation enables the determination of the unknown position of the CM of the system and the spatial motion of other bodies at each point in time, but maintains the decoupling between the translational and rotational inertial forcing, which facilitates numerical integration of the EOMs.

C. Theory

The coordinate systems associated with the 3-body model are introduced in Section 1. The translational and rotational EOMs of the entire floating wind turbine system are then derived in Section 2, where the effect of the unconstrained CM of the system is considered. The calculations of the angular momentum of the system in the rotational EOMs and its derivative are addressed separately to generalize and standardize the derivation. The external loads on the system, i.e. restoring and environmental forcing, are calculated in Sections 3, in which the effects of the unknown CM of the system are hightlighted.

1. Coordinate Systems

The implementation of the new method first requires the selection of a set of coordinates to unequivocally define the motion of the multibody system and derive the EOMs; coordinate selection is based on first selecting proper coordinate systems. There are two global earth-fixed coordinate systems, plus three body-fixed coordi-

nate systems attached to each of the three bodies, plus one system-fixed coordinate system.

Fig. 27 shows both the (X, Y, Z) and the (X_M, Y_M, Z_M) systems, which are earth-fixed global coordinate systems with the origin located at the CM of the undisplaced tower and the still water level respectively. The (x_t, y_t, z_t), (x_n, y_n, z_n) and (x_r, y_r, z_r) coordinate systems are body fixed and originate at the instantaneous CM of the tower, nacelle and rotor, consecutively. There is also a coordinate system for the entire system, (x_s, y_s, z_s). This system-fixed (x_s, y_s, z_s) is parallel to (x_t, y_t, z_t) and originates at the time-varying CM of the entire system, instantaneous change of which depends on arbitrarily located CM of each body and relative motion among bodies.

The (X, Y, Z) system is used for application of Newton's second Law. The (X_M, Y_M, Z_M) system is not used in the calculations and is defined only to enable comparison of simulation results with those of FAST, in which the reference point is usually prescribed to be on the still water level. The body-fixed coordinate systems, (x_t, y_t, z_t), (x_n, y_n, z_n) and (x_r, y_r, z_r) , are assumed to be on the principal axes of inertia in order to simplify the calculation of angular momentum of the three rigid bodies. The system-fixed (x_s, y_s, z_s) system is used for application of the theorem of conservation of angular momentum to the entire system. Additionally, the external excitation applied in the dynamic equations is computed consecutively and projected into the corresponding coordinate systems.

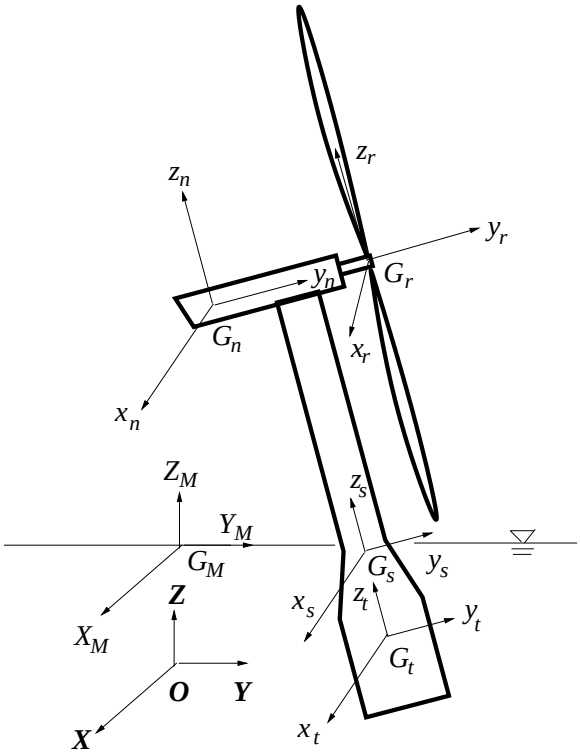

Fig. 27. Coordinate systems used in the 3-body model

The coordinates (X_1, X_2, X_3) measured from the (X, Y, Z) system are used to define the absolute motion of the CM of the system, G_s. These coordinates are further transferred to the translations of the CM of the tower, G_t, which are notated by the coordinates (X_{1t}, X_{2t}, X_{3t}) and defined as 3 translational DOFs of the tower. Similar to Chapter 3, the 1-2-3 sequence of Euler angles are selected; the coordinates (X_4, X_5, X_6) denote these angles, which are 3 rotational DOFs of the tower and describe the position of the rotating tower. Additionally, the prescribed mechanical DOFs are denoted by two relative coordinates: the vector $\vec{\omega}_{yaw}$ describes the rotation

of the nacelle to the tower in the (x_t, y_t, z_t) system; the vector $\dot{\vec{\psi}}$ describes the rotation of the rotor to the nacelle (x_n, y_n, z_b) system.

2. Equations of Motion of the System

Applying the conservation of momentum to the system can avoid the calculation of internal forcing between contiguous rigid bodies. The conservation of angular momentum is directly applied to the entire wind turbine system to derive the rotational EOMs; and the conservation of linear momentum (Newton's second Law) is applied to establish the translational EOMs. The resulting 6 EOMs of the multibody system include terms representing each of the three rigid bodies: the tower, the nacelle and the rotor. Six unknown DOFs of the tower (translation and rotation) and two prescribed mechanical DOFs (nacelle yaw and rotor spinning) are considered in the model. Thus, the EOMs of the entire system are used to solve the unknown general motion of the tower in the space. Tower motions and prescribed yaw and spin can then be used to obtain the motions of the nacelle and rotor.

a. Rotational Equations of Motion

Beginning with conservation of angular momentum, the sum of the moments resulting from externally applied forces about the CM of a system of particles in the translating-rotating system, (x_s, y_s, z_s), equals the change of amplitude of the momentum within the coordinate system plus the change of direction of the momentum with respect to global coordinate system (e.g. [58]). The rotational EOMs can be shown as:

$$\sum \vec{M} = \left(\dot{\vec{H}}^{s}_{G_s}\right)_{x_s y_s z_s} + \vec{\omega}_s \times \vec{H}^{s}_{G_s} \tag{4.1}$$

where $\vec{H}^{s}_{G_s}$ is the angular momentum of the system. The form is similar to that used in the derivation of the conventional Euler dynamic equations applied to only one rigid body. A significant difference here is that the conservation of angular momentum is applied to the entire system. The single vector representing the total angular momentum in Eqn. (4.1) is the sum of the angular momentum of each body. The summation of angular momentum of each body needs a unified coordinate system. Here, calculation of angular momentum and its derivative is greatly simplified because the translating-rotating system, (x_s, y_s, z_s), has been prescribed to be parallel to the body-fixed coordinate system (x_t, y_t, z_t). The vector $\vec{\omega}_s$ describes the angular velocity of (x_s, y_s, z_s) with respect to the global coordinate system (X, Y, Z). The LHS of Eqn. (4.1), $\sum \vec{M}$, represents the moments from all external forces: $\sum \vec{M} = \vec{M}_{wind} + \vec{M}_{wave} + \vec{M}_{restoring}$, where the restoring moment $\vec{M}_{restoring}$ includes the effect of both hydrostatics and mooring lines; the environmental moments $\vec{M}_{wind}$ and $\vec{M}_{wave}$ result from wind and wave forces.

Calculation of Angular Momentum The angular momentum of the entire system results from summing the angular momentum of each rigid body. The application of conservation of angular momentum by Eqn. (4.1) needs the angular momentum of the complete system about the CM of the system, G_s, which can be obtained by summing up the angular momentum of each rigid body about G_s. Summing the momenta requires they be calculated about the same reference point and

projected into the same coordinate system. Here the angular momentum of each body is computed in the coordinate system including its principal axes of inertia, then transformed into the unified (x_s, y_s, z_s) system and finally transferred to the origin of the (x_s, y_s, z_s) system. Combining the first two steps, the total angular momentum of the system can be expressed by:

$$\vec{H}^s_{G_s} = \vec{H}^s + \vec{H}_{ETR} \tag{4.2}$$

in which the vector $\vec{H}^s$ is the total angular momentum of three bodies projected into the (x_s, y_s, z_s) system but calculated about respective CM of each body, i.e. $\vec{H}^s = \vec{H}^s_{G_t} + \vec{H}^s_{G_n} + \vec{H}^s_{G_r}$; the term $\vec{H}_{ETR}$ represents the effect of transferring the reference point from the CM of each body to G_s. The angular momenta of three rigid bodies taken about respective CM can be expressed as:

$$\begin{aligned} \vec{H}^s_{G_t} &= T_{t\to s}(I_t\vec{\omega}_t) \\ \vec{H}^s_{G_n} &= T_{n\to s}(I_n\vec{\omega}_n) \\ \vec{H}^s_{G_r} &= T_{r\to s}(I_r\vec{\omega}_r) \end{aligned} \tag{4.3}$$

where I_t, I_n and I_r are the inertia tensors of three rigid bodies, with diagonal elements equal to the moments of inertia about respective principal axes. The transformation matrix from the body-fixed coordinate system of the tower to the unified system, $T_{t\to s}$, is an identity matrix because the (x_t, y_t, z_t) system is parallel to the (x_s, y_s, z_s) system. The other two transformation matrixes about the nacelle and rotor can be

shown to be (e.g. [52]):

$$
\begin{aligned}
T_{n\to s}(\beta) &= \begin{bmatrix} \cos\beta & -\sin\beta & 0 \\ \sin\beta & \cos\beta & 0 \\ 0 & 0 & 1 \end{bmatrix} \\
T_{r\to s}(\alpha) &= T_{n\to s}T_{r\to n} = T_{n\to s}\begin{bmatrix} \cos\alpha & 0 & \sin\alpha \\ 0 & 1 & 0 \\ \sin\alpha & 0 & \cos\alpha \end{bmatrix}
\end{aligned} \tag{4.4}
$$

Here the angle α describes the relative spin of the rotor to the nacelle and is positive along the y_r-axis; the angle β describes the relative yaw of the nacelle to the tower and is positive along the z_t-axis. The absolute angular velocities in Eqn. (4.3) are component-wise projections in the body-fixed coordinate systems of each of three bodies [70]:

$$
\begin{aligned}
\vec{\omega}_t &= \begin{bmatrix} \dot{X}_4\cos X_5\cos X_6 + \dot{X}_5\sin X_6 \\ -\dot{X}_4\cos X_5\sin X_6 + \dot{X}_5\cos X_6 \\ \dot{X}_4\sin X_5 + \dot{X}_6 \end{bmatrix} \\
\vec{\omega}_n &= T_{t\to n}(\vec{\omega}_t + \vec{\omega}_{yaw}) \\
\vec{\omega}_r &= T_{n\to r}(\vec{\omega}_n + \dot{\vec{\psi}})
\end{aligned} \tag{4.5}
$$

where the vector $\vec{\omega}_{yaw}$ has positive nacelle yaw component along z_t-direction; the spinning vector $\dot{\vec{\psi}}$ is positive along y_r-direction. The angular momentum of the system without consideration of the transfer of reference point can be obtained by

substituting Eqns. (4.4)-(4.5) into Eqn. (4.3):

$$\begin{aligned}\vec{H}^s &= (T_{t\to s}I_t + T_{n\to s}I_nT_{t\to n} + T_{r\to s}I_rT_{t\to r})\vec{\omega}_t \\ &\quad +(T_{n\to s}I_nT_{t\to n} + T_{r\to s}I_rT_{t\to r})\vec{\omega}_{yaw} \\ &\quad +T_{r\to s}I_rT_{n\to r}\dot{\vec{\psi}} \end{aligned} \tag{4.6}$$

where the first bracket associated with $\vec{\omega}_t$ represents the angular momentum of the entire system in absence of the relative motion between contiguous components; the terms including the nacelle yaw rate $\vec{\omega}_{yaw}$ and the spinning velocity $\dot{\vec{\psi}}$ indicate the contribution of relative motion to the total angular momentum. Each of the three angular velocities is first transferred to the local coordinate systems of its rigid body to calculate the angular momentum and then transferred to the unified coordinate system (x_s, y_s, z_s), so it can be included in sum. The decreasing number of transformations for $\vec{\omega}_t$, $\vec{\omega}_{yaw}$, and $\dot{\vec{\psi}}$ is because of the cascading nature of the transformation matrix.

Eqn. (4.6) has not included the effect of transferring the reference point, i.e. the term $\vec{H}_{ETR}$ in Eqn. (4.2). A simple way to transfer the reference point in the calculation of angular momentum of a rigid body is to combine the angular momentum about the CM of the rigid body to the effect of change of the reference point. For example, the angular momentum of the tower calculated about G_s can be shown as [58]:

$${}^t\vec{H}^s_{G_s} = \vec{H}^s_{G_t} + \vec{\rho}_{G_t/G_s} \times m_t\vec{v}_{G_t/G_s} \tag{4.7}$$

The cross product term in Eqn. (4.7) is one component in $\vec{H}_{ETR}$ relative to the

tower, which depends on the radius vector originated from G_s to G_t, $\vec{\rho}_{G_t/G_s}$, and the relative velocity of G_t to G_s, $\vec{v}_{G_t/G_s}$. The angular momenta of the nacelle and the rotor about G_s can be expressed similar to Eqn. (4.7) and result in $\vec{H}_{ETR} = \vec{\rho}_{G_t/G_s} \times m_t \vec{v}_{G_t/G_s} + \vec{\rho}_{G_n/G_s} \times m_n \vec{v}_{G_n/G_s} + \vec{\rho}_{G_r/G_s} \times m_r \vec{v}_{G_r/G_s}$. Thus, the radius vectors $\vec{\rho}_{G_t/G_s}$, $\vec{\rho}_{G_n/G_s}$ and $\vec{\rho}_{G_r/G_s}$ need to be determined to include the effect of transfer of reference points.

Computing the CM of the wind turbine system requires the spatial position of the CM of each rigid body expressed in a common coordinate system. Careful selection of this common system can significantly simplify the EOMs. Here the body-fixed coordinate system of the base body, the (x_t, y_t, z_t) system, is chosen to measure the relative positions of the CM of each body to that of the system because it enables expressions of the locations of the tower, nacelle and rotor relative to the CM of the system as three single radius vectors and depends on only the prescribed rotational DOFs between bodies.

Firstly, the radius vectors originated from the CM of the tower (G_t) to the CM of other rigid bodies (G_n and G_r) are decomposed in the translating-rotating (x_t, y_t, z_t) system based on the initial configuration of the bodies and a transformation matrices representing the relative rotation between the bodies. Then the CM of the system is calculated in this coordinate system to decouple the translational and rotational EOMs:

$$\begin{aligned} \vec{\rho}_{G_n/G_t} &= \vec{\rho}_{J_n/G_t} + T_{n\to t}\vec{\rho}_{G_n/J_n} \\ \vec{\rho}_{G_r/G_t} &= \vec{\rho}_{G_n/G_t} + T_{n\to t}\vec{\rho}_{G_r/G_n} \end{aligned}$$

$$\vec{\rho}_{G_t/G_s} = -\vec{\rho}_{G_s/G_t} = -\frac{m_n\vec{\rho}_{G_n/G_t} + m_r\vec{\rho}_{G_r/G_t}}{m_t + m_n + m_r} \tag{4.8}$$

where m_t,m_n and m_r are the masses of the tower, the nacelle and the rotor, respectively. The relative positions between the centers of mass are connected by means of the positions of the joints measured from the proper body-fixed coordinate systems in order to avoid the influence of spatial rotation. Here the mechanical joint J_n is located between the tower and nacelle; the radius vectors $\vec{\rho}_{J_n/G_t}$ and $\vec{\rho}_{G_n/J_n}$ are projected into the (x_t, y_t, z_t) and (x_n, y_n, z_n) systems, respectively. Both of them result from the initial geometrical configuration within the multibody system and remain as constants, as shown in Fig. 27. The radius vector $\vec{\rho}_{G_r/G_n}$ can be obtained following the pattern of $\vec{\rho}_{G_n/G_t}$, i.e. $\vec{\rho}_{G_r/G_n} = \vec{\rho}_{J_r/G_n} + T_{r\to n}\vec{\rho}_{G_r/J_r}$. The CM of the nacelle and the rotor w.r.t that of the system can be obtained by means of $\vec{\rho}_{G_t/G_s}$, e.g. $\vec{\rho}_{G_n/G_s} = \vec{\rho}_{G_n/G_t} + \vec{\rho}_{G_t/G_s}$. Obviously, that part of the angular momentum associated with the effect of the transfer of the reference point does not depend on the translation of the system, which facilitates the numerical integration dramatically.

Calculation of Derivative of Angular Momentum The absolute derivative of the angular momentum of the system includes the local derivative in the unified coordinate system (x_s, y_s, z_s) (the change of magnitude of the momentum) and the rotational effect (the change of direction of the momentum) in Eqn. (4.1). In theory, the angular momentum of any system can be decomposed into any arbitrary coordinate system. Here, the (x_s, y_s, z_s) coordinate system in the presented method is prescribed to be parallel to the body-fixed coordinate system of the tower, (x_t, y_t, z_t), to realize two important benefits. First, it eliminates complication of computing the

derivative of the angular momentum, and more importantly, it decouples the velocity terms in the inertia forcing of Eqn. (4.1). The absolute derivative of the angular momentum of the system in Eqn. (4.1) can be expanded to:

$$\frac{d\vec{H}^s_{G_s}}{dt} = \left(\dot{\vec{H}}^s_{G_s}\right)_{x_s y_s z_s} + \vec{\omega}_s \times \vec{H}^s_{G_s} \tag{4.9}$$

in which

$$\vec{H}^s_{G_s} = \vec{H}^s + \vec{\rho}_{G_t/G_s} \times m_t \vec{v}_{G_t/G_s} + \vec{\rho}_{G_n/G_s} \times m_n \vec{v}_{G_n/G_s} + \vec{\rho}_{G_r/G_s} \times m_r \vec{v}_{G_r/G_s} \tag{4.10}$$

where the notation $(\dot{\ })_{x_s y_s z_s}$ represents the local derivative within the (x_s, y_s, z_s) system, i.e. the time change of the magnitude of each component in the vector. The angular velocity of the (x_s, y_s, z_s) system, $\vec{\omega}_s$, is equal to rotational velocity of the tower shown in Eqn. (4.5). The local derivative of the vector $\vec{H}^s$ can be obtained by directly taking derivative of Eqn. (4.6), which includes the derivative of the transformation matrixes and the angular velocities. The derivative of three cross product terms needs further investigation. Here a symmetric matrix $(\bar{\rho})$ is introduced to simplify the calculation of derivative. Take the term associated with the tower for example:

$$\begin{aligned}
\vec{v}_{G_t/G_s} &= \frac{d\vec{\rho}_{G_t/G_s}}{dt} = \left(\dot{\vec{\rho}}_{G_t/G_s}\right)_{x_s y_s z_s} + \vec{\omega}_s \times \vec{\rho}_{G_t/G_s} \\
\left(\vec{\rho}_{G_t/G_s} \times \dot{m_t \vec{v}}_{G_t/G_s}\right)_{x_s y_s z_s} &= \vec{\rho}_{G_t/G_s} \times m_t \left(\ddot{\vec{\rho}}_{G_t/G_s}\right)_{x_s y_s z_s} \\
&\quad + \left[\vec{\rho}_{G_t/G_s} \times m_t (\dot{\vec{\omega}}_s \times \vec{\rho}_{G_t/G_s})\right]_{x_s y_s z_s} \\
&= \vec{\rho}_{G_t/G_s} \times m_t \left(\ddot{\vec{\rho}}_{G_t/G_s}\right)_{x_s y_s z_s} + m_t (\dot{\bar{\rho}}\dot{\vec{\omega}}_s)_{x_s y_s z_s} \\
&= m_t \vec{\rho}_{G_t/G_s} \times \left(\ddot{\vec{\rho}}_{G_t/G_s}\right)_{x_s y_s z_s} + m_t (\dot{\bar{\rho}})_{x_s y_s z_s} \vec{\omega}_s
\end{aligned}$$

$$+m_t\bar{\rho}(\dot{\vec{\omega}}_s)_{x_sy_sz_s} \tag{4.11}$$

where the relative velocity $\vec{v}_{G_t/G_s}$ is calculated by the absolute derivative of the radius vector $\vec{\rho}_{G_t/G_s}$. The symmetric matrix $\bar{\rho}$ is introduced to simplify the calculation of the derivative [34]:

$$\bar{\rho} = \begin{bmatrix} \rho_2^2+\rho_3^2 & -\rho_1\rho_2 & -\rho_1\rho_3 \\ -\rho_1\rho_2 & \rho_1^2+\rho_3^2 & -\rho_2\rho_3 \\ -\rho_1\rho_3 & -\rho_2\rho_3 & \rho_1^2+\rho_2^2 \end{bmatrix} \tag{4.12}$$

in which $\vec{\rho}_{G_t/G_s} = [\rho_1, \rho_2, \rho_3]$. The derivative of the radius vector $\vec{\rho}_{G_t/G_s}$ can be obtained from Eqn. (4.8), which depends on the derivatives of various transformation matrixes. If the amplitude of the radius vector $\vec{\rho}_{G_t/G_s}$ is assumed to be constant, i.e. that the CM of the system is at a fixed point on a body, the velocity and acceleration terms resulting from this vector, $\left(\ddot{\vec{\rho}}_{G_t/G_s}\right)_{x_sy_sz_s}$ and $(\dot{\bar{\rho}})_{x_sy_sz_s}$, will disappear from Eqn. (4.11), which allows this methodology to degenerate to the specific case presented in Chapter 3. The derivatives related to the vectors $\vec{\rho}_{G_n/G_s}$ and $\vec{\rho}_{G_r/G_s}$ in Eqn. (4.10) are calculated similarly. The introduction of symmetric matrix ($\bar{\rho}$) facilitates the combination of similar terms from each rigid body and the separation of rotational DOFs ($\vec{\omega}_s$) from cross product terms, which guarantees the numerical integration of the rotational EOMs can be achieved by efficient matrix form.

b. Translational Equations of Motion

Similar to the rotational EOMs, the conservation of linear momentum is applied to the entire wind turbine system directly to avoid the calculation of internal forces

between rigid bodies:

$$\sum \vec{F} \;=\; m_s \vec{a}_{G_s} \tag{4.13}$$

where $\vec{a}_{G_s}$ is the linear acceleration of the CM of the system, $\vec{a}_{G_s} = [\ddot{X}_1, \ddot{X}_2, \ddot{X}_3]$; m_s is the mass of the whole system, i.e. $m_s = m_t + m_n + m_r$; the force vector $\sum \vec{F}$ represents the external forces of the entire system in the inertia coordinate system (X, Y, Z), including environmental forces, restoring forces and gravity: $\sum \vec{F} = \vec{F}_{wind} + \vec{F}_{wave} + \vec{F}_{restoring} + \vec{G}$. Each of these components must be decomposed to the inertia coordinate system (X, Y, Z) for application of Newton's second Law. Restoring forcing, $\vec{F}_{restoring}$, include contributions from buoyancy of the hull and tension of the mooring lines. The solution to this set of 3 translational EOMs is the motion of the CM of the system measured from the (X, Y, Z) system. This CM is a mathematical convenience, the position of which may be constantly changing relative to both the (X, Y, Z) system and any of the three bodies making up the wind turbine model. The spatial position of the CM of the tower relative to G_s can be expressed as:

$$\vec{\rho}^{\,I}_{G_t/O} \;=\; \vec{\rho}^{\,I}_{G_s/O} + T_{s\to I}\vec{\rho}_{G_t/G_s} \tag{4.14}$$

where the radius vectors $\vec{\rho}^{\,I}_{G_s/O}$ and $\vec{\rho}_{G_t/G_s}$ result from the integration result of Eqn. (4.13) as well as Eqn. (4.8), respectively; the transformation matrix from (x_s, y_s, z_s) to (X, Y, Z) can be calculated by Eqn. (3.13) in Chapter 3. The translational DOFs of the tower are determined as the motion of G_t measured from the (X, Y, Z) system, i.e. $\vec{\rho}^{\,I}_{G_t/O} = [X_{1t}, X_{2t}, X_{3t}]$, which is specified as the initial con-

dition of translation and transferred to that of G_s by Eqn. (4.14) for numerical integration of the translational EOMs. Similarly, the motion of G_s from Eqn. (4.13) is transferred to that of G_t for the calculation of external forcing at each time step.

3. External Forcing

The external forcing (including both the external forces and moments) is composed of restoring forcing from hydrostatics and mooring lines and the environmental forcing due to wind and waves. The LHS of the rotational EOMs (Eqn. (4.1)) is the sum of the external moments in the translating-rotating system (x_s, y_s, z_s); the LHS of the translational EOMs (Eqn. (4.13)) is the external forces in the inertial system (X, Y, Z). The calculation of nonlinear external forcing is similar to the method presented in Chapter 3. Here, the effects of 3-body configuration and the unconstrained G_s are highlighted.

a. Restoring Forcing

The large-amplitude motion of the wind turbine system results in nonlinear restoring forcing, which cannot be calculated by the conventional linear stiffness matrix method. Here the hydrostatic restoring forcing are calculated directly from the instantaneous buoyancy and the buoyancy center of the floater, which are nonlinear for large-amplitude motions. The floater (Fig. 27) includes two cylinders: a small surface-piercing cylinder and a larger subsurface cylinder, which are connected by a tapered structural cone. The lower cylinder and taper are fully submerged and therefore have constant buoyancy and fixed buoyancy center. The surface-piercing

cylinder has buoyancy and the buoyancy center that change with position of the cylinder. The constantly changing buoyancy and the buoyancy center of the entire floater can be obtained by combining those of previous two parts.

The instantaneous buoyancy of the surface-piercing cylinder in the inertial coordinate system (X, Y, Z) is $\vec{F}_B^I = (0, 0, \rho g \pi r^2 h_1)$ [67], where ρ is the density of sea water; g is the gravitational acceleration; r is the radius of the cylinder; h_1 is instantaneous submerged length of the cylinder along the centerline. This variable length can be shown as the function of heave motion and leaning angle of the cylinder:

$$h_1 = \frac{\rho_{G_M/G_t} - X_{3t}}{cos\theta_1} - \rho_{G_M/G_t} + h_0 \tag{4.15}$$

where ρ_{G_M/G_t} is the distance measured from still water level to the CM of the tower in its equilibrium position; θ_1 is the leaning angle of the cylinder with respect to vertical, $cos\theta_1 = cosX_4 cosX_5$; h_0 is the initial length of h_1, i.e. the draft of the cylinder in equilibrium position.

The variable center of buoyancy of this partially submerged cylinder piercing the water surface at an angle is described by the radius vector in the (x_t, y_t, z_t) system, i.e. $\vec{\rho}_{B/G_t} = (x_t^B, y_t^B, z_t^B)$, and can be calculated by Eqn. (3.15) in Chapter 3. The hydrostatic restoring moment from the cylinder can be expressed as $\vec{M}_B^s = \vec{\rho}_{B/G_s} \times (T_{I\to s}\vec{F}_B^I)$, in which the radius vector $\vec{\rho}_{B/G_s}$ can be calculated by $\vec{\rho}_{B/G_s} = \vec{\rho}_{B/G_t} + \vec{\rho}_{G_t/G_s}$. This moment is decomposed into the translating-rotating system (x_s, y_s, z_s) to be consistent with the inertia forcing in the RHS of Eqn. (4.1). The restoring forcing from the fully submerged part of the floater (taper and lower larger cylinder) is combined to previous contribution from surface-piercing cylinder to estimate total

hydrostatic force.

The calculation of mooring forcing from four radial taut lines is similar to Chapter 3 by determining the position of the fairlead of each line with respect to the CM of the tower. The radius position of any one fairlead (point A) in the inertia coordinate system (X, Y, Z) is $\vec{\rho}_{A/O} = \vec{\rho}_{G_t/O} + T_{t\to I}\vec{\rho}_{A/G_t}$, where the radius vector $\vec{\rho}_{G_t/O}$ results from Eqn. (4.14); $\vec{\rho}_{A/G_t}$ is the radius position of point A in the (x_t, y_t, z_t) system. The tension along a neutrally buoyant taut line in the (X, Y, Z) system can be obtained by Eqn. (3.16) in Chapter 3. The restoring force of the mooring system is obtained by summing the force from each line. Similarly, the restoring moment from each line in the (x_s, y_s, z_s) system is summed to obtain the contribution from the entire mooring system.

b. Environmental Forcing

The wind force in the (X, Y, Z) system and wind moment calculated about G_s in the (x_s, y_s, z_s) system are needed in the application of equations of motion of the system. The wind thrust force is assumed to be applied on the center of the blade area (G_r in Fig. 27) and along the B-axis, i.e., perpendicular to the swept blade area. The amplitude of wind force (F_b) depends on relative wind velocity and can be calculated by Eqn. (3.19) in Chapter 3.

The amplitude of relative velocity, V_{rb}, is computed by projecting both the wind velocity and structural velocity onto the B-axis through dot product, i.e. $V_{rb} = \vec{V}^I_{wind} \cdot \vec{u}^I_B - \vec{V}^I_{G_r} \cdot \vec{u}^I_B$, in which $\vec{V}^I_{wind}$ is the wind velocity measured from the (X, Y, Z) system. The structural velocity of the center of the blade area can be expressed as:

$\vec{V}^I_{G_r} = [\dot{X}_1\, \dot{X}_2\, \dot{X}_3]^T + T_{s\to I}\vec{v}_{G_r/G_s}$, where the relative velocity $\vec{v}_{G_r/G_s}$ can be obtained by similar form to Eqn. (4.11). The unit vector $\vec{u}^I_B$ indicates the direction of the B-axis in the (X, Y, Z) system by $\vec{u}^I_B = T_{r\to I}\vec{u}^r_B$, where $\vec{u}^r_B$ is the unit vector along B-axis in the (x_r, y_r, z_r) system, i.e. $\vec{u}^r_B = (0, 1, 0)$. The transformation matrix from (x_r, y_r, z_r) to (X, Y, Z), $T_{r\to I}$, is obtained by multiplication of the transformation matrix: $T_{r\to I} = T_{s\to I}T_{r\to s}$.

Finally the wind force in the (X, Y, Z) system and the wind moment in the (x_s, y_s, z_s) system are expressed as:

$$\vec{F}_{wind} = T_{r\to I}\vec{F}^r_{wind} \tag{4.16}$$

$$\vec{M}_{wind} = \vec{\rho}_{G_r/G_s} \times \vec{F}^r_{wind} \tag{4.17}$$

where $\vec{F}^r_{wind}$ is the wind force in the (x_r, y_r, z_r) system: $\vec{F}^r_{wind} = (0, -F_b, 0)$. The aerodynamic torque is modeled as a constant using rated power divided by rotor speed, which is added to the wind moment.

Similar to Chapter 3, the generalized Morison equation (Eqn. (3.22)) is used to calculate the wave forces per unit length normal to the axis of the leaning cylinder. The structural velocity and acceleration of the segment along the tower can be obtained by the kinematics of rigid body:

$$\vec{V}_t = \vec{V}_{G_t} + T_{s\to I}(\vec{\omega}_t \times \vec{\rho}_{i/G_t}) \tag{4.18}$$

$$\dot{\vec{V}}_t = \vec{a}_{G_t} + T_{s\to I}[\dot{\vec{\omega}}_t \times \vec{\rho}_{i/G_t} + \vec{\omega}_t \times (\vec{\omega}_t \times \vec{\rho}_{i/G_t})] \tag{4.19}$$

where $\vec{V}_{G_t}$ and $\vec{a}_{G_t}$ are the linear velocity and acceleration of the CM of the tower, G_t, in the inertial coordinate system (X, Y, Z); $\vec{\rho}_{i/G_t}$ is the vector radius from G_t to

the segment with unit length.

The wave force on the cylinder is obtained by summing the force on each segment from Eqn. (3.22). The wave moment in the (x_s, y_s, z_s) coordinate system can be computed by transforming the resulting forces from Eqn. (3.22) into the (x_s, y_s, z_s) system and then numerically integrating over the submerged length of the tower. In the calculation of wave moment from each segment, the arm can be expressed by $\vec{\rho}_{i/G_s} = \vec{\rho}_{i/G_t} + \vec{\rho}_{G_t/G_s}$.

D. Example

A compliant floating wind turbine design is obtained by truncating the spar cylinder of OC3-Hywind model [60] from from 120 m to 84.4 m, saving about 2500 tonnes, or about or about 30% in total weight. This reduction also reduces the available hydrostatic restoring moment and allows larger pitch angle. OC3-Hywind is the numerical model based on Statoil's original Hywind system, but was modified to support the NREL 5-MW wind turbine. The topsides (nacelle and rotor) of the truncated model are the same as that in OC3-Hywind: the moment of inertia of nacelle about yaw axis is 2.61×10^6 kg·m^2; the moment of inertia of rotor about spin axis is 3.54×10^7 kg·m^2. The displaced volume of water is reduced from the original 8.03×10^3 m^3 to 5.56×10^3 m^3. The moments of inertia of the tower (including hull) w.r.t. the (x_t, y_t, z_t) system originated from G_t are 5.85×10^9 kg·m^2 and 1.12×10^8 kg·m^2 in the tilt (roll and/or pitch) and yaw, respectively. The four taught-leg mooring lines are each assumed to be a straight axial spring with stiffness of 6.81×10^5 N/m and length of 564-m in a 320-m water depth location. The origin of

the global coordinate system (X, Y, Z) is the initial position of the CM of the tower, i.e. 58.67 m below still water level.

The truncated design is first used to verify the new method by comparison with the popular wind turbine dynamics software FAST [46] for a small-amplitude motion case. The same model is then applied to large-amplitude motion. Results for a 2-body system in Chapter 3 and 3-body system are critically compared to quantify the influence of including small changes to the position of the CM of the system (G_s) caused by nacelle yaw. Finally, the new method is applied to simulate the general motion of the compliant design subject to nacelle yaw associated with a rapid wind shift.

1. Free Vibration Verified by FAST

Figs. 28–29 show time histories computed using FAST and those computed using conservation of momentum method for a small-amplitude free vibration case. The rotational DOFs of the tower are transferred to the inertial coordinate system used in FAST to enable direct comparison between (X_4, X_5, X_6) and pitch, roll and yaw, which is valid for small-amplitude rotation [69]. The translational DOFs, (X_{1t}, X_{2t}, X_{3t}), are transferred to the waterplane to enable direct comparison with the sway, surge and heave computed in FAST, which are measured from the (X_M, Y_M, Z_M) system in Fig. 27. Constant nacelle yaw (1.2 deg/sec) and rotor spin (12.1 rpm) are prescribed during the simulation. Here both hydrodynamics and aerodynamics have been disabled in FAST. The only external forces acting on the body are from the mooring lines and buoyancy, both of which are represented in

the user-defined subroutine (UserPtfmLd) in FAST as a 6×6 restoring matrix, with values to be consistent with the method presented in Section 3 but linearized near the average tilt angle and tuned to reproduce the correct natural frequencies. The initial conditions of six DOFs of tower motion are zero. The CM of the nacelle is not directly above the axis of the tower, so nacelle yaw motion changes the position of the CM of the system relative to the tower, which causes the tower motion. Figs. 28–29 show that the global motions of FAST and the momentum method are virtually indistinguishable. The spin axis is initially parallel to the surge direction. The influence of the moving G_s is clearly observable in the coupled motion of translational and rotational moving DOFs. For example, both pitch and surge are minimized (zero crossing) when the nacelle yaw angle is 90 deg (at 75 sec), while roll and sway are maximized. The observed yaw motion results from gyro moments associated with rotor spin coupled with roll and pitch.

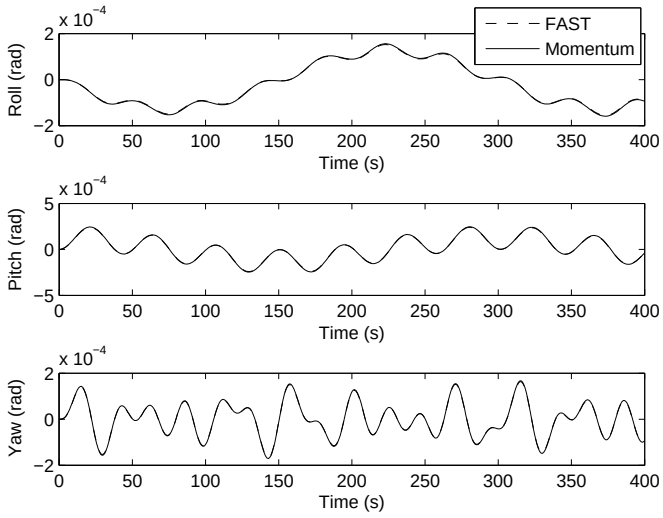

Fig. 28. Rotation compared to FAST (3-body)

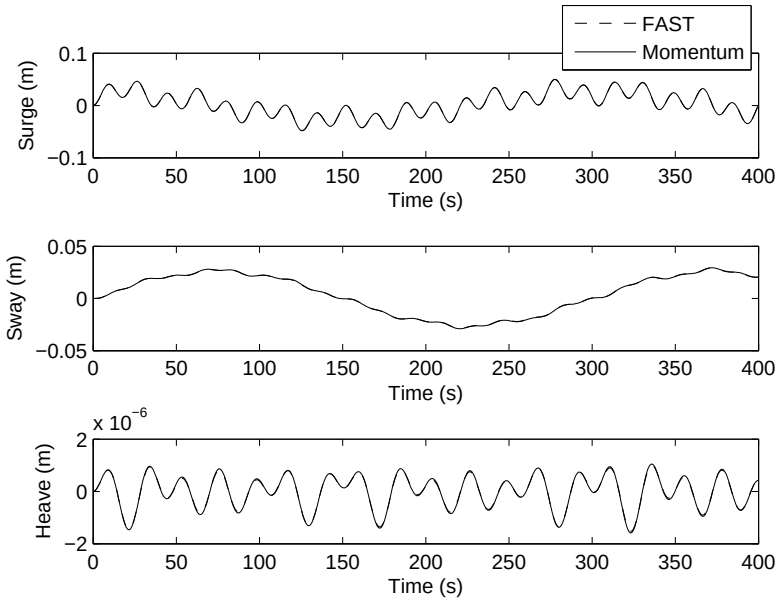

Fig. 29. Translation compared to FAST (3-body)

2. Effect of a Variable Center of Mass on Free Vibration

Figs. 30–31 show the comparison of global motion between the 2-body in Chapter 3 and 3-body systems using the same truncated model. As in the prior example, this is a free-vibration case in which the only externally applied forces are the restoring forces from the mooring lines and hydrostatics. The large-amplitude initial conditions are prescribed to be $X_4 = X_5 = 0.4$ rad. Constant nacelle yaw (0.3 deg/sec) and rotor spin (12.1 rpm) are also prescribed. Figs. 30–31 show the significant influence of

the unconstrained G_s on the global motion (only X_6 and X_{3t} shown). In the 2-body system, the CM of the system (G_s) is constrained to the tower axis and independent of nacelle yaw, because the 2-body representation requires that the radius vector from G_s to the CM of each body (e.g. $\vec{\rho}_{G_t/G_s}$) remains constant. However, the more accurate modeling of the 3-body system enables correct calculation of changes to the CM of G_s associated with nacelle yaw. The effect is that the 3-body model includes changes to both the angular momentum and external moments in rotational EOMs (Eqn. (4.1)) associated with the change of reference point G_s at each time step, which results in significant differences in computed rotation about the tower axis (Figs. 30,X_6). These refinements results cannot be captured by the 2-body model.

Accurate simulation of the unconstrained G_s has a similar effect on vertical motion. The motion of G_s from the 2-body model is transferred to that of G_t through rigid body motion. The moving G_s in the 3-body model, captured by Eqn. (4.14) and coupled with the roll and pitch motions of the tower, introduces the change of the vertical motion of G_t (X_{3t}). In a separate simulation, the overhang length of the rotor in the 3-body system was adjusted to make the CM of the topsides exactly on the top of the tower, such that the 3-body system effectively degenerated to the 2-body system. In this case, the general motion of the 3-body system matched the 2-body system perfectly (plot of results not shown).

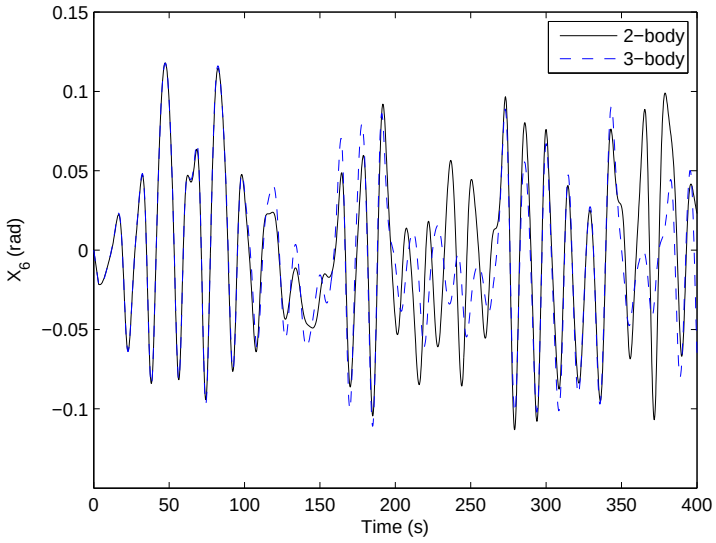

Fig. 30. Rotation comparison between the 2-body and 3-body models

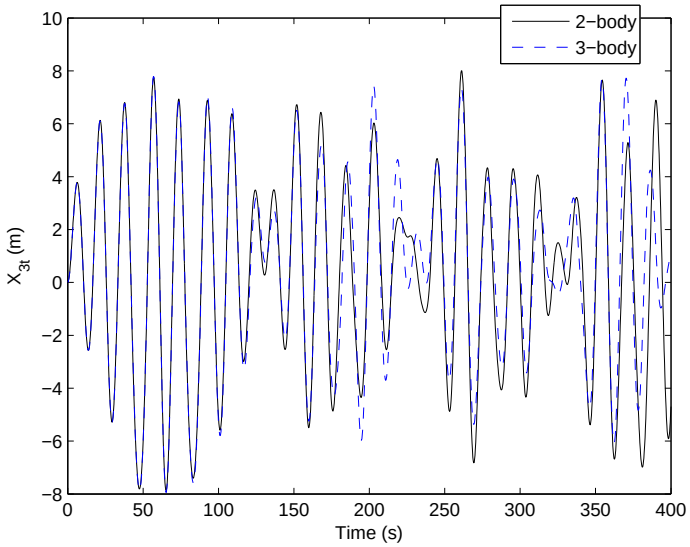

Fig. 31. Translation comparison between the 2-body and 3-body models

3. Forced Vibration with Nacelle Yaw

Figs. 32–34 show global motion for the same compliant spar model subject to realistic environmental forcing. The mean wind velocity at hub height is 18.2 m/s. Irregular wind velocities are simulated using TurbSim [62]. The wave environment is represented by a JONSWAP spectrum with a significant wave height of 5.0 m and peak period of 10 sec. The wind is along the negative direction of the Y-axis during the first 100 sec and then suddenly shifts by $\pi/4$ rad towards the negative direction of the X-axis in the XOY plane. The wind shift causes the nacelle yaw control to activate at 100 sec, yaw the nacelle at a constant 0.3 deg/sec, and then deactivate at around 250 sec. Wave forces are computed using the Morison equation from a first-order time-domain representation of irregular waves simulated directly from the wave spectrum using a uniform phase distribution. The inertia coefficient C_m in Eqn. (3.22) is assumed to be 2.0; the added mass coefficient C_a is assumed to be 1.0; the drag coefficient C_d is assumed to be 0.6. Fig. 32 shows simulation results of 1-2-3 sequenced Euler angles, in which wind forces are computed using the variable thrust coefficient based on Fig. 14. Fig. 33 shows the associated motion of G_t measured from the global coordinate system (X, Y, Z). The nonzero means of X_4 and X_{3t} indicate that the tower is always leaning away from the wind. The change in the mean of X_5 from zero to nonzero is due to the wind shift. Fig. 34 shows the results of a simulation in which wind forces are computed using a fixed thrust coefficient of $C_T = 0.15$ in Eqn. (3.19). Both the sway of G_s (X_1) and roll of the tower (X_5) clearly show the transition of mean between 100 sec and 250 sec. The positive damping introduced by fixed thrust coefficient decreases both the maxima

and the envelope of the motion considerably, as was previously noted by Nielsen [63].

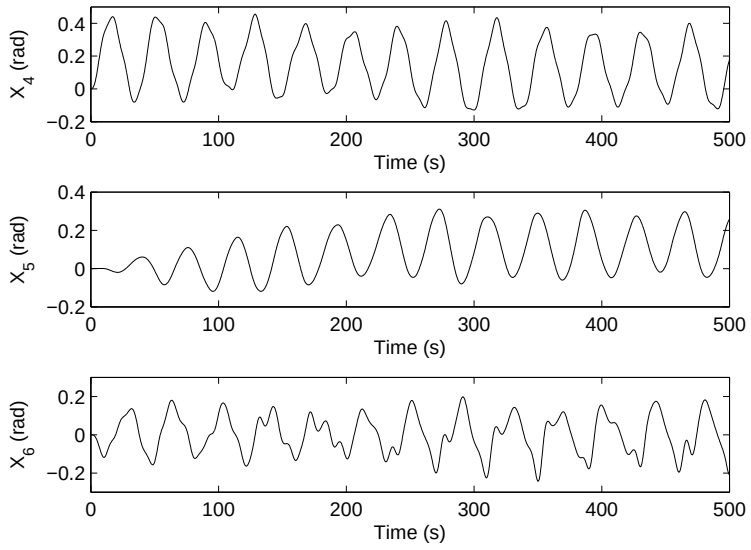

Fig. 32. Rotation with variable thrust coefficient

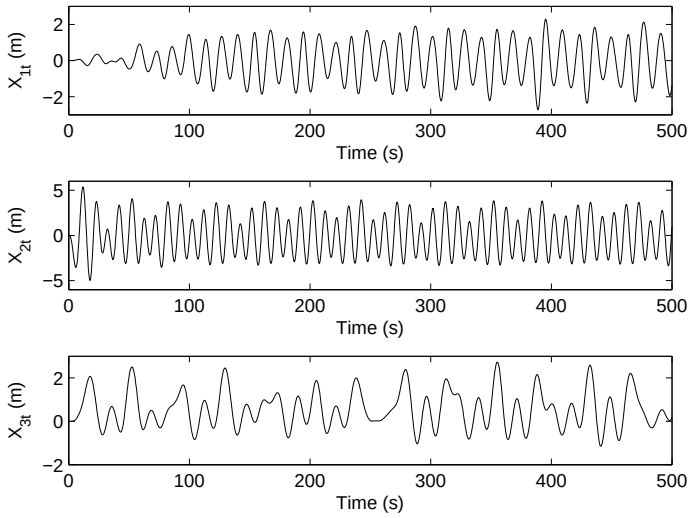

Fig. 33. Translation with variable thrust coefficient

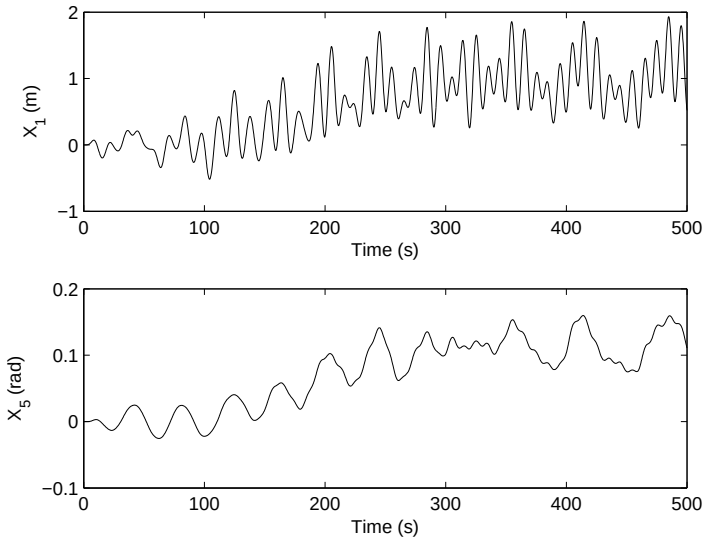

Fig. 34. Motion with fixed thrust coefficient

E. Conclusions

A new formulation of multibody dynamics has been developed to directly apply the conservation of angular momentum to a 3-body compliant floating wind turbine system including tower, nacelle and rotor. An important extension beyond Chapter 3 is that the unconstrained CM of the system due to the relative motion among rigid bodies is considered in the derivation. The coupling between translational and rotational inertial forcing is eliminated by choosing the body-fixed coordinate system of the base body (tower) to derive unknown relative radius vectors between the CM of the system and that of each body. The resulting position and velocity of each body is applied in the calculation of restoring forcing and environmental forcing, which preserves the fully nonlinear coupling between external forcing and large-amplitude motion of the system. The new method is verified by comparison with the well-known software FAST for small-amplitude motion. Comparison of motions between 2-body system in Chapter 3 and 3-body system here is shown to quantify the influence of the unconstrained CM of the system. The new method is also used to simulate the general motion of the compliant design subject to nacelle yaw. A major strength of this new method is that it can be readily expanded and applied to the wind turbine system including more rigid bodies.

CHAPTER V

CONSERVATION OF MOMENTUM FOR N-BODY MODEL

A. Overview

In this Chapter, the method in Chapter 4 is generalized for application to any N-body system. First, the coordinates used in the derivation are standardized: the absolute translation and rotation of a prescribed base body within the system are chosen to be the reference point coordinates, which is equivalent to the unknown degrees of freedom (DOFs) of the multibody system; the relative rotations between contiguous bodies along the kinematic chain within the system are chosen to be relative coordinates, which are mechanically controlled and equivalent to prescribed known DOFs of the system. The theoretical derivations for both forward and inverse dynamics are then systematized using standardized notations. The generalized formulation procedure is named the momentum cloud method (MCM) and it can be applied to establish the EOMs using standard vector and matrix calculations. The resulting EOMs are not coupled between translation and rotation beyond the first-order and so facilitate numerical integration. A key advantage over conventional energy methods is that the MCM avoids tedious rederivation of the EOMs if new rigid bodies are added to the system. The standardization of the new method starts from a simple 2-body model, and is then generalized to the serial N-body system connected by revolute joints with prescribed relative rotation, and finally expanded to more complicated forms and joints. A simulation example is presented for a 6-body floating wind turbine system to demonstrate the results of forward and inverse

dynamics, which are verified by critical comparison with those of the popular wind turbine dynamics software FAST.

B. Introduction and Background

In Chapter 3 and 4, the multibody dynamics of compliant floating wind turbines are investigated by directly applying conservation of momentum to the entire systems. The presented method in this Chapter is an expansion of prior work for application to a generalized rigid multibody system connected by revolute or prismatic joints with prescribed relative motions between contiguous bodies. The main focus is systematic formulation of six basic EOMs associated with the two decoupled 3×3 mass matrices by the momentum cloud method (MCM). In addition to these basic EOMs, a generalized N-body system may also include the EOMs of the unknown DOFs of mechanically controlled joints (control equations) and EOMs describing kinematic relation between selected coordinates (constraint equations). In this case, expansion of the six basic EOMs requires consideration of the effects of both the control and constraint equations through use of numerous system coordinates, including six reference point coordinates of the base body and unknown relative coordinates among contiguous bodies.

The generalization of multibody formulation methods first requires standard notations, based on which systematic theoretical derivation and numerical implementation are then achieved. To mention a few examples, Lucassen [71] analyzes optimal body-fixed coordinate systems in the NE method using standardized parameters and derivaiton. Stoneking [34] presents the systematic derivation of the exact

nonlinear dynamic EOMs for a multibody spacecraft system based on the improved NE method. Garrad [72] investigates the symbolic computing of the EL method and applies it to the research on wind turbine dynamics. In his work, the mathematical formulation of the EOMs is described first in a form suitable for manual derivation and then generalized as a step by step process suitable for automation.

Regardless of the physical theories, the general form of the EOMs is based on the representation of a mass matrix for use in computing the inertial forcing, which is then set equal to the external forcing. The EOMs in this general form are convenient to be written in the first-order decoupled form $\dot{x} = f(x, t)$ for numerical integration [73]. Featherstone [36] investigates the formulation and solution of the EOMs in this general form from the perspective of coding. Orden [74] analyzes the computational methods and applications of multibody dynamics. Some programs based on analytical methods have also been documented in literatures [75]. The efficiency of numerical integration depends on the degree to which the elements in mass matrix are coupled, or say the number of nonzero off-diagonal elements. In this sense, the formulation of current methods introduces a common computational inefficiency: a large number of coupled differential EOMs must be solved simultaneously. To decouple the EOMs including different DOFs as much as possible, a base body is prescribed within the multibody system, and the EOMs of the entire system are projected into the coordinate system relevant to this body. Only six basic EOMs of the system are required to capture 6 unknown DOFs of the base body when mechanical DOFs between contiguous bodies are prescribed. The 6×6 mass matrix is actually composed of two decoupled 3×3 mass matrices for translation and

rotation, respectively. Each element within the matrix includes the inertial effects of all bodies. This condensation decreases the coupling between elements in the mass matrix, and so minimizes the computational demand. This new formulation method is later expanded to multibody systems with more complicated joints and connection types.

Derivation of the MCM first requires selection of a set of proper coordinates. In the sections that follow, these coordinates are developed and applied to a simple 2-body model for which the basic EOMs are formulated. The method is then generalized to a serial N-body system, such as a serial manipulator in robotics, and finally generalized to more complicated forms with branches or loops. The formulation can also be used on the inverse dynamic problem to calculate the internal forcing. An example is presented in which the dynamics of a 6-body floating wind turbine system are simulated. The tower, nacelle, hub and the three blades are each represented as rigid bodies. Results of the forward and inverse dynamics are critically compared with the well-recognized NREL FAST aero-elastic simulator [45].

C. Theory

The coordinate systems and relevant coordinates associated with the N-body model are standardized in Section 1. The basic EOMs for a simple 2-body model are formulated in Section 2. The method is then generalized to a serial N-body system to form the MCM in Section 3 and expanded for systems with more complicated forms and connection joints in Section 4. Finally, inverse dynamics is investigated in Section 5.

1. Coordinate Systems and Dependent Coordinates

A set of proper coordinates is needed to unequivocally define the kinematics of a multibody system [33]. Here, the corresponding coordinate systems are first illustrated by a simple 2-body model. Then the coordinates measured from such coordinate systems are demonstrated and generalized for an N-body system. Finally, the reasons and advantages for such choice of coordinates are investigated.

In the MCM, the reference point coordinates are used to describe the motion of base body; the relative coordinates are used to define the relative motions between contiguous bodies. Several proper coordinate systems are needed to define those coordinates. Fig. 35 shows the detailed definitions of various coordinate systems through a simple 2-body model. B_1 and B_2 are two rigid bodies connected by revolute joint J with known relative rotation. B_1 is specified as the base body. The angular rotation of B_2 relative to B_1 is always expressed relative to its initial position B_2^0. For example, the base body (B_1) is a moving tower, on the top of which is mounted a clock face and rotating hour hand. If the hour hand is initially at 12:00 (B_2^0), then all future positions of B_2 are measured relative to 12:00, regardless of motion of the tower. The coordinate systems (x_1, y_1, z_1) (C_1 system) and (x_2, y_2, z_2) (C_2 system) are body fixed and originate at the CM of bodies, G_1 and G_2, respectively. The C_2^0 system originates at the CM of B_2^0 (G_2^0) and indicates the initial position of the C_2 system. The system-fixed coordinate system (x_s, y_s, z_s) (C_s system) is located at the CM of the system (G_s), and is prescribed to be parallel to the C_1 system. The inertial coordinate system (X, Y, Z) (C_I system) has its origin defined by the initial position of the CM of the base body, such that the radius vector originated from O

to G_1 is the location of G_1 relative to its initial position.

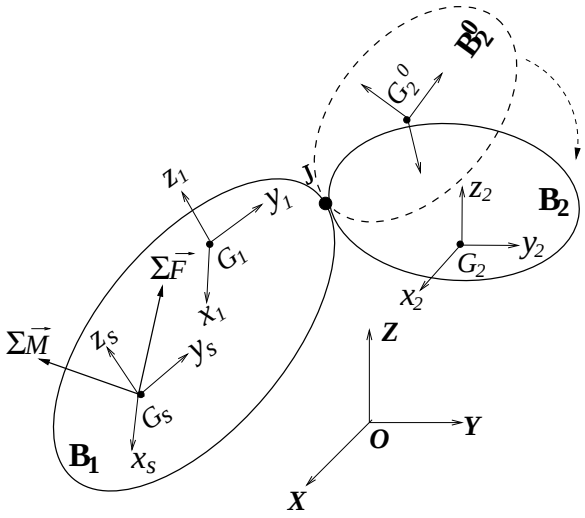

Fig. 35. Two bodies connected by a joint

The dependent coordinates for an N-body system can be defined using similar coordinate systems as that in 2-body model. The reference point coordinates describe the translation and rotation of the base body measured from the inertial coordinate systems. The coordinates (X_1, X_2, X_3) measured from the C_I system are used to define the absolute motion of the CM of the C_s system, G_s. These coordinates are further transferred to the translations at the CM of the C_1 system, G_1, which are notated by the coordinates (X_{1b}, X_{2b}, X_{3b}) and defined as 3 translational DOFs of the base body. The large-amplitude rotation of the base body w.r.t. the C_I system is described by introducing the 1-2-3 sequenced Euler angles X_4-X_5-X_6, which are

3 rotational DOFs of the base body. Thus, the reference point coordinates of the N-body system are represented by (X_{1b}, X_{2b}, X_{3b}) and (X_4, X_5, X_6). The relative coordinates of the N-body system can be measured by the rotation of C_i relative to the C_i^0 system and denoted by the angular velocity vector $\vec{\omega}_{B_i}^{C_i^0}$, which is the rotation of C_2 relative to the C_2^0 system in the 2-body model. Here the relative coordinates include only one prescribed relative angular velocity to simplify the formulation of the EOMs. More unknown relative coordinates can be applied, such as unknown relative rotation angles and orientations of the rotational axes, and can be interconnected through the control and constraint equations.

The reference point coordinates includes two unconventional features. First, they are used to describe the motion of an arbitrarily selected based body: the absolute translation at its CM and the absolute rotation as described by Euler angles. Second, only three rotational reference point coordinates (Euler angles) ultimately appear in the basic EOMs. Relative coordinates define the motion of each successive body (B_i) relative to its neighbor (B_{i-1}) along the kinematic chain by the DOFs allowed by the connecting joint. A cascading procedure is then applied to determine the absolute position of each body other than the base body.

Generally, the dependency of all coordinates are represented by the combination of six basic EOMs, control and constraint equations. In the derivation here, all relative coordinates at different joints are mechanically controlled, which is equivalent to the explicit solution to the control EOMs. The constraint equations are minimized in the derivation by prescribing certain relative coordinates equal to zero and simplifying the associated transformation matrices. However, the MCM can be easily

expanded to the multibody system needing all three kinds of EOMs. In general case, the number of the basic and control EOMs is equal to the unknown DOFs of the system; the number of the constraint equations is equal to the difference between the number of dependent coordinates and that of the DOFs of the system. The control equations can be of any complexity, e.g. from the response of a spring to a highly complex numerical control system. The solution to the control equations at a single point of time actually imposes a constraint at that time. In this sense, the control and constraint equations receive comparable treatment in the MCM: the solutions to them are represented in six basic EOMs in the form of various transforms.

An ideal selection of the coordinates both simplifies formulation of the EOMs and increases the efficiency of the numerical integration. Any coordinate introduced to a multibody dynamics problem becomes an unknown, which require an additional equation to solve. The combination of reference point and relative coordinates guarantees that some dependent coordinates can be eliminated from the basic EOMs with only trivial computational demand. The basic coupled differential EOMs of the system are by far the most computationally demanding to solve, so minimizing the number of coordinates in these equations is of primary importance. Here, a very large number of coordinates is applied to facilitate the establishment of the EOMs, but the formulation enables elimination of all but six reference point coordinates from the basic EOMs.

2. Equations of Motion for 2-Body System

The methodology is developed for a simple 2-body model connected by one revolute joint with one prescribed relative angular velocity (Fig. 35). Future sections will further generalize the derivation to more complex system.

a. Rotational Equations of Motion

Beginning with conservation of angular momentum, the sum of the moments resulting from externally applied forces about the CM of a system of particles in the translating-rotating system, (x_s, y_s, z_s), equals the change of amplitude of the momentum within the coordinate system plus the change of direction of the momentum with respect to global coordinate system (e.g. [58]). The rotational EOMs can be shown by Chapter 4 as:

$$ {}^{B_1}\vec{M}_{G_s}^{C_s} + {}^{B_2}\vec{M}_{G_s}^{C_s} \;=\; \left({}^{s}\dot{\vec{H}}_{G_s}^{C_s}\right)_{C_s} + \vec{\omega}_{C_s} \times {}^{s}\vec{H}_{G_s}^{C_s} \tag{5.1} $$

where the notation $(\dot{\ })_{C_s}$ is the local derivative within the C_s system, i.e. the rate of change of the total quantity with respect to time. For the 2-body system shown in Fig. 35, ${}^{s}\vec{H}_{G_s}^{C_s}$ is the sum of the angular momenta of B_1 and B_2 w.r.t. the CM of the system, G_s, which is totally different from the angular momentum of one rigid body in the conventional Euler dynamic equations. The vector $\vec{\omega}_{C_s}$ describes the angular velocity of the C_s system w.r.t. the inertial coordinate system C_I. The moment vectors ${}^{B_1}\vec{M}_{G_s}^{C_s}$ and ${}^{B_2}\vec{M}_{G_s}^{C_s}$ represent the external moments applied to B_1 and B_2, which are calculated about G_s and decomposed onto the C_s system.

Application of the theorem of conservation of angular momentum to a system

requires that the momentum be calculated about the CM of the system. Here, the momentum of each body is computed about G_s, and projected onto a coordinates system parallel to the C_1 system. Computation of the absolute derivative of the angular momentum of each rigid body is simplified by decomposing its absolute angular velocity onto a body-fixed coordinate system (C_i) , then projecting the resulting momentum back into the system-fixed coordinate system (C_s) in accordance with conventional Euler dynamics equations (e.g. [58]). Using this method, the angular momentum of each body is computed in its body-fixed coordinate system and transferred to the C_s system without introducing any new coordinates.

In a 2-body system, the angular momentum of each of the two rigid bodies is first calculated in the body-fixed coordinate system C_1 or C_2 about G_1 or G_2, then transformed to the unified C_s system and finally transferred to the unified reference point, G_s. The angular momentum of the 2-body system with respect to G_s and projected to the C_s system is:

$$ {}^{s}\vec{H}^{C_s}_{G_s} = {}^{B_1}\vec{H}^{C_s}_{G_s} + {}^{B_2}\vec{H}^{C_s}_{G_s} \tag{5.2} $$

where ${}^{B_1}\vec{H}^{C_s}_{G_s}$ and ${}^{B_2}\vec{H}^{C_s}_{G_s}$ are the angular momenta of B_1 and B_2 w.r.t. G_s and projected to the C_s system, respectively, and can be shown to be:

$$ \begin{aligned} {}^{B_1}\vec{H}^{C_s}_{G_s} &= T_{C_1\to C_s}\,{}^{B_1}\vec{H}^{C_1}_{G_1} + \vec{\rho}^{C_s}_{G_1/G_s}\times m_1\vec{v}^{C_s}_{G_1/G_s} \\ &= T_{C_1\to C_s}\left(I_{B_1}\vec{\omega}^{C_1}_{B_1}\right) + \vec{\rho}^{C_s}_{G_1/G_s}\times m_1\vec{v}^{C_s}_{G_1/G_s} \\ {}^{B_2}\vec{H}^{C_s}_{G_s} &= T_{C_2\to C_s}\,{}^{B_2}\vec{H}^{C_2}_{G_2} + \vec{\rho}^{C_s}_{G_2/G_s}\times m_2\vec{v}^{C_s}_{G_2/G_s} \\ &= T_{C_2\to C_s}\left(I_{B_2}\vec{\omega}^{C_2}_{B_2}\right) + \vec{\rho}^{C_s}_{G_2/G_s}\times m_2\vec{v}^{C_s}_{G_2/G_s} \end{aligned} \tag{5.3} $$

in which the angular momentum of each body is first calculated in the C_1 or C_2 system about G_1 or G_2 ($^{B_1}\vec{H}_{G_1}^{C_1}$ or $^{B_2}\vec{H}_{G_2}^{C_2}$), and then transformed into the unified C_s system by transformation matrixes $T_{C_1\to C_s}$ or $T_{C_2\to C_s}$. Finally, addition of the radius cross-product terms transfers the local momentum to the unified reference point G_s. I_{B_1} and I_{B_2} are the tensors of moment of inertia w.r.t. the C_1 and C_2 systems. $\vec{\omega}_{B_1}^{C_1}$ and $\vec{\omega}_{B_2}^{C_2}$ are the absolute angular velocities of B_1 and B_2 and decomposed to the C_1 and C_2 systems, respectively, which can be shown to be:

$$\begin{aligned}
\vec{\omega}_{B_1}^{C_1} &= \begin{bmatrix} \dot{X}_4\cos X_5\cos X_6 + \dot{X}_5\sin X_6 \\ -\dot{X}_4\cos X_5\sin X_6 + \dot{X}_5\cos X_6 \\ \dot{X}_4\sin X_5 + \dot{X}_6 \end{bmatrix} \\
\vec{\omega}_{B_2}^{C_2} &= T_{C_1\to C_2}\vec{\omega}_{B_1}^{C_1} + T_{C_2^0\to C_2}\vec{\omega}_{B_2}^{C_2^0}
\end{aligned} \tag{5.4}$$

where the expressions of $\vec{\omega}_{B_1}^{C_1}$ are Euler kinematic equations [69] associated with the rotational reference point coordinates (X_4, X_5, X_6) and are equal to $\vec{\omega}_{C_s}$ in Eqn. (5.1) because the C_s system is parallel to the C_1 system; $\vec{\omega}_{B_2}^{C_2}$ is obtained along the kinematic chain by combining the effects of $\vec{\omega}_{B_1}^{C_1}$ and $\vec{\omega}_{B_2}^{C_2^0}$ and transforming the results into the common C_2 system. The prescribed angular velocity of B_2 relative to B_1, $\vec{\omega}_{B_2}^{C_2^0}$, is measured relative to the C_2^0 system, which is fixed to B_1 and parallel to the initial position of B_2. The C_2^0 system is introduced as a convenient reference for relative rotation between B_2 and B_1. The transformation matrix $T_{C_1\to C_2}$ can be obtained as $T_{C_1\to C_2} = T_{C_2^0\to C_2}T_{C_1\to C_2^0}$, in which $T_{C_1\to C_2^0}$ is the direction cosine matrix between two body-fixed coordinate systems. $T_{C_1\to C_2^0}$ is time-independent and can be obtained from initial positions; $T_{C_2^0\to C_2}$ is time-dependent and can be calculated

from known mechanical rotations at the joint.

The cross product terms in Eqn. (5.3) transfer the reference point of angular momentum from the CM of the body to the CM of the system (e.g. [58]). The CM of the system, G_s, is time-varying and not constrained to any rigid body, as dictated by arbitrary relative motion between rigid bodies. The CM of each body (G_1 and G_2) and of the system (G_s) are expressed through defining all relative motions due to joint rotations in the body-fixed C_1 system, which makes the radius vectors ($\vec{\rho}^{C_s}_{G_1/G_s}$ and $\vec{\rho}^{C_s}_{G_2/G_s}$) independent of the absolute motion of G_s. This independence makes the inertial forcing in three basic rotational EOMs independent of (X_1, X_2, X_3), which dramatically simplifies the formulation and solution of the EOMs.

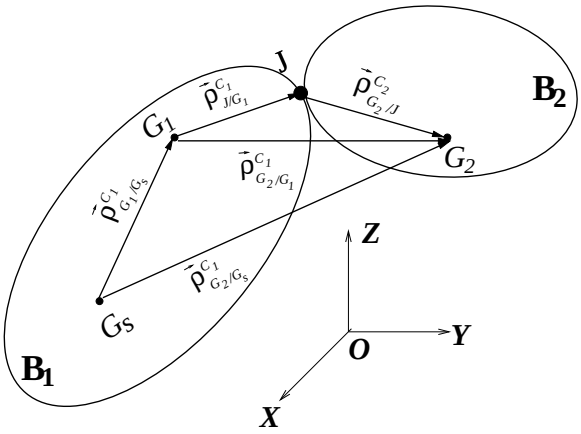

Fig. 36. Calculation of radius vectors

The relative positions of G_1 and G_2 to G_s are obtained by vectorial combina-

tion; the CM of the system, G_s, is computed as a weighted average; and motions between bodies are computed directly from transformation matrix representing joint rotations.

$$\begin{aligned}
\vec{\rho}^{C_s}_{G_1/G_s} &= \vec{\rho}^{C_1}_{G_1/G_s} = \vec{\rho}^{C_1}_{G_1/G_1} - \vec{\rho}^{C_1}_{G_s/G_1} \\
\vec{\rho}^{C_s}_{G_2/G_s} &= \vec{\rho}^{C_1}_{G_2/G_s} = \vec{\rho}^{C_1}_{G_2/G_1} - \vec{\rho}^{C_1}_{G_s/G_1} \\
\vec{\rho}^{C_1}_{G_s/G_1} &= \frac{m_1\vec{\rho}^{C_1}_{G_1/G_1} + m_2\vec{\rho}^{C_1}_{G_2/G_1}}{m_1+m_2} \\
\vec{\rho}^{C_1}_{G_2/G_1} &= \vec{\rho}^{C_1}_{J/G_1} + T_{C_2\to C_1}\vec{\rho}^{C_2}_{G_2/J}
\end{aligned} \tag{5.5}$$

in which vector $\vec{\rho}^{C_1}_{G_1/G_1}$ has zero magnitude, but is included here for completeness because it aids in the generalization to an N-body system. Radius vectors $\vec{\rho}^{C_1}_{J/G_1}$ and $\vec{\rho}^{C_2}_{G_2/J}$ indicate the fixed locations of the joint on two rigid bodies. The final radius vectors in the C_s system, $\vec{\rho}^{C_s}_{G_1/G_s}$ and $\vec{\rho}^{C_s}_{G_2/G_s}$, are equal to the correspondents in the C_1 system.

The relative linear velocities in Eqn. (5.3), $\vec{v}^{C_s}_{G_1/G_s}$ and $\vec{v}^{C_s}_{G_2/G_s}$, are computed as the absolute derivatives of the radius vectors of $\vec{\rho}^{C_s}_{G_1/G_s}$ and $\vec{\rho}^{C_s}_{G_2/G_s}$, respectively:

$$\begin{aligned}
\vec{v}^{C_s}_{G_1/G_s} &= \frac{d\vec{\rho}^{C_s}_{G_1/G_s}}{dt} = \left(\dot{\vec{\rho}}^{C_s}_{G_1/G_s}\right)_{C_s} + \vec{\omega}_{C_s}\times\vec{\rho}^{C_s}_{G_1/G_s} \\
\vec{v}^{C_s}_{G_2/G_s} &= \frac{d\vec{\rho}^{C_s}_{G_2/G_s}}{dt} = \left(\dot{\vec{\rho}}^{C_s}_{G_2/G_s}\right)_{C_s} + \vec{\omega}_{C_s}\times\vec{\rho}^{C_s}_{G_2/G_s}
\end{aligned} \tag{5.6}$$

the form of which is similar to Eqn. (5.1) because $\vec{\rho}^{C_s}_{G_1/G_s}$ and $\vec{\rho}^{C_s}_{G_2/G_s}$ are decomposed into the rotating C_s system. It is significant that the translation of the system, (X_1, X_2, X_3), do not appear in Eqns. (5.5) and (5.6), such that motions due to rotations are calculated independent from translation of the system, which greatly

facilitates the numerical integration.

b. Translational Equations of Motion

Similar to the rotational EOMs, the conservation of linear momentum is applied to the 2-body system directly to avoid the calculation of internal forces between rigid bodies:

$$\vec{F}_{B_1}^{C_I} + \vec{F}_{B_2}^{C_I} = (m_1 + m_2)\vec{a}_{G_s}^{C_I} \tag{5.7}$$

where $\vec{a}_{G_s}^{C_I}$ is the linear acceleration of the CM of the system, $\vec{a}_{G_s}^{C_I} = [\ddot{X}_1, \ddot{X}_2, \ddot{X}_3]$; m_1 and m_2 are the masses of two bodies; the force vectors $\vec{F}_{B_1}^{C_I}$ and $\vec{F}_{B_2}^{C_I}$ represent the external forces applied to B_1 and B_2 in the inertial coordinate system (X, Y, Z). The solution to this translational EOMs is the motion of the CM of the system (G_s) measured from the (X, Y, Z) system. G_s is not constrained to any body. However, Eqn. (5.7) is solved directly for motion of G_s because it enables decoupling of translations from rotations.

The absolute position of each body is needed to compute the external forcing, and can be found by combining translations from the direct integration result of Eqn. (5.7) with rotations from integration result of Eqn. (5.1):

$$\begin{aligned} \vec{\rho}_{G_1/O}^{C_I} &= \vec{\rho}_{G_s/O}^{C_I} + T_{C_s \to C_I} \vec{\rho}_{G_1/G_s}^{C_s} \\ \vec{\rho}_{G_2/O}^{C_I} &= \vec{\rho}_{G_s/O}^{C_I} + T_{C_s \to C_I} \vec{\rho}_{G_2/G_s}^{C_s} \end{aligned} \tag{5.8}$$

where the radius vector $\vec{\rho}_{G_s/O}^{C_I}$ is the position of the CM of the system: $\vec{\rho}_{G_s/O}^{C_I} = [X_1, X_2, X_3]$; $\vec{\rho}_{G_1/G_s}^{C_s}$ and $\vec{\rho}_{G_2/G_s}^{C_s}$ result from Eqn. (5.5). The resulting $\vec{\rho}_{G_1/O}^{C_I}$ has ad-

ditional significance in that it describes the position of the base body represented by 3 translational reference point coordinates: $\vec{\rho}^{C_I}_{G_1/O} = [X_{1b}, X_{2b}, X_{3b}]$. The transformation matrix from (x_s, y_s, z_s) to (X, Y, Z), $T_{C_s \to C_I}$, needed in Eqn. (5.8) can be calculated by Eqn. (3.13) in Chapter 3.

Application of this method in a numerical time-domain simulation tool requires the initial displacement of G_s. This initial condition is computed from the prescribed initial displacements of the base body and initial joint displacements by solving the first line in Eqn. (5.8) for $\vec{\rho}^{C_I}_{G_s/O}$. Eqn. (5.8) is applied in future time steps to transform the motion of G_s resulting from integration of Eqn. (5.7) to G_1 and G_2 for the calculation of external forcing. Thus, Eqn. (5.8) can be used as both preprocessing and postprocessing procedures in the new method.

3. Generalization to a Serial N-Body System

This section generalizes the 2-body derivation to a serial N-body system. Six basic EOMs are formulated for a series of N bodies connected by revolute joints with prescribed relative angular velocities. Eqns. (5.1) and (5.7) are the basic EOMs resulting from the conservation of linear and angular momenta. Application of the same derivation to a serial N-body system results in vector equations representing three translational and three rotational EOMs, respectively:

$$\begin{aligned} \sum_{i=1}^{N} \vec{F}^{C_I}_{B_i} &= \left(\sum_{i=1}^{N} m_i \right) \vec{a}^{C_I}_{G_s} \\ \sum_{i=1}^{N} {}^{B_i}\vec{M}^{C_s}_{G_s} &= \left({}^{s}\dot{\vec{H}}^{C_s}_{G_s} \right)_{C_s} + \vec{\omega}_{C_s} \times {}^{s}\vec{H}^{C_s}_{G_s} \end{aligned} \tag{5.9}$$

The forces $\sum_{i=1}^{N} \vec{F}_{B_i}^{C_I}$ are externally applied and projected into the inertial C_I system; $\sum_{i=1}^{N} m_i$ is the mass of the entire system; $\vec{a}_{G_s}^{C_I}$ is the acceleration of the CM of the system (G_s). In the rotational EOMs, the external moments on each body, ${}^{B_i}\vec{M}_{G_s}^{C_s}$, are calculated about G_s and projected into the system-fixed C_s coordinate system; ${}^{s}\vec{H}_{G_s}^{C_s}$ is the total angular momentum of the N-body system, which is also calculated about G_s and projected into the C_s system; the absolute angular velocity of the C_s system, $\vec{\omega}_{C_s}$, can be obtained using Eqn. (5.4). Similar to Eqn. (5.8), the absolute position of each rigid body is specified as radius vector to the origin of inertial coordinate system (X, Y, Z):

$$\vec{\rho}_{G_i/O}^{C_I} = \vec{\rho}_{G_s/O}^{C_I} + T_{C_s \to C_I} \vec{\rho}_{G_i/G_s}^{C_s} \quad (i \geqslant 1) \tag{5.10}$$

in which the vector $\vec{\rho}_{G_s/O}^{C_I}$ is the absolute motion of G_s in the C_I system and results from the integration of the translational EOMs; radius vector $\vec{\rho}_{G_i/G_s}^{C_s}$ is from G_s to the CM of each rigid body, G_i, and is measured in the C_s system.

The logic underlying the N-body derivation is only slightly more complicated than that of the 2-body case. Conservation of angular momentum for an N-body system first requires development of general expressions of total angular momentum of the system and its local derivative. Then systematic application, including final formulation of the EOMs and numerical implementation, is presented.

a. Calculation of Angular Momentum

The total angular momentum can be summed over the N-body system:

$$ {}^{s}\vec{H}^{C_s}_{G_s} = \sum_{i=1}^{N} {}^{B_i}\vec{H}^{C_s}_{G_s} \tag{5.11} $$

of which Eqn. (5.2) is a special case, and for which the angular momentum of the i-th body about G_s and projected into the C_s system ($^{B_i}\vec{H}^{C_s}_{G_s}$) results from generalization of Eqn. (5.3):

$$ {}^{B_i}\vec{H}^{C_s}_{G_s} = T_{C_i \to C_s} {}^{B_i}\vec{H}^{C_i}_{G_i} + \vec{\rho}^{C_s}_{G_i/G_s} \times m_i \vec{v}^{C_s}_{G_i/G_s} \tag{5.12} $$

Each term in Eqn. (5.12) is calculated individually, and then substituted back to Eqn. (5.11) to obtain the total angular momentum.

First, $^{B_i}\vec{H}^{C_i}_{G_i}$ is the angular momentum of B_i calculated about the CM of the body, G_i, and decomposed onto C_i, the body-fixed coordinate system of B_i. This angular momentum of a rigid body is:

$$ {}^{B_i}\vec{H}^{C_i}_{G_i} = I_{B_i} \vec{\omega}^{C_i}_{B_i} \tag{5.13} $$

in which I_{B_i} is the tensor of moment of inertia of B_i. The absolute angular velocity of bodies numbered sequentially outward from the base body can be computed as the second expression of Eqn. (5.4) in a cascading format:

$$ \begin{aligned} \vec{\omega}^{C_i}_{B_i} &= T_{C_{i-1} \to C_i} \vec{\omega}^{C_{i-1}}_{B_{i-1}} + T_{C_i^0 \to C_i} \vec{\omega}^{C_i^0}_{B_i} \quad (i \geqslant 2) \\ T_{C_{i-1} \to C_i} &= T_{C_i^0 \to C_i} T_{C_{i-1} \to C_i^0} \end{aligned} \tag{5.14} $$

in which the C_i^0 system describes the initial position of B_i relative to B_{i-1}; $T_{C_{i-1} \to C_i^0}$

is time invariant and results from the initial direction cosine matrix between B_{i-1} and B_i^0; $T_{C_i^0 \to C_i}$ represents mechanical rotation.

Back to Eqn. (5.12), the transformation matrix for any body motion relative to the base body can be expressed by the consecutive multiples of the transformation matrices between contiguous bodies along the kinematic chain:

$$T_{C_i \to C_s} = T_{C_i \to C_1} = \prod_{j=2}^{i} T_{C_j \to C_{j-1}} = \prod_{j=2}^{i} T_{C_j^0 \to C_{j-1}} T_{C_j \to C_j^0} \quad (i \geqslant 2) \tag{5.15}$$

The cross product term in Eqn. (5.12) is related to the unconstrained CM of the system, G_s. Relative radius vector ($\vec{\rho}^{\,C_s}_{G_i/G_s}$) and its derivative ($\vec{v}^{\,C_s}_{G_i/G_s}$) are derived using the same methodology as Eqns. (5.5) and (5.6):

$$\begin{aligned}
\vec{\rho}^{\,C_{i-1}}_{G_i/G_{i-1}} &= \vec{\rho}^{\,C_{i-1}}_{J_{i-1}/G_{i-1}} + T_{C_i \to C_{i-1}} \vec{\rho}^{\,C_i}_{G_i/J_{i-1}} \quad (i \geqslant 2) \\
\vec{\rho}^{\,C_1}_{G_i/G_1} &= \vec{\rho}^{\,C_1}_{G_{i-1}/G_1} + T_{C_{i-1} \to C_1} \vec{\rho}^{\,C_{i-1}}_{G_i/G_{i-1}} \quad (i \geqslant 3) \\
\vec{\rho}^{\,C_1}_{G_s/G_1} &= \frac{\sum_{i=1}^{N} m_i \vec{\rho}^{\,C_1}_{G_i/G_1}}{\sum_{i=1}^{N} m_i} \\
\vec{\rho}^{\,C_s}_{G_i/G_s} &= \vec{\rho}^{\,C_1}_{G_i/G_s} = \vec{\rho}^{\,C_1}_{G_i/G_1} - \vec{\rho}^{\,C_1}_{G_s/G_1} \quad (i \geqslant 1) \\
\vec{v}^{\,C_s}_{G_i/G_s} &= \frac{d\vec{\rho}^{\,C_s}_{G_i/G_s}}{dt} = \left(\dot{\vec{\rho}}^{\,C_s}_{G_i/G_s}\right)_{C_s} + \vec{\omega}_{C_s} \times \vec{\rho}^{\,C_s}_{G_i/G_s} \quad (i \geqslant 1)
\end{aligned} \tag{5.16}$$

This methodology offers the same computational advantage for an N-body system as for a 2-body system: decoupling the rotational reference point coordinates, (X_4, X_5, X_6), from the absolute motion of G_s, (X_1, X_2, X_3).

Eqns. (5.11)-(5.16) can be condensed into a single expression for the total angular

momentum of the N-body system about the reference point G_s:

$$\begin{aligned} {}^{s}\vec{H}_{G_s}^{C_s} &= \sum_{i=1}^{N}\left(T_{C_i\to C_s}\,{}^{B_i}\vec{H}_{G_i}^{C_i} + \vec{\rho}_{G_i/G_s}^{C_s}\times m_i\vec{v}_{G_i/G_s}^{C_s}\right) \\ &= P_1\vec{\omega}_{B_1}^{C_1} + Q_1 + P_2\vec{\omega}_{B_1}^{C_1} + Q_2 \end{aligned} \tag{5.17}$$

in which the terms $P_1\vec{\omega}_{B_1}^{C_1}$ and Q_1 represent the total angular momentum of each body calculated about its own CM (G_i) but projected into the unified C_s system, i.e. $\sum_{i=1}^{N} T_{C_i\to C_s}\,{}^{B_i}\vec{H}_{G_i}^{C_i}$; the terms $P_2\vec{\omega}_{B_1}^{C_1}$ and Q_2 represent the effect of transferring from the CM of each body (G_i) to the unified reference point(G_s), i.e. $\sum_{i=1}^{N}\vec{\rho}_{G_i/G_s}^{C_s}\times m_i\vec{v}_{G_i/G_s}^{C_s}$. Each of the four coefficients represents a sum over the entire system:

$$\begin{aligned} P_1 &= \sum_{i=1}^{N} T_{C_i\to C_s} I_{B_i} T_{C_1\to C_i} \\ Q_1 &= \sum_{i=2}^{N}\left[\left(\sum_{j=i}^{N} T_{C_j\to C_s} I_{B_j} T_{C_i^0\to C_j}\right)\vec{\omega}_{B_i}^{C_i^0}\right] \\ P_2 &= \sum_{i=1}^{N} m_i\bar{\rho}_{G_i/G_s} \\ Q_2 &= \sum_{i=1}^{N} m_i\vec{\rho}_{G_i/G_s}^{C_s}\times\left(\dot{\vec{\rho}}_{G_i/G_s}^{C_s}\right)_{C_s} \end{aligned} \tag{5.18}$$

where the calculation of $P_2\vec{\omega}_{B_1}^{C_1}$ is simplified through use of a matrix identity $\vec{\rho}_{G_i/G_s}^{C_s}\times(\vec{\omega}_{B_1}^{C_1}\times\vec{\rho}_{G_i/G_s}^{C_s}) = \bar{\rho}_{G_i/G_s}\vec{\omega}_{B_1}^{C_1}$ [34]. $\bar{\rho}_{G_i/G_s}$ is introduced as a computational convenience and calculated by Eqn. (4.12) in Chapter 4. The three elements of any radius vector $\vec{\rho}_{G_i/G_s}^{C_s}$ are represented by $[\rho_1, \rho_2, \rho_3]$. This matrix identity enables extraction of the angular velocity ($\vec{\omega}_{B_1}^{C_1}$) from the double cross product term, which facilitates the establishment of first-order decoupled EOMs and greatly simplifies derivative

calculations.

b. Calculation of Local Derivative of Angular Momentum

The rotational EOMs in Eqn. (5.9) require the local derivative of the total angular momentum within the C_s system, which is calculated from Eqn. (5.17):

$$\left({}^{s}\dot{\vec{H}}^{C_s}_{G_s}\right)_{C_s} = (P_1 \dot{+} P_2)_{C_s}\vec{\omega}^{C_1}_{B_1} + (P_1 + P_2)\left(\dot{\vec{\omega}}^{C_1}_{B_1}\right)_{C_s} + (Q_1 \dot{+} Q_2)_{C_s} \tag{5.19}$$

in which $(P_1 \dot{+} P_2)_{C_s} = (\dot{P}_1)_{C_s} + (\dot{P}_2)_{C_s}$, $(Q_1 \dot{+} Q_2)_{C_s} = (\dot{Q}_1)_{C_s} + (\dot{Q}_2)_{C_s}$. Eqn. (5.19) includes the local derivatives of four coefficients in Eqn. (5.18) and the angular velocity of the base body in Eqn. (5.4), which are calculated consecutively.

First, taking the derivative of Eqn. (5.18):

$$\begin{aligned}
(\dot{P}_1)_{C_s} &= \sum_{i=1}^{N} \dot{T}_{C_i\to C_s} I_{B_i} T_{C_1\to C_i} + T_{C_i\to C_s} I_{B_i} \dot{T}_{C_1\to C_i} \\
(\dot{Q}_1)_{C_s} &= \sum_{i=2}^{N} \Bigg\{ \left[\sum_{j=i}^{N} \left(\dot{T}_{C_j\to C_s} I_{B_j} T_{C^0_i\to C_j} + T_{C_j\to C_s} I_{B_j} \dot{T}_{C^0_i\to C_j} \right) \right] \vec{\omega}^{C^0_i}_{B_i} \\
&\quad + \left(\sum_{j=i}^{N} T_{C_j\to C_s} I_{B_j} T_{C^0_i\to C_j} \right) \dot{\vec{\omega}}^{C^0_i}_{B_i} \Bigg\} \\
(\dot{P}_2)_{C_s} &= \sum_{i=1}^{N} m_i \ddot{\vec{\rho}}_{G_i/G_s} \\
(\dot{Q}_2)_{C_s} &= \sum_{i=1}^{N} m_i \vec{\rho}^{C_s}_{G_i/G_s} \times \left(\ddot{\vec{\rho}}^{C_s}_{G_i/G_s} \right)_{C_s}
\end{aligned} \tag{5.20}$$

in which the derivatives of transformation matrices can be obtained by a cascading method. For example, the matrix derivative $\dot{T}_{C_1\to C_i}$ can be expressed as:

$$\dot{T}_{C_1\to C_i} = \dot{T}_{C_{i-1}\to C_i} T_{C_1\to C_{i-1}} + T_{C_{i-1}\to C_i} \dot{T}_{C_1\to C_{i-1}} \quad (i \geqslant 2) \tag{5.21}$$

in which the derivative of transformation matrix $T_{C_{i-1}\to C_i}$ can be obtained by $\dot{T}_{C_{i-1}\to C_i} = \dot{T}_{C_i^0\to C_i} T_{C_{i-1}\to C_i^0}$ by considering that $\dot{T}_{C_{i-1}\to C_i^0} = 0$, since the direction cosine matrix $T_{C_{i-1}\to C_i^0}$ is time independent. The matrix derivative $\dot{T}_{C_1\to C_2}$ is the starting point of the previous cascading method.

The matrix derivative $\dot{\bar{\rho}}_{G_i/G_s}$ in Eqn. (5.20) can be obtained by:

$$\dot{\bar{\rho}}_{G_i/G_s} = \begin{bmatrix} 2\left(\rho_2\dot{\rho}_2 + \rho_3\dot{\rho}_3\right) & -\dot{\rho}_1\rho_2 - \rho_1\dot{\rho}_2 & -\dot{\rho}_1\rho_3 - \rho_1\dot{\rho}_3 \\ -\dot{\rho}_1\rho_2 - \rho_1\dot{\rho}_2 & 2\left(\rho_1\dot{\rho}_1 + \rho_3\dot{\rho}_3\right) & -\dot{\rho}_2\rho_3 - \rho_2\dot{\rho}_3 \\ -\dot{\rho}_1\rho_3 - \rho_1\dot{\rho}_3 & -\dot{\rho}_2\rho_3 - \rho_2\dot{\rho}_3 & 2\left(\rho_1\dot{\rho}_1 + \rho_2\dot{\rho}_2\right) \end{bmatrix} \tag{5.22}$$

where the local derivative $\left(\dot{\bar{\rho}}^{C_s}_{G_i/G_s}\right)_{C_s}$ is defined as $\left(\dot{\bar{\rho}}^{C_s}_{G_i/G_s}\right)_{C_s} = [\dot{\rho}_1, \dot{\rho}_2, \dot{\rho}_3]$ and can be obtained by taking the derivative of Eqn. (5.16):

$$\begin{aligned}
\left(\dot{\bar{\rho}}^{C_{i-1}}_{G_i/G_{i-1}}\right)_{C_{i-1}} &= \dot{T}_{C_i\to C_{i-1}}\bar{\rho}^{C_i}_{G_i/J_{i-1}} \quad (i \geqslant 2) \\
\left(\dot{\bar{\rho}}^{C_1}_{G_i/G_1}\right)_{C_1} &= \left(\dot{\bar{\rho}}^{C_1}_{G_{i-1}/G_1}\right)_{C_1} + \dot{T}_{C_{i-1}\to C_1}\bar{\rho}^{C_{i-1}}_{G_i/G_{i-1}} + T_{C_{i-1}\to C_1}\left(\dot{\bar{\rho}}^{C_{i-1}}_{G_i/G_{i-1}}\right)_{C_{i-1}} \quad (i \geqslant 3) \\
\left(\dot{\bar{\rho}}^{C_1}_{G_s/G_1}\right)_{C_1} &= \frac{\sum_{i=1}^{N} m_i\left(\dot{\bar{\rho}}^{C_1}_{G_i/G_1}\right)_{C_1}}{\sum_{i=1}^{N} m_i} \\
\left(\dot{\bar{\rho}}^{C_s}_{G_i/G_s}\right)_{C_s} &= \left(\dot{\bar{\rho}}^{C_1}_{G_i/G_1}\right)_{C_1} - \left(\dot{\bar{\rho}}^{C_1}_{G_s/G_1}\right)_{C_1} \quad (i \geqslant 1)
\end{aligned} \tag{5.23}$$

in which $\bar{\rho}^{C_i}_{G_i/J_{i-1}}$ in the first expression is time-independent, which simplifies the calculation of derivative. Similarly, the second order derivative in Eqn. (5.20), i.e. $\left(\ddot{\bar{\rho}}^{C_s}_{G_i/G_s}\right)_{C_s}$, can be obtained by taking the derivative of Eqn. (5.23).

Back to Eqn. (5.19), the local derivative of the angular velocity of the base body

can be found by taking derivative of the first expression in Eqn. (5.4):

$$\left(\vec{\omega}_{B_1}^{\dot{C}_1}\right)_{C_s} = T_\omega \begin{bmatrix} \ddot{X}_4 \\ \ddot{X}_5 \\ \ddot{X}_6 \end{bmatrix} + RE \tag{5.24}$$

where the angular acceleration vector is expressed in terms of the general matrix form by extracting the vector $[\ddot{X}_4\, \ddot{X}_5\, \ddot{X}_6]$, which enables the explicit expression of these three rotational reference point coordinates for numerical simulation. The vector RE and the matrix T_ω can be expressed by:

$$\begin{aligned} RE &= \begin{bmatrix} -\dot{X}_4\dot{X}_5 \sin X_5 \cos X_6 - \dot{X}_4\dot{X}_6 \cos X_5 \sin X_6 + \dot{X}_5\dot{X}_6 \cos X_6 \\ \dot{X}_4\dot{X}_5 \sin X_5 \sin X_6 - \dot{X}_4\dot{X}_6 \cos X_5 \cos X_6 - \dot{X}_5\dot{X}_6 \sin X_6 \\ \dot{X}_4\dot{X}_5 \cos X_5 \end{bmatrix} \\ T_\omega &= \begin{bmatrix} \cos X_5 \cos X_6 & \sin X_6 & 0 \\ -\cos X_5 \sin X_6 & \cos X_6 & 0 \\ -\sin X_5 & 0 & 1 \end{bmatrix} \end{aligned} \tag{5.25}$$

c. Application

The derivation results for total angular momentum and its derivative can be directly applied to formulate the EOMs of N-body systems. Numerical implementation of the new method is also presented.

Eqn. (5.17) can be applied to express the total angular momentum of the N-body system required by the rotational EOMs in Eqn. (5.9). The first two terms, $P_1\vec{\omega}_{B_1}^{C_1}$ and Q_1, represent the angular momentum of the entire system projected into the unified

C_s system but calculated about the CM of individual bodies. $P_1\vec{\omega}_{B_1}^{C_1}$ represents the instantaneous angular momentum of the N-body system rotating with the base body. The coefficient P_1 can be generalized by first transferring the angular velocity of the base body ($\vec{\omega}_{B_1}^{C_1}$) to each rigid body through the transformation matrix ($T_{C_1 \to C_i}$), then multiplying the result with the corresponding inertia tensor (I_{B_i}) and finally transforming the angular momentum back to the unified coordinate system (C_s) and summing up. The term Q_1 represents the contribution of relative rotation among the bodies ($\vec{\omega}_{B_i}^{C_i^0}$) to the total angular momentum. The angular velocity at each joint ($\vec{\omega}_{B_i}^{C_i^0}$) is transferred to all of the bodies affected by this joint along the kinematic chain, then multiplied by the corresponding inertia tensor and finally transformed back to the unified C_s system.

The effect of transferring the reference points is represented in $P_2\vec{\omega}_{B_1}^{C_1}$ and Q_2, in which radius vector $\vec{\rho}_{G_i/G_s}^{C_s}$ and matrix $\bar{\rho}_{G_i/G_s}$ represent the effect of the unconstrained CM of the system and need to be formulated. First, the kinematic chain is decomposed into individual links similar to Fig. 36 to apply Eqn. (5.16). Each of links is made of two contiguous bodies (B_{i-1} and B_i) connected by a mechanical joint (J_{i-1}). The radius vector from G_{i-1} to G_i, $\vec{\rho}_{G_i/G_{i-1}}^{C_{i-1}}$, is projected into the C_{i-1} system and calculated for each link. The fixed radius vectors between each body and connecting joint, $\vec{\rho}_{J_{i-1}/G_{i-1}}^{C_{i-1}}$ and $\vec{\rho}_{G_i/J_{i-1}}^{C_i}$, are time-independent if expressed in body-fixed coordinate systems C_{i-1} and C_i. Second, the cascading expressions in the first two lines of Eqn. (5.16) are applied repeatedly to calculate the radius vector, $\vec{\rho}_{G_i/G_1}^{C_1}$, from the CM of the base body to that of each body along the chain. Third, the CM of the system (G_s) within the C_1 system is calculated as a weighted average. Finally, the

radius vectors needed in the coefficients P_2 and Q_2, $\vec{\rho}^{C_s}_{G_i/G_s}$ and $\vec{v}^{C_s}_{G_i/G_s}$, are obtained by vector combination and absolute derivative calculation, respectively. The local derivative of the relative radius vector $\left(\dot{\vec{\rho}}^{C_s}_{G_i/G_s}\right)_{C_s}$ needed in the velocity expression of Eqn. (5.16) can be obtained by calculating the derivative of each element within $\vec{\rho}^{C_s}_{G_i/G_s}$. Eqn. (4.12) in Chapter 4 is used to update $\bar{\rho}_{G_i/G_s}$ based on $\vec{\rho}^{C_s}_{G_i/G_s}$.

Generally, the local derivative of the total angular momentum in Eqn. (5.19) can be formulated through Eqns. (5.20) and (5.24). The angular acceleration of the base body is decoupled from the translational acceleration, which facilitates the explicit expression of $[\ddot{X}_4, \ddot{X}_5, \ddot{X}_6]$ without consideration of $[\ddot{X}_1, \ddot{X}_2, \ddot{X}_3]$.

Finally, Eqn. (5.9) can be rearranged as an explicit expression of unknown accelerations:

$$\begin{aligned}
\sum_{i=1}^{N} m_i \begin{bmatrix} \ddot{X}_1 \\ \ddot{X}_2 \\ \ddot{X}_3 \end{bmatrix} &= \sum_{i=1}^{N} \vec{F}^{C_I}_{B_i} \\
(P_1 + P_2) T_\omega \begin{bmatrix} \ddot{X}_4 \\ \ddot{X}_5 \\ \ddot{X}_6 \end{bmatrix} &= \sum_{i=1}^{N} {}^{B_i}\vec{M}^{C_s}_{G_s} - (P_1 \dot{+} P_2)_{C_s} \vec{\omega}^{C_1}_{B_1} - (Q_1 \dot{+} Q_2)_{C_s} \\
&\quad -(P_1 + P_2) RE - \vec{\omega}_{C_s} \times {}^{s}\vec{H}^{C_s}_{G_s}
\end{aligned} \tag{5.26}$$

Eqn. (5.26) includes six basic EOMs of the N-body system and represents the balance between the inertial forcing and external forcing. The LHS is the inertial forcing, which depends on translational and rotational accelerations; those terms other than external moments ($\sum_{i=1}^{N} {}^{B_i}\vec{M}^{C_s}_{G_s}$) in the RHS of basic rotational EOMs

are also the inertial forcing, but these terms are independent of unknown reference point coordinates, including the velocity-dependent inertia terms [33], the vectors $(P_1 \dot{+} P_2)_{C_s} \vec{\omega}_{B_1}^{C_1}$, $(P_1 + P_2)RE$ and $\vec{\omega}_{C_s} \times {}^s\vec{H}_{G_s}^{C_s}$, and the acceleration term $(Q_1 \dot{+} Q_2)_{C_s}$ that depends on known relative coordinates. Thus, the influence of prescribed relative coordinates between contiguous bodies has been included in the basic EOMs. The factor $\sum_{i=1}^{N} m_i$ is the total mass of the N-body system. It can be simply expanded to an equivalent diagonal mass matrix relevant to absolute motion of G_s, (X_1, X_2, X_3); $(P_1 + P_2)T_\omega$ is the mass matrix associated with the rotational reference point coordinates of the base body, (X_4, X_5, X_6). These two matrices combine the total effect of the elements of the mass and inertia tensor of each body within the multibody system and are equivalent to collapsing the larger mass matrices of conventional methods. More importantly, rotational and translational mass matrices are decoupled, a significant advantage over other analytical methods.

The first-order decoupled EOMs for numerical integration can be easily obtained from Eqn. (5.26). All of the matrices and vectors in Eqn. (5.26) are to be updated at each time step. The decoupling between the previous two mass matrices enables the separate integrations of the three translational and three rotational basic EOMs. The kinematics of the translational and rotational reference point coordinates (including velocity and acceleration) are thoroughly decoupled in the inertial forcing: the translational inertial forcing depends on only translational reference point coordinates; the rotational inertial forcing depends on only rotational reference point coordinates. This formulation advantage facilitates the numerical integration. The coordinates (X_1, X_2, X_3) are connected with the translational reference point coordi-

nates of the base body, (X_{1b}, X_{2b}, X_{3b}), and the positions of the CM of other bodies through pre- and postprocessing procedures in Eqn. (5.10). These procedures are used to prescribe initial conditions about G_1 at the beginning of the first time step and compute external forcing applied to each body in the future time steps.

4. Expansion for General N-Body System

The derivation for the serial N-body systems is applicable to more general N-body systems with only minor expansion. These more complicated systems may include open-chains with branches and closed-chain loops of rigid bodies. The final basic EOMs (Eqn. (5.26)) remain unchanged, but some intermediate equations requires additional explanations. The increased complexity of the joints requires additional relative coordinates between contiguous bodies, which may introduce additional control and constraint equations. Application to more complicated systems is first discussed, followed by applications including more complicated joints.

The previous derivation was for a serial kinematic chain which enabled sequential numbering, starting from the base body and progressing through all rigid bodies. However, a simple kinematic chain does not exist for an open-chain system with branches (a tree system) or for the combination of a tree system and a closed-chain system. The expansion of the new method only requires that each body be connected by some kinematic chain to the base body, and that each body be uniquely numbered. As in the serial case, radius vectors between the CM of each body and its contiguous joints and transformation matrices between contiguous bodies must be determined, after which the position and orientation of any body relative to the base body can

be obtained by choosing a kinematic chain connecting them. Two equations need to be reexamined for application to non-serial N-body systems: Eqn. (5.16) and (5.18). The first and second expressions in Eqn. (5.16) can be applied to any kinematic chain in a non-serial N-body system as long as the bodies and joints are uniquely numbered from 1 to N. The calculation of the relative position of G_s in the C_1 system ($\vec{\rho}^{C_1}_{G_s/G_1}$) in the third expression already considers the relative positions of all bodies within the N-body system, and can be used directly, as can the fourth and fifth expressions of $\vec{\rho}^{C_s}_{G_i/G_s}$ and $\vec{v}^{C_s}_{G_i/G_s}$. The only change required to Eqn. (5.18) is to modify the internal summation in Q_1 to exclude bodies not affected by the relative angular velocity $\vec{\omega}^{C_i^0}_{B_i}$, i.e. to exclude bodies on other branches.

Just as the method can be applied to systems of any complexity, it can also be applied to joints of any complexity. Any joint can be represented by relative coordinates between contiguous bodies. As long as the relative motion described by these additional relative coordinates are prescribed, no additional EOMs need to be solved beyond six basic EOMs. For example, a cylindrical joint allowing both translation and rotation requires one additional relative coordinate to describe the prescribed translation of the joint hinge relative to its initial position. This motion is added to the constant vector $\vec{\rho}^{C_i}_{G_i/J_{i-1}}$ in Eqn. (5.16).

Generally, if the relative coordinates at joints are unknown, the control and constraint equations governing these coordinates are fully coupled with six basic EOMs. The sum $(Q_1 \dot{+} Q_2)_{C_s}$ in Eqn. (5.20) introduces accelerations of unknown relative coordinates into the basic EOMs. The control and constraint equations may also depend on accelerations of six reference point coordinates, in which case, the accel-

erations of relative coordinates in these equations can be expressed as a function of the accelerations of the reference point coordinates and substituted into $(Q_1 \dot{+} Q_2)_{C_s}$ in the basic EOMs to compute $(\ddot{X}_4, \ddot{X}_5, \ddot{X}_6)$. The translational accelerations of the base body, $(\ddot{X}_1, \ddot{X}_2, \ddot{X}_3)$, still result from the first equation in Eqn. (5.26). Finally, explicit expressions of all the accelerations of the chosen coordinates are applied prior to the numerical integration.

5. Inverse Dynamics of N-body System

The computational efficiency of the overall method is enhanced by avoiding the need to calculate internal forces and moments between bodies. However, it is commonly necessary to quantify this internal forcing. Inverse dynamics is conventionally used to calculate internal forces and moments between arbitrarily selected contiguous bodies using the kinematics resulting from a forward dynamic simulation.

The first step is to divide the N-body system into two subsystems based on the position of unknown internal forcing. These two subsystems are connected by either one or two common joints. The latter indicates a loop composed of rigid bodies that needs to be broken into two separate subsystems. Known time histories of both inertial and external forcing on each body are used for the calculation of the internal forcing by applying the conservation of momentum to one (for one-joint case) or two (for two-joint case) subsystems. The new method is first derived for the one-joint case and then simply expanded to the two-joint case.

Two subsystems (s_1 and s_2) in the original system (s) are connected by one common joint J. The conservation of linear momentum (Newton's second Law)

can be applied to either of these two subsystems to determine forces between them. Subsystem s_1 includes N_1 bodies. Newton's second Law applied to subsystem s_1 is:

$$^{s}\sum_{i=1}^{N_1}\vec{F}_{B_i}^{C_I}+\vec{F}_{J}^{C_I} \;=\; \left(\sum_{i=1}^{N_1} m_i\right)\vec{a}_{G_{s_1}}^{C_I} \tag{5.27}$$

The unknown force on the joint J is internal for the original s system and external for the subsystem s_1. This force is denoted as $\vec{F}_J^{C_I}$ and equal to the difference between the external forces applied to each body in the s_1 system and $^{s}\sum_{i=1}^{N_1}\vec{F}_{B_i}^{C_I}$, the external forces on all N_1 bodies in the original s system. The vector $^{s}\sum_{i=1}^{N_1}\vec{F}_{B_i}^{C_I}$ is known from the first expression of Eqn. (5.9) in the forward dynamic simulation. The vector $\vec{a}_{G_{s_1}}^{C_I}$ in the RHS is the acceleration of G_{s_1} (the CM of the subsystem s_1) and can be expressed by $\vec{a}_{G_{s_1}}^{C_I} = \ddot{\vec{\rho}}_{G_{s_1}/O}^{C_I}$. Similar to the third expression in Eqn. (5.16), the radius vector $\vec{\rho}_{G_{s_1}/O}^{C_I}$ can be shown to be: $\vec{\rho}_{G_{s_1}/O}^{C_I} = \frac{\sum_{i=1}^{N_1} m_i\vec{\rho}_{G_i/O}^{C_I}}{\sum_{i=1}^{N_1} m_i}$, in which the radius vectors $\vec{\rho}_{G_i/O}^{C_I}$ are known and result from Eqn. (5.10) in the forward dynamic simulation. To summarize, the unknown internal forces ($\vec{F}_J^{C_I}$) can be obtained by: first saving the time histories of $^{s}\sum_{i=1}^{N_1}\vec{F}_{B_i}^{C_I}$ and $\vec{\rho}_{G_i/O}^{C_I}$ in forward dynamics; then using $\vec{\rho}_{G_i/O}^{C_I}$ to calculate the time history of $\vec{\rho}_{G_{s_1}/O}^{C_I}$; numerically calculating the second order derivative of $\vec{\rho}_{G_{s_1}/O}^{C_I}$ to obtain the acceleration of G_{s_1} and further the RHS $\left(\sum_{i=1}^{N_1} m_i\right)\vec{a}_{G_{s_1}}^{C_I}$; finally subtracting the time history of $^{s}\sum_{i=1}^{N_1}\vec{F}_{B_i}^{C_I}$ from that of the RHS to obtain $\vec{F}_J^{C_I}$.

Moments between subsystems connected by a single joint are found by a similar procedure. The conservation of angular momentum (Newton's second Law) can be

applied to the subsystem s_1 to determine internal moments in the original s system:

$$ {}^{s}\sum_{i=1}^{N_1} {}^{B_i}\vec{M}_{G_{s_1}}^{C_s} + \vec{M}_{F_J}^{C_s} + \vec{M}_J^{C_s} = \left({}^{s_1}\dot{\vec{H}}_{G_{s_1}}^{C_s} \right)_{C_s} + \vec{\omega}_{C_s} \times {}^{s_1}\vec{H}_{G_{s_1}}^{C_s} \tag{5.28} $$

where the LHS includes both the force moments (moments resulting from a force) and couple moments (moments resulting from pairs of equal and opposite applied forces). The force moments are calculated about G_{s_1}, while the couple moments are free vectors and independent of the reference point. The paired forces do not appear in the balance of forces in Eqn. (5.27), but their effects do appear in the balance of moments in Eqn. (5.28). Here, ${}^{s}\sum_{i=1}^{N_1} {}^{B_i}\vec{M}_{G_{s_1}}^{C_s}$ represents the external force and couple moments on all N_1 bodies in the original s system and is computed from the forward dynamic simulation. $\vec{M}_{F_J}^{C_s}$ is the force moments applied on the joint J and can be shown as $\vec{\rho}_{J/G_{s_1}}^{C_s} \times (T_{C_I \to C_s} \vec{F}_J^{C_I})$, in which the internal force $\vec{F}_J^{C_I}$ is calculated by Eqn. (5.27); the radius vector $\vec{\rho}_{J/G_{s_1}}^{C_s}$ can be obtained by: $\vec{\rho}_{J/G_{s_1}}^{C_s} = T_{C_{N_1} \to C_s} \vec{\rho}_{J/G_{N_1}}^{C_{N_1}} + \vec{\rho}_{G_{N_1}/G_{s_1}}^{C_s}$. The couple moments on the joint J ($\vec{M}_J^{C_s}$) are the desired internal moments (e.g. [35]). In the RHS, the vector ${}^{s_1}\vec{H}_{G_{s_1}}^{C_s}$ is the total angular momentum of N_1 bodies about the CM of the subsystem s_1 (G_{s1}): ${}^{s_1}\vec{H}_{G_{s_1}}^{C_s} = {}^{s_1}\vec{H}_{G_s}^{C_s} - \vec{\rho}_{G_s/G_{s_1}}^{C_s} \times m_{s_1} \vec{v}_{G_s/G_{s_1}}^{C_s}$. Here, the vector ${}^{s_1}\vec{H}_{G_s}^{C_s}$ is the total angular momentum of N_1 bodies about G_s; the vector $\vec{\rho}_{G_s/G_{s_1}}^{C_s}$ can be calculated as $\vec{\rho}_{G_s/G_{s_1}}^{C_s} = \vec{\rho}_{G_s/G_1}^{C_s} - \vec{\rho}_{G_{s_1}/G_1}^{C_s}$. Thus, the inertial forcing in the RHS of Eqn. (5.28) is computed from results for all N_1 bodies in the forward dynamic simulation. The unknown internal moments ($\vec{M}_J^{C_s}$) are obtained by subtracting ${}^{s}\sum_{i=1}^{N_1} {}^{B_i}\vec{M}_{G_{s_1}}^{C_s}$ and $\vec{M}_{F_J}^{C_s}$ from the time history of the inertial forcing, i.e. the RHS of Eqn. (5.28).

A two-joint case is solved in a similar manner using Eqns. (5.27) and (5.28). Ap-

plication of Eqn. (5.27) to each of the two subsystems results in two sets of equations with two unknown internal forces, which can be solved simultaneously. After obtaining the two internal forces, Eqn. (5.28) can be applied to each of the two subsystems and solved simultaneously for the internal moments at the two joints.

Configurations may exist for which the number of the desired unknown internal forces or moments is greater than 2, and so not all unknowns can be obtained simultaneously for these cases. Multiple application of the presented method can be implemented through dividing the original s system into one-joint or two joint cases. Calculation of internal forcing for overdetermined systems is not covered here.

D. Example

The new multibody formulation (MCM) is applied to a 6-body compliant floating wind turbine design. The physical properties of the model are the same as that in Chapter 4. The 6-body model includes the tower (body 1), nacelle (body 2), hub (body 3) and three blades (bodies 4-6). The tower is considered as the base body.

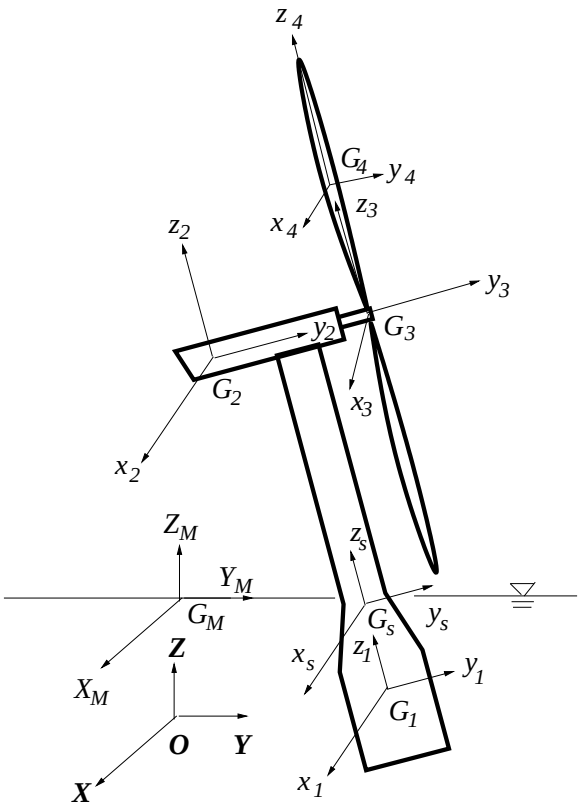

Fig. 37. Coordinate systems used in the 6-body model

Fig. 37 shows the coordinate systems used for the MCM; only the body-fixed coordinate system on one of the three blades is shown. The (X_M, Y_M, Z_M) system is defined to enable comparison of simulation results with those of FAST, in which the reference point is usually prescribed to be on the still water level. The six unknown reference point coordinates are three translational DOFs of the CM of the tower and three rotational DOFs of the base body. The known relative coordinates are the yaw rate of the nacelle relative to the tower, the spin rate of the hub relative to the

nacelle and the three blade-pitch rates relative to hub.

The 6-body model is first decomposed to three serial kinematic chains to apply the MCM. Each chain starts from the base body (tower) and ends at one of the three blades. Along each chain, the angular velocity of each body and the transformation matrix between contiguous bodies are obtained by Eqn. (5.14). The common part of all chains (including bodies 1, 2 and 3) needs derivation only once. The transformation matrix along each chain is obtained by Eqn. (5.15). Then the position of each joint relative to the CM of the contiguous body is prescribed to determine the kinematics of each body relative to the CM of the system using Eqn. (5.16). The angular momentum of the system and its local derivative can be written directly through Eqns. (5.17) and (5.19). The resultant rotational EOMs are further connected with the translational EOMs by Eqns. (5.10).

The MCM is verified through comparison of results from the multibody wind turbine model with those from the popular wind turbine dynamics software FAST [46]. FAST uses Kane's method to formulate the EOMs of the wind turbine system. Under the free vibration case, both the global motion from forward dynamics and internal forcing from inverse dynamics are compared to simulation results from FAST.

1. Global Motion from Forward Dynamics

Figs. 38–39 show time histories of global motion computed using FAST and those computed using the MCM for a small-amplitude free vibration case. The rotational DOFs of the tower are transferred to the inertial coordinate system used in FAST to enable direct comparison between (X_4, X_5, X_6) and pitch, roll and yaw, which

is valid for small-amplitude rotation [69]. The translational DOFs, (X_{1b}, X_{2b}, X_{3b}), are transferred to the waterplane to enable direct comparison with the sway, surge and heave computed in FAST, which are measured from the (X_M, Y_M, Z_M) system in Fig. 37. Constant nacelle yaw (1.2 deg/sec), hub spin (12.1 rpm) and blade-pitch rate (1.2 deg/sec) are prescribed during the simulation. Here, both hydrodynamics and aerodynamics have been disabled in FAST. The only external forces acting on the base body are from the mooring lines and buoyancy, both of which are represented in the user-defined subroutine (UserPtfmLd) in FAST as a 6×6 restoring matrix, with values consistent with the method presented in Chapter 3 but linearized near the average tilt angle and tuned to reproduce the correct natural frequencies. The initial conditions in all six DOFs of the tower are zero. The CM of the nacelle is not directly above the axis of the tower, so nacelle yaw motion changes the position of the CM of the system relative to the tower, which causes the tower motion. Figs. 38–39 show that the global motions of FAST and the MCM are virtually indistinguishable. The spin axis is initially parallel to the surge direction. The influence of the moving G_s is clearly observable in the coupled motion of translational and rotational moving DOFs. For example, both pitch and surge are minimized (zero crossing) when the nacelle yaw angle is 90 deg (at 75 sec), while roll and sway are maximized. The observed yaw motion results from gyro moments associated with rotor spin coupled with roll and pitch.

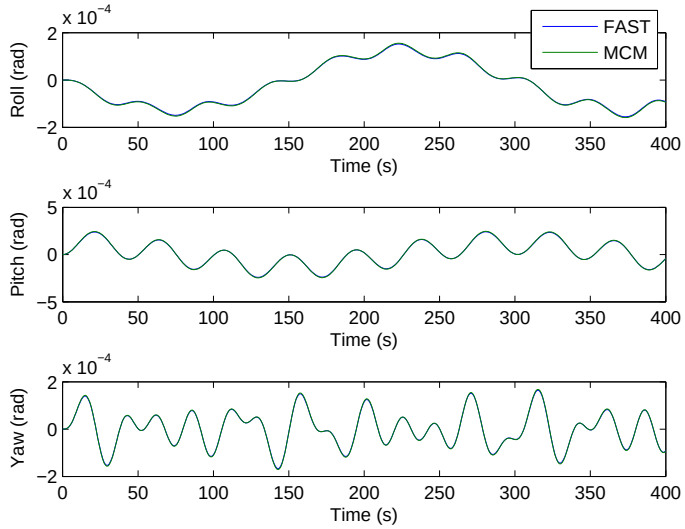

Fig. 38. Rotation compared to FAST (6-body)

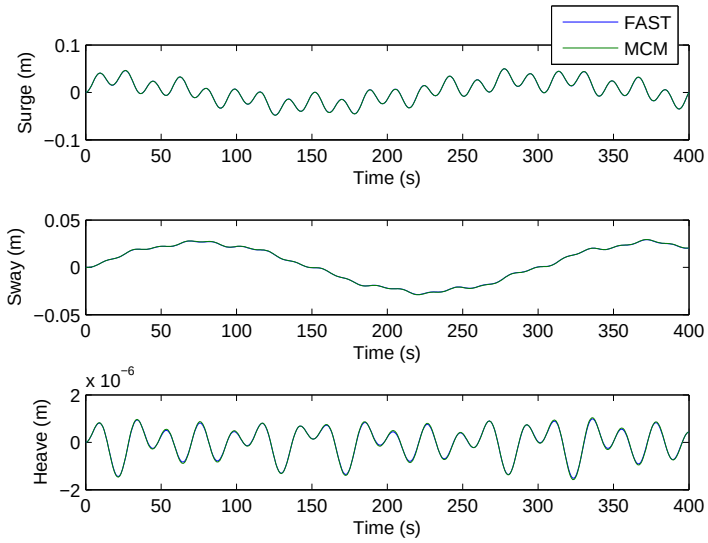

Fig. 39. Translation compared to FAST (6-body)

2. Internal Forcing from Inverse Dynamics

Figs. 40–43 show the corresponding internal forcing resulting from inverse dynamics. The internal forces and moments applied by the nacelle on the tower are decomposed into the body-fixed (x_1, y_1, z_1) system and shown by Figs. 40 and 41, in which the nearly constant internal force along the tower axis due to the topsides weight is not shown. The results from the tower-top coordinate system in FAST are transferred to the (x_1, y_1, z_1) system to compare with the MCM and show perfect agreement. The natural frequency of tower pitch shown in Fig. 38 dominates the time histories of internal forces, which further affect the internal moments. Meanwhile, the effect of nacelle yaw is represented in both internal forces and moments. The internal forces and moments applied by the hub on the blade are decomposed into the body-fixed (x_4, y_4, z_4) system and shown by Figs. 42 and 43. The results from the blade coordinate system in FAST are transferred to the (x_4, y_4, z_4) system to compare with the MCM. The numerical differentiation is applied in the MCM to calculate the acceleration of the CM of the blade, which causes results slightly different from those of FAST. In this free vibration case, the internal edgewise and flapwise forces at the blade root dominate the blade bending moments, while the external wind forces applied on the blades dominate the bending moments in a practical forced vibration case.

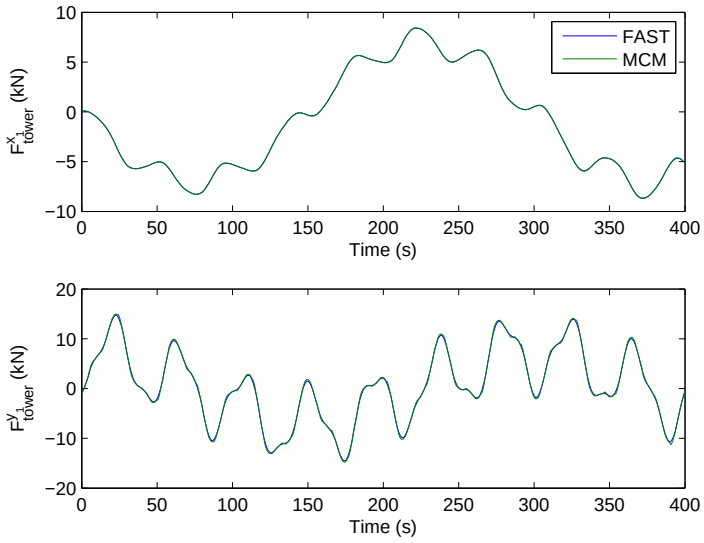

Fig. 40. Internal forces applied by the nacelle on the tower

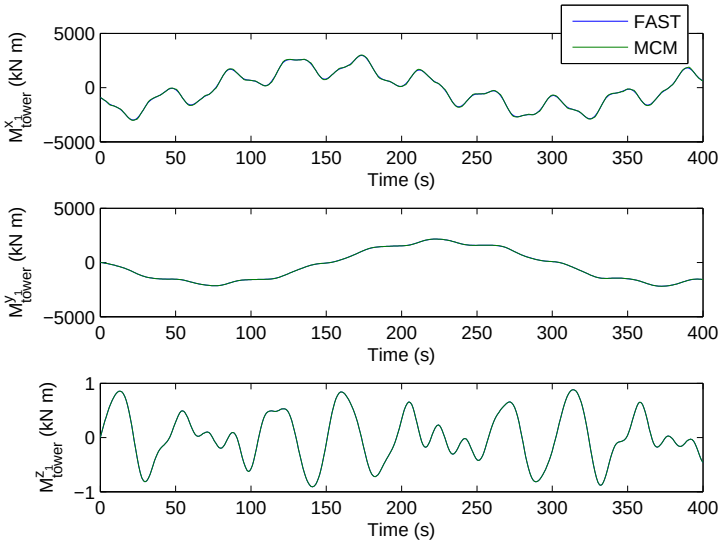

Fig. 41. Internal moments applied by the nacelle on the tower

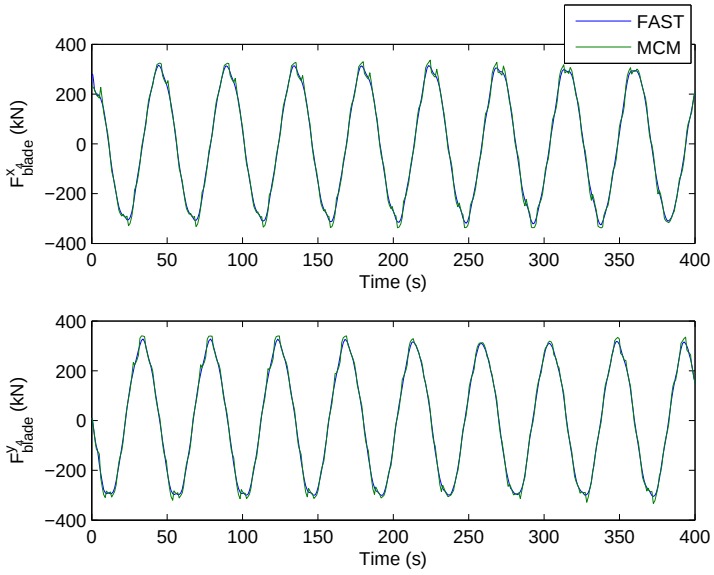

Fig. 42. Internal forces applied by the hub on the blade

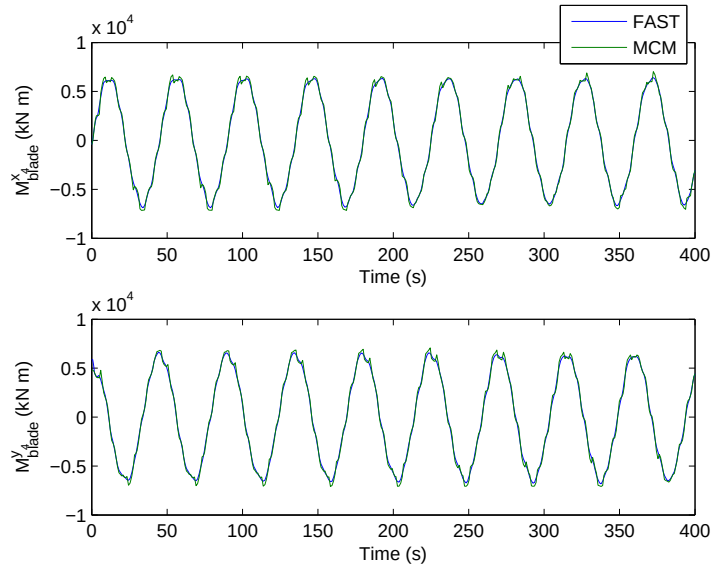

Fig. 43. Internal moments applied by the hub on the blade

E. Conclusions

A new multibody dynamics formulation method (MCM) is presented to obtain the explicit first-order decoupled EOMs for numerical integration. The underlying concept is to directly apply the conservation of momentum to the entire rigid multibody system. Various advantages of current multibody dynamics formulations are combined in the MCM: the calculation of internal forcing can be avoided and the rederivation due to a newly added body in the system is simplified. The 1-2-3 sequenced Euler angles are applied to describe the large-amplitude rotations of the floating base body, which preserves the fully nonlinearly in the EOMs. More importantly, the MCM represents the conservation of momentum of entire system using only six basic EOMs, in which the translational and rotational inertial forcing are decoupled. The 6×6 mass matrix in the basic EOMs is actually composed of two 3×3 decoupled mass matrices, which increases the efficiency of numerical integration dramatically. The selection of coordinates makes it simple to expand the MCM to multibody systems with more complicated forms and connection joints. The unknown relative motion at joints can be solved by combining six basic EOMs with the constraint and control equations. Inverse dynamics can also be applied to conveniently find internal forcing between any two contiguous bodies using the results of forward dynamics. The MCM is verified by the well-recognized multibody dynamics software through a 6-body compliant wind turbine model.

CHAPTER VI

SUMMARY

A. Conclusions

In this dissertation, a new multibody dynamics formulation method underlying the time-domain simulation of compliant floating wind turbine designs is presented to obtain the explicit first-order decoupled EOMs for numerical integration. The EOMs of multibody systems are established by applying the theorem of conservation of momentum. Development of the new methodology is based on improvement of wind turbine models and refinement of theoretical derivation.

In Chapter 2, Euler dynamic equations based on the conservation of angular momentum are applied to each body of a simple 2-body wind turbine model, respectively. The selection of two sets of 3-1-3 sequenced Euler angles simplifies Euler kinematic equations. The application of geometrical constraints decreases the DOFs of the system. All of these advantages facilitate the establishment of the first-order decoupled EOMs.

As the work progresses, new EOMs are established and gradually refined to enable an increased number of bodies. Significant improvements of the formulation method result from direct application of the conservation of both linear and angular momenta to the entire multibody system. In Chapter 3, previous 2-body model is applied to highlight the uniqueness of the new formulation methodology using a simple derivation. A set of 1-2-3 sequenced Euler angles are selected to describe the rotation of the tower because they are more consistent with conventional pitch-roll-

yaw of floating structures. Decoupling between translational and rotational EOMs is simplified by prescribing the CM of the wind turbine system to be constrained to the tower axis and writing the EOMs about that point.

In Chapter 4, the new method is improved by introducing a 3-body model with an unconstrained CM of the system. The coupling between translational and rotational inertial forcing is eliminated by: writing the translational EOMs about the CM of the system, though this point is not longer constrained to a body; a separate coordinate system fixed to the base body (tower) is applied to derive unknown relative radius vectors between the CM of the system and that of each body in the rotational EOMs. This decoupling enables generation of two decoupled mass matrices, one translational and one rotational, which greatly facilitates the numerical integration. The introduction of the 3-body model with the unconstrained CM of the system leads to the generalization of theoretical derivation to the N-body system presented in Chapter 5.

In Chapter 5, the new methodology is generalized using a serial N-body system to form the momentum cloud method (MCM). The selection of coordinate systems and corresponding coordinates is standardized. The theoretical derivations for both forward and inverse dynamics are systematized using standardized notations, which enables application of the MCM to formulate the first-order decoupled EOMs using standard vector and matrix calculation methods. A key advantage over conventional energy methods is that the MCM avoids tedious rederivation of the EOMs if new rigid bodies are added to the system. A six-body wind turbine model is used to verify the MCM. The new method has clear application beyond derivation of the

EOMs of floating wind turbines. It is expanded for application to other multibody systems with more complicated forms and more complicated joints through use of additional constraint and control equations.

The new method is demonstrated by simulation of the motion and internal forcing of highly compliant floating wind turbines, the results of which are verified by critical comparison with those of the popular wind turbine dynamics software FAST. The time-domain simulation tool based on the new method is also applied to roughly investigate the feasibility of compliant designs. Specific two-component gyroscopic moments of compliant designs are shown (Fig. 11). Large pitch angles reduce the effective blade swept area perpendicular to the wind, but this effect has been shown to have only a modest effect on energy capture (Fig. 26). It is also shown, counter-intuitionally, that in some cases reduced stiffness actually lowers dynamic loading. For sinusoidal motion, the amplitude of the inertial loads is the product of the moment of inertia, the amplitude of the motion, and the square of the circular frequency. Decreasing the stiffness reduces the pitch and roll natural frequencies (Fig. 19), which decreases inertial loading. However, such a change may require special consideration in the design of the rotor speed and blade-pitch controllers.

B. Future Work

This dissertation summarizes the work regarding a new multibody dynamic formulation using conservation of momentum and its application to the time-domain dynamic simulation of compliant floating wind turbines. There are several possible developments for future work:

1) When the control equations governing the relative motions at joints need to be solved simultaneously with six basic EOMs, various real-time control mechanisms, such as nacelle-yaw, blade-pitch and rotor-spin control, are critical for better design of compliant floating wind turbines, and so merit further investigation.

2) Calculation of external loads should be improved. The simulation tool could be connected to AeroDyn [30] to calculate wind loads. The radiation-diffraction may be considered in the calculation of wave loads. The restoring loads could be obtained using catenary mooring lines.

3) General multibody systems may include the joints of any complexity. Current constraint equations are actually minimized by prescribing the rotation axis of the joint, which simplifies the transformations between contiguous bodies. More general joints with 6-DOFs can be introduced by using existing parametrization system, such as the Denavit-Hartenberg parameters.

4) The MCM can be expanded to multibody systems with complicated forms, such as open-chains with branches or closed-chains. However, the serial kinematic chains need to be first prescribed before application. Future work on topology of multibody systems could be combined with the current derivation to formulate the automatic generalization of model-based EOMs.

5) Structural flexibility of individual bodies is not presently considered using the MCM, which is currently applicable to rigid multibody systems. The flexible body could be considered as an assembly of a series of rigid bodies connected by joints represented by springs and dampers. The modal superposition method could be investigated as a possible means to obtain the relative position of an assembly of rigid

bodies, which could then be combined with the newly presented MCM to simulate a flexible body as an assembly of rigid bodies. Structural stiffness and damping of the connecting joints could be treated as the dynamic factors in the constraint equations.

REFERENCES

[1] W. Musial and S. Butterfield, "Future for offshore wind energy in the United States," Tech. Rep. NREL/CP-500-36313, National Renewable Energy Laboratory, Golden, CO, 2004.

[2] W. Musial, S. Butterfield, and B. Ram, "Energy from offshore wind," Tech. Rep. NREL/CP-500-39450, National Renewable Energy Laboratory, Golden, CO, 2006.

[3] P. Sclavounos, "Floating offshore wind turbines," *Journal of Marine Technology Society*, vol. 42, no. 2, pp. 39–43, 2008.

[4] A. R. Henderson, C. Morgan, B. Smith, H. C. Sorensen, R. J. Barthelmie, and B. Boesmans, "Offshore wind energy in Europe: A review of the state-of-the-art," *Journal of Wind Energy*, vol. 6, pp. 35–52, 2003.

[5] J. F. Manwell, C. N. Elkinton, A. L. Rogers, and J. G. McGowan, "Review of design conditions applicable to offshore wind energy systems in the United States," *Journal of Renewable and Sustainable Energy Reviews*, vol. 11, pp. 210–234, 2007.

[6] G. M. Simon-Philippe Breton, "Status, plans and technologies for offshore wind turbines in Europe and North America," *Journal of Renewable Energy*, vol. 34, pp. 646–654, 2009.

[7] W. Musial, S. Butterfield, and A. Boone, "Feasibility of floating platform systems for wind turbines," Tech. Rep. NREL/CP-500-34874, National Renewable Energy Laboratory, Golden, CO, 2004.

[8] S. Butterfield, W. Musial, J. Jonkman, and P. Sclavounos, "Engineering challenges for floating offshore wind turbines," Tech. Rep. NREL/CP-500-38776, National Renewable Energy Laboratory, Golden, CO, 2005.

[9] A. R. Henderson and J. H. Vugts, "Prospects for floating offshore wind energy," in *Proceedings of the European Wind Energy Conference*, pp. 627–630, Jun. 2001.

[10] D. Roddier, C. Cermelli, A. Aubault, and A. Weinstein, "WindFloat: A floating foundation for offshore wind turbines," *Journal of Renewable and Sustainable Energy*, vol. 2, no. 3, pp. 033104–1–033104–34, 2010.

[11] A. Neville, "Top plants: Hywind floating wind turbine, North Sea, Norway," *Power*, pp. 37–42, Dec. 2009.

[12] "Rules and regulations for fixed offshore platforms," Tech. Rep. API, American Petroleum Institute, Washington, DC, U.S., 2000.

[13] "Wind turbines - part 1: Design requirements," Tech. Rep. IEC 61400-1 ed. 3, International Electrotechnical Commission, Geneva, Switzerland, 2005.

[14] "Wind turbines - part 3: Design requirements for offshore wind turbines," Tech. Rep. IEC 61400-3 ed. 1.0, International Electrotechnical Commission, Geneva, Switzerland, 2009.

[15] "Design of offshore wind turbine structures," Tech. Rep. DNV-OS-J101, Det Norske Veritas, Oslo, Norway, 2010.

[16] T. Krogh, "HAWC load simulation of generic 5MW offshore wind turbine model," Tech. Rep. Riso-R-1475, Riso National Laboratory, Roskilde, Denmark, 2004.

[17] K. Freudenreich and K. Argyriadis, "Wind turbine load level based on extrapolation and simplified methods," *Journal of Wind Energy*, vol. 11, pp. 589–600, May 2008.

[18] A. R. Henderson and M. H. Patel, "On the modelling of a floating offshore wind turbine," *Journal of Wind Energy*, vol. 6, pp. 53–86, 2003.

[19] E. Bush, "A comparison of alternate foundation models for offshore wind turbines and resulting long-term loads," Master's thesis, University of Texas at Austin, 2009.

[20] A. R. Henderson and P. W. Cheng, "Wave loads on slender offshore structures, comparison of theory & measurement," in *Proceedings of the 6th German Wind Energy Conference*, pp. 521–524, Oct. 2002.

[21] T. R. Camp, E. A. Bossanyi, and D. C. Quarton, "Design loads for offshore wind turbines," in *Proceedings of the 21st British Wind Energy Association Conference*, pp. 393–394, 1999.

[22] E. Anahua, S. Barth, and J. Peinke, "Markovian power curves for wind turbines," *Journal of Wind Energy*, vol. 11, pp. 219–232, 2008.

[23] A. Write, L. Fingersh, and K. Stol, "Designing and testing controls to mitigate tower dynamic loads in the controls advanced research turbine," Tech. Rep. NREL/CP-500-40932, National Renewable Energy Laboratory, Golden, CO, 2007.

[24] K. H. Lee, "Responses of floating wind turbines to wind and wave excitation," Master's thesis, Massachusetts Institute of Technology, 1998.

[25] E. Wayman, "Coupled dynamics and economic analysis of floating wind turbine systems," Master's thesis, Massachusetts Institute of Technology, 2006.

[26] J. E. Withee, *Fully Coupled Dynamic Analysis of a Floating Wind Turbine System*. PhD thesis, Massachusetts Institute of Technology, 2004.

[27] B. Skaare, T. D. Hanson, and F. G. Nielsen, "Integrated dynamic analysis of floating offshore wind turbines," Tech. Rep. Riso, Riso National Laboratory, Roskilde, Denmark, 2007.

[28] J. M. Jonkman and P. D. Sclavounas, "Development of fully coupled aeroelastic and hydrodynamic models for offshore wind turbines," Tech. Rep. NREL/CP-500-39066, National Renewable Energy Laboratory, Golden, CO, 2006.

[29] J. M. Jonkman and M. L. J. Buhl, "Development and verification of a fully coupled simulator for offshore wind turbines," Tech. Rep. NREL/CP-500-40979, National Renewable Energy Laboratory, Golden, CO, 2007.

[30] D. J. Laino and A. C. Hansen, "User's guide to the wind turbine aerodynamics computer software AeroDyn," Tech. Rep. TCX-9-29209-01, National Energy

Renewal Laboratory, Golden, CO, 2002.

[31] C. H. Lee and J. N. Newman, "WAMIT user manual," Tech. Rep. Version 6.4, WAMIT, Inc., Chestnut Hill, MA, 2008.

[32] D. Matha, "Model development and loads analysis of an offshore wind turbine on a tension leg platform, with a comparison to other floating turbine concepts," Tech. Rep. NREL/SR-500-45891, National Renewable Energy Laboratory, Golden, CO, 2009.

[33] J. G. Jalon and E. Bayo, *Kinematic and Dynamic Simulation of Multibody Systems: The Real-Time Challenge*. New York: Springer, 1993.

[34] E. Stoneking, "Newton-Euler dynamic equations of motion for a multi-body spacecraft," in *Proceedings of the AIAA Guidance, Navigation, and Control Conference*, pp. 1368–1380, Aug. 2007.

[35] T. R. Kurfess, *Robotics and Automation Handbook*. Boca Raton, FL: CRC Press, 2004.

[36] R. Featherstone, *Rigid Body Dynamics Algorithms*. New York: Springer, 2008.

[37] A. Shabana, *Dynamics of Multibody Systems*. Indianapolis, IN: Wiley, 1989.

[38] R. Huston, *Multibody Dynamics*. Oxford, U.K.: Butterworth-Heinemann, 1990.

[39] R. T. D. Luca, "A brief synopsis of kanes method and a few applications," Tech. Rep. CMU, Carnegie Mellon University, Pittsburgh, PA, 2000.

[40] M. T. Mason, *Mechanics of Robotic Manipulation.* Cambridge, MA: MIT Press, 2001.

[41] A. Garrad, "An approximate method for the dynamic analysis of two-bladed horizontal axis wind turbine systems," in *Proceedings of the 4th International Symposium on Wind Energy Systems*, pp. 445–461, 1982.

[42] A. Garrad, "Dynamics of wind turbines," in *Proceedings of IEE. Physical Science, Measurement and Instrumentation, Management and Education, Reviews*, pp. 523–530, 1983.

[43] D. Quarton and A. Garrad, "Some comments on the stability analysis of horizontal axis wind turbines," in *Proceedings of the 6th BWEA Wind Energy Conference*, pp. 197–209, 1984.

[44] A. Garrad and U. Hassan, "Dynamic analysis of wind turbines for fatigue life prediction," in *Proceedings of the 8th British Wind Energy Association Conference*, pp. 179–185, 1986.

[45] J. M. Jonkman and M. L. J. Buhl, "FAST user's guide," Tech. Rep. NREL/EL-500-38230, National Renewable Energy Laboratory, Golden, CO, 2005.

[46] J. M. Jonkman, "Dynamic modeling and loads analysis of an offshore floating wind turbine," Tech. Rep. NREL/TP-500-41958, National Energy Renewal Laboratory, Golden, CO, 2007.

[47] M. Hansena, J. Sorensen, S. Voutsinas, N. Soensen, and H. Madsen, "State of the art in wind turbine aerodynamics and aeroelasticity," *Journal of Progress*

in Aerospace Sciences, vol. 42, pp. 285–330, 2006.

[48] H. Matsukuma and T. Utsunomiya, "Motion analysis of a floating offshore wind turbine considering rotor-rotation," *The IES Journal Part A: Civil and Structural Engineering*, vol. 1, no. 4, pp. 268–279, 2008.

[49] S. Shim and M. H. Kim, "Rotor-floater-tether coupled dynamic analysis of offshore floating wind turbines," in *Proceedings of the 18th International Offshore and Polar Engineering Conference*, pp. 455–460, Jul. 2008.

[50] S. Chandrasekaran and A. K. Jainb, "Dynamic behaviour of square and triangular offshore tension leg platforms under regular wave loads," *Journal of Ocean Engineering*, vol. 29, no. 3, pp. 279–313, 2002.

[51] M. J. Amoruso, "Euler angles and quaternions in six degree of freedom simulations of projectiles," Tech. Rep. ADA417259, US Army Armament Research Development and Engineering Center, Picatinny Arsenal, NJ, 1996.

[52] D. Eberly, "Euler angle formulas," Tech. Rep. MS, Magic Software, Chapel Hill, NC, 1999.

[53] A. Guran, "Studies in spatial motion of a gyro on an elastic-foundation," *Journal of Mechanics of Sturctures and Machines*, vol. 21, no. 1, pp. 185–199, 1993.

[54] T. Amer, "On the rotational motion of a gyrostat about a fixed point with mass distribution," *Journal of Nonlinear Dynamics*, vol. 54, no. 3, pp. 189–198, 2008.

[55] J. M. Longuski, "Real solutions for the attitude motion of a self-excited rigid body," *Journal of Acta Astronautica*, vol. 25, no. 3, pp. 131–139, 1991.

[56] N. H. Hughes, "Quaternion to Euler angle conversion for arbitrary rotation sequence using geometric methods," Tech. Rep. BT, Braxton Technologies, Colorado Springs, CO, 2008.

[57] J. Van Der Ha, "Pertubation solution of attitude motion under body-fixed torques," *Journal of Acta Astronautica*, vol. 12, no. 10, pp. 861–869, 1985.

[58] R. C. Hibbeler, *Engineering Mechanics - Statics and Dynamics*. Upper Saddle River, NJ: Pearson Prentice Hall, 2004.

[59] B. Sweetman and L. Wang, "Large-angle rigid body dynamics of a floating offshore wind turbine using Euler's equations of motion," in *Proceedings of the NSF CMMI Research and Innovation Conference*, pp. 671–682, Jan. 2011.

[60] J. Jonkman, "Definition of the floating system for phase IV of OC3," Tech. Rep. NREL/TP-500-47535, National Energy Renewal Laboratory, Golden, CO, 2010.

[61] D. J. Laino, "NWTC Design Codes (IECWind)," Tech. Rep. v5.01.01, National Renewable Energy Laboratory, Golden, CO, 2010.

[62] N. Kelley and B. Jonkman, "NWTC Design Codes (TurbSim)," Tech. Rep. v1.50, National Renewable Energy Laboratory, Golden, CO, 2009.

[63] F. G. Nielsen, T. D. Hanson, and B. Skaare, "Integrated dynamic analysis of floating offshore wind turbines," in *Proceedings of the 25th International Conference on Offshore Mechanics and Arctic Engineering*, pp. 671–679, Jun. 2006.

[64] T. Sarpkaya and M. Issacson, *Mechanics of Wave Forces on Offshore Structures*. New York: Van Nostrand Reinhold Company, 1981.

[65] M. T. U. Mulk and J. Falzarano, "Complete six-degrees-of-freedom nonlinear ship rolling motion," *Journal of Offshore Mechanics and Artics Engineering*, vol. 116, no. 4, pp. 191–201, 1994.

[66] T. R. Kane and D. A. Levinson, *Dynamics: Theory and Applications*. New York: MacGraw-Hill Book Company, 1985.

[67] X. H. Zeng and X. P. Shen, "Nonlinear dynamics response of floating circular cylinder with taut tether," in *Proceedings of the 15th Offshore and Polar Engineering Conference*, pp. 218–224, Jun. 2005.

[68] E. Leimanis, *The General Problem of the Motion of Coupled Rigid Bodies About a Fixed Point*. New York: Springer-Verlag, 1965.

[69] M. A. Abkowitz, *Stability and Motion Control of Ocean Vehicles*. Cambridge, MA: M.I.T. Press, 1969.

[70] L. Wang and B. Sweetman, "Simulation of large-amplitude motion of floating wind turbines using conservation of momentum," *Journal of Ocean Engineering*, vol. 42C, pp. 155–164, Mar. 2012.

[71] F. Lucassen and H. van de Ven, "Optimal body fixed coordinate systems in Newton/Euler modelling," Tech. Rep. EUT Report 88-E-210, Eindhoven University of Technology, Eindhoven, Netherlands, 1988.

[72] A. D. Garrad and D. C. Quarton, "Symbolic computing as a tool in wind turbine dynanics," *Journal of Sound and Vibration*, vol. 109, no. 1, pp. 65–78, 1986.

[73] A. Meghdari and F. Fahimi, "On the first-order decoupling of dynamical equations of motion for elastic multibody systems as applied to a two-link flexible manipulator," *Journal of Multibody System Dynamics*, vol. 5, pp. 1–20, 2001.

[74] J. C. G. Orden, J. M. Goicolea, and J. Cuadrado, *Multibody Dynamics: Computational Methods and Applications*. New York: Springer, 2010.

[75] P. Nikravesh, *Computer-Aided Analysis of Mechanical Systems*. Upper Saddle River, NJ: Prentice-Hall, 1988.

VITA

NAME: Lei Wang

ADDRESS: Ocean Engineering Program, 3136 TAMU
College Station, TX 77843-3136

EMAIL : lei.ray@hotmail.com

EDUCATION: B.S., Naval Architecture and Ocean Engineering,
Tianjin University, China, 2001

M.S., Naval Architecture and Ocean Engineering,
Tianjin University, China, 2004

RELEVANT PUBLICATIONS:

[1] B. Sweetman and L. Wang, "Floating offshore wind turbine dynamics: large-angle motions in Euler space," *Journal of Offshore Mechanics and Arctic Engineering*, vol. 134, iss. 3, Aug. 2012.

[2] L. Wang and B. Sweetman, "Simulation of large-amplitude motion of floating wind turbines using conservation of momentum," *Journal of Ocean Engineering*, vol. 42C, pp. 155-164, Mar. 2012.

[3] L. Wang and B. Sweetman, "Conceptual design of floating wind turbines with large-amplitude motion," in *Proceedings of the Society of Naval Architects and Marine Engineers Conference*, pp. 58-67, Nov. 2011.